

CITY, UNIVERSITY OF LONDON

MSC IN DATA SCIENCE

PROJECT REPORT

2018/2019

**Integrating data science into immunological
research to determine patterns in neutrophil
shape and movement**

Author:

Lara Chammas

Supervised by:

Dr Constantino Carlos

Reyes-Aldasoro

Dr Cagatay Turkay

October 1, 2019

Declaration of Authorship

By submitting this work, I declare that this work is entirely my own except those parts duly identified and referenced in my submission. It complies with any specified word limits and the requirements and regulations detailed in the assessment instructions and any other relevant programme and module documentation. In submitting this work I acknowledge that I have read and understood the regulations and code regarding academic misconduct, including that relating to plagiarism, as specified in the Programme Handbook. I also acknowledge that this work will be subject to a variety of checks for academic misconduct.

Signed:

Lara Chammas

Abstract

Video microscopy techniques are revolutionizing immunological research, as they allow cells to be monitored in real time. The integration of data science into immunology research has become integral in data processing. Previous research initiatives have focused on improving the preprocessing of images to segment and identify cells. Now, this focus must shift to investigation the potential of data science tools for analysing images for biological significance. This project takes raw images and preprocessed numerical features of neutrophils within a zebrafish model to identify and quantify different behaviours. These behaviours and features are then compared statistically between neutrophils under different experimental conditions. New cell behaviours classified in this project include cell shape, nucleus elongation, and directional movement. The classification of cell shapes was automated using a random forest algorithm. Nucleus elongation and directional movement were classified using thresholding and descriptive statistics. Systematically identifying these unique moments suggests the position of the neutrophil nucleus contributes to regulating cell velocity, that nucleus elongation contributes to persistent directional movement, and that the cytoskeleton plays a large role in modulating the morphology of the neutrophil nucleus.

Keywords: immunology, image classifier, behaviour classifier, random forest, statistical hypothesis testing

Contents

| | |
|---|-----------|
| Declaration of Authorship | i |
| Abstract | ii |
| 1 Introduction and Objectives | 1 |
| 1.1 Background | 1 |
| 1.2 Aims and Objectives | 2 |
| 1.2.1 Beneficiaries | 3 |
| 1.3 Introduction to Methods and Work Plan | 3 |
| 1.3.1 Changes in Methods and Work Plan | 3 |
| 1.4 Structure of the Report | 4 |
| 2 Context | 6 |
| 2.1 Data Science in Immunology | 6 |
| 2.2 The Neutrophil and its Nucleus | 8 |
| 2.3 Origins of the Data | 11 |
| 3 Methods | 13 |
| 3.1 Materials | 13 |
| 3.2 Cell Shape Image Classifier | 13 |
| 3.2.1 Random Forest | 14 |
| 3.2.2 Extracting Features | 15 |
| 3.2.3 Building the models | 16 |
| 3.2.4 Training and Testing Data | 17 |
| 3.2.5 Hyperparameter Tuning and Grid Search | 17 |
| 3.3 Defining Nuclear Elongation | 19 |
| 3.4 Detecting and Defining Movement | 20 |

| | |
|---|------------|
| 3.5 Biological Experiment Analysis | 20 |
| 3.5.1 Questions and Metrics | 21 |
| 3.5.2 T-Test, Anova, and Tukey Multicomparsion Correction Tests | 24 |
| 3.5.3 Fisher's Exact Test & Odd's Ratio | 26 |
| 4 Results | 28 |
| 4.1 Final data set | 28 |
| 4.2 Cell Image Classifier | 29 |
| 4.3 Elongation Event Analysis | 32 |
| 4.4 Directional Change Analysis | 33 |
| 4.5 Biological Experimental Group Analysis | 34 |
| 4.5.1 Tissue Injury: Non-injured (Group 1) versus Injured (Group 2) | 35 |
| 4.5.2 LBR Mutation: Wildtype (Group 4) versus LBR Mutant (Group 5) | 37 |
| 4.5.3 Drug Groups: Group 7 (Control) vs Group 3 and Group 10 | 40 |
| 5 Discussion | 44 |
| 6 Evaluation, Reflections and Conclusions | 48 |
| Bibliography | 50 |
| A RMPI Project Proposal | 56 |
| B Model Training Figures | 67 |
| B.1 Out of the bag classification error plots | 67 |
| B.2 Confusion matrices | 68 |
| C Image Classifier Hyperparameter Tuning Results | 72 |
| D Histograms of Metrics | 89 |
| E Behaviour Classifier Validation Notes | 93 |
| F Screenshots of metrics data table | 119 |

1 Introduction and Objectives

1.1 Background

The goal of immunological research is to develop complete models of how different aspects of the immune system work synergistically to maintain health. Immune system components include physical barriers such as the skin, immune cells such as macrophages and neutrophils, and regulatory components such as interleukins and chemokines (de Oliveira et al. 2013). Most immunological studies are “wet lab experiments”, comprising of small-scale experiments on an isolated component of the immune system, observing how it reacts to different experimental conditions. These conditions include environmental changes such as tissue injury, and genetic modifications such as protein receptor deletion (Elks et al. 2011, Ritter et al. 1998). Once the data has been collected, statistical hypothesis testing and correlation analysis determines whether there is a significant difference between groups and quantifies the size of these differences. This analysis is then assessed in the context of known immunological research, allowing for a model to be generated of the system as a whole (Castro et al. 2016, Moreau et al. 2018). These models then lead to the development of vaccines, anti-bacterial drugs, and cancer treatments (Gaudreau et al. 2016).

With advances in image processing, video microscopy is an increasingly viable method to study immune cells as it allows for in-vivo, or within organism, study. Observing active cells within the context of their natural environment provides a more realistic representation of behaviour than in-vitro observation in a test-tube or petri-dish enviroment (Kan 2017). Though more accurate, scale becomes a limiting factor, as the bottle neck of immunology research shifts from data collection to data processing (Henry et al. 2013). Within a single video frame, there can be hundreds of cells which require tracking. Automating the process of categorising images and extracting features for cell behaviour analysis is paramount to making biology a more quantitative science (Danuser 2011, Kan 2017). This project aims to address this quantitative

gap and advance the integration of the data science toolkit into immunological research. It does this by investigating the question *to what extent can outputs of cell tracking algorithms, and other quantitative analysis techniques, be used to determine patterns in immune cell shape and movement?*

This project builds upon a partnership between Monash University PhD candidate Harriet Manley and Dr Constantino Carlos Reyes-Aldasoro of City, University of London. Manley conducted various experiments on neutrophils inside zebrafish models and used fluorescent video microscopy to capture the neutrophils moving within the organism. These videos were then pre-processed by Dr Reyes-Aldasoro, who segmented each cell into a video time-lapse before generating various metrics about the cell's shape and movement. Further examining these processed videos, this project builds upon Reyes-Aldasoro's initial metrics to suggest answers to the immunological problems that Manley is researching. Ultimately, this partnership seeks to publish in peer-reviewed publications, and therefore the full data set used cannot be provided. However, Appendix F.1 and F.2 contain screenshot examples of the final metrics table generated by myself and various figures throughout the report show examples of the video and image stills generated by Manley and Reyes-Aldasoro.

1.2 Aims and Objectives

The main aim of this project is to determine patterns in neutrophil nucleus shape and movement under different experimental conditions by automating the generation of quantitative metrics that have been detected qualitatively by the biologists' eye. Any cell features generated during this project will be verified against hand-annotated samples by Harriet Manley, who will also verify any biological results to ensure they are in-line with current findings. The outcome of this project is to add new knowledge to the immunology field and to show the feasibility of integrating data science techniques into biological research.

To meet this aim, the project objectives are:

- Generate features and metrics which reflect biological characteristics of the cells including shape and movement
- Analyze cells' behavior using these metrics to determine whether there are any patterns unique to each condition group

- Investigate any statistical differences between the features of the various condition groups
- If there is significance, quantify the effect of each condition on metrics of interest

1.2.1 Beneficiaries

The main beneficiaries of this project include firstly Harriet Manley, who will use the metrics and results generated in this report directly in the completion of her PhD thesis. Next, immunologists and other biological researchers will benefit from this project's demonstration of the scope for integrating different processing techniques in the automation of quantitative research. It shall also demonstrate scope for future interdisciplinary work between data scientists and biological researchers in advancing biological data processing and research more generally.

1.3 Introduction to Methods and Work Plan

The first stage of this project involved creating a machine learning algorithm which could classify the shape of a cell based on its image. The next stage was defining moments of nucleus elongation and then classifying which cells exhibited this behaviour. Next, analysis was conducted on the cell's movement patterns. This included first detecting if movement was occurring, then in which direction, and lastly identifying when the cell changed direction. These outputs, along with other metrics generated by Dr Reyes-Aldasoro, were then combined to create a final data set of metrics for each cell over time. This data was then used to determine the physiological functions behind many neutrophil behaviours by conducting hypothesis statistical testing between different experimental groups using Fisher's exact test, t-tests, and ANOVA with Tukey multicomparison tests.

1.3.1 Changes in Methods and Work Plan

The original proposal discussed modeling the movement of the cells to determine if chemotaxis or random motility was occurring (Tranquillo et al. 1988). This analysis could not be conducted over the course of the project however, as the data collected was not calibrated for directional movement analysis. Therefore, the movement modeling aspect of the project was generalised to understanding the direction of movement versus the type of movement. The creation of a

cell shape image classifier was not discussed in the original proposal, but was added to the project plan after the initial data analysis stage. A revised work-plan is shown below in Figure 1.1.

1. Initial Data Analysis
2. Cell Shape Classification
 - a. Manually label training data
 - b. Hyperparameter model training and testing
 - c. Final model selection
3. Cell Behaviour Classification
 - a. Nucleus Elongation Identification
 - b. Directional Movement Identification
4. Experimental Biology Data Analysis
 - a. Statistical hypothesis testing
 - i. T-Test
 - ii. ANOVA
 - iii. Fisher's Exact Test
 - b. Statistical Significance difference estimation
 - i. Absolute mean difference
 - ii. Confidence Intervals
 - c. Analysing the results in the context of current scientific literature

FIGURE 1.1: Updated workplan for this project.

1.4 Structure of the Report

The structure of the remaining report is as follows:

- Chapter 2 provides the critical context surrounding the project motivation and the methods used through an analysis of pertinent literature. It outlines the current state of data science in immunology, provides information on what is a neutrophil, and outlines the experimental set-up of the data analyzed in the project.
- Chapter 3 describes in detail the materials of the project and the methods used.
- Chapter 4 gives the the results of training the image classifiers and the statistical analysis conducted on the data, providing both the statistical outputs directly and their corresponding biological interpretation.

- Chapter 5 discusses first if the project met the aims and objectives set in Chapter 1. Then, it discusses how the results found in chapter 4 fit into current immunological understanding of the neutrophil and provide new insights in the field.
 - Chapter 6 reflects and evaluates the project as a whole, including its limitations and contributions, and recommends areas for further work.
-
- Appendix A contains the original RMPI project proposal submitted in April.
 - Appendix B contains the validation classification error plots for each of image classification models during hyperparameter training. It also contains the testing classification confusion matrices for the six tuned models.
 - Appendix C contains the pdf print out of all the hyperparameter tuning model results for classification accuracy and error
 - Appendix D contains histograms for each of the metrics analysed during the biological experimental group analysis.
 - Appendix E contains scanned versions of the notes taken while validating the nucleus elongation classifier and cell movement classifier.
 - Appendix F contains screenshots of the first 24 rows of the analyzed data set.
-
- Additional files are submitted in the submission area. These are the MATLAB files used to generate the analysis (including the extracted features and labels to train the image classification models), the LATEX files that generate this document (including the jpg figures), and copies of the scanned pdfs attached in the appendix.

2 Context

2.1 Data Science in Immunology

Immunological research is going through a revolution with the advancement of video and image processing techniques. This is because video microscopy techniques allow for in-vivo, study of immune cells in different environmental and genetic conditions. These studies are conducted using zebrafish larvae which are transparent, allowing for direct viewing of their internal structures. With florescent labeling, immune cells become easily identifiable in images and videos generated through the microscopy (Reyes-Aldasoro et al. 2009, Liepe et al. 2012).

Processing the images and videos can be facilitated by applying data science techniques. The first step is to segment individual cells in each frame and follow them over-time. Once individual tracks and segments have been identified, statistics and metrics of the cell's movement, shape, and interactions within the zebrafish can be calculated. Thus far, most work in biological microscopy image and video analysis has focused on improving the algorithms used for segmentation and tracking. The aim has been to make the algorithms more accurate and adaptable to situations such as cells touching and moving in and out of the field of the camera (Thomas & John 2017, Solís-Lemus et al. 2018). Now, these tools require further development to fully explore the extent to which they can improve biological research through automating the detection and identification of hidden cell behaviours (Kadirkamanathan et al. 2012). This requires moving beyond the generation of standard measurements such as cell velocity and cell count towards more nuanced measurements including directional persistence and cell shape. By comparing the values of these metrics between different experimental groups, biological function and pathology can be deduced.

Current literature using video microscopy techniques relies heavily on human processing of each image to detect patterns in behaviour. This includes Mathias et al. (2006), who tracked 25

different neutrophils over time and quantitatively calculated the movement of the cells using directional persistence. Mathias nonetheless used manual annotation to detect patterns in shape, such as that neutrophils develop a rounded morphology upon reaching a wound site. This has been verified quantitatively in Henry et al. (2013), where it was discovered that neutrophil volume increases as the cell migrates towards a site of injury. The cell volume in this paper was determined using image processing techniques, a fast computer based process, whereas previously detecting the volume of a cell would require planning and running of a specific in-vitro experimental protocol (Ritter et al. 1998). This shows how data science techniques allow for rapid re-purposing of data to answer questions that emerge through the analysis of biological data without needing to run expensive and time consuming wet-lab experiments.

An example of a data science tool that can automate biological research is image classification algorithms (Thomas & John 2017). This is useful because there can be hundreds of cells to label and manual identification is time consuming and prone to human errors (Marée et al. 2007, Danuser 2011). In cell biology, the two most prominent categories of image classification algorithms are feature engineering and machine learning, and artificial neural networks (Shifat-E-Rabbi et al. 2019). An example of an image classifier built using feature engineering and machine learning is Putzu et al. (2014). They developed a cell image classifier which could correctly identify if an image contained white blood cells with leukemia or not by training a support vector machine to discriminate between pre-extracted morphological features, such as eccentricity and elongation, of cells labeled having leukemia or not. Their model had a 92% accuracy rate. To reduce the time needed for pre-processing to extract features, Marée et al. (2007) show the feasibility of using more generalized features, based on the raw image pixels, for four different cell biology classification tasks. Hamilton et al. (2007) also uses raw image pixels as features instead of specific shape features for cell phenotype classification with classification accuracy results over 90%. These studies show the possibility of building image classifiers without previous knowledge of the features that distinguish the objects of interest.

Neural network algorithms, such as convolutional neural networks (CNN), have become increasingly popular in cell biology image processing and classification (Kusumoto & Yuasa 2019). Convolutional neural networks do not require feature engineering, as they are able to directly extract features from an image to build the classifier (Rawat & Wang 2017). This is called end-to-end learning. Lin et al. (2019) used convolutional neural networks to classify

white blood cells in an image without the need to predetermine features. Nishimoto et al. (2018) used a convolutional neural network to predict the movement of a cell based on its current shape. By examining the features that the CNN used to distinguish each movement class, the researchers were able to identify morphological features that can influence the cell's movement. This shows how data science techniques can not advance biological research through the automate of tasks, but by also provide new insights into future areas of research that could not be detected by humans alone.

This project utilized feature extraction with machine learning to build a cell shape image classifier because the number of labeled training samples was low. This would reduce the accuracy of a CNN, which require large sample numbers for training. Standard machine learning algorithms also require less computation time, and have been shown to be as effective as CNNs when using features that best describe the objects to be classified (Shifat-E-Rabbi et al. 2019, Rawat & Wang 2017).

2.2 The Neutrophil and its Nucleus

Neutrophils are one of the many different white blood cells, or leukocytes, that make up the immune system. They are created in the bone marrow and circulate throughout the body searching for foreign pathogens and signs of infection. Upon meeting a pathogen, neutrophils have various techniques to kill them such as phagocytosis, granulation, and NETosis. Alongside their anti-microbial function, neutrophils have been shown to have regulatory functions within the immune system including the resolution of inflammation and recruitment of other immune cells (Rosales 2018).

Neutrophils are highly plastic cells, exhibiting a diverse range of shapes and movement patterns. They are classified as amoeboid cells, meaning that they use a series of extending and contracting pseudopodia, or arm-like extensions, to move around (Salvermoser et al. 2018). They also exhibit a diverse range of shapes, including a U-shape and a Y-shape, alongside the standard circular cell morphology (Manley et al. 2018). Another unique property of neutrophils is their ability to migrate from the blood stream into tissues by squeezing between endothelial cells (Davidson et al. 2014, Manley et al. 2018). Endothelial cells are the cells that make up the inner lining of blood vessels, and the space between them is much smaller than the size of a

neutrophil (Félétou 2011). A drawing of the neutrophil's localization within the body and its role in fighting bacteria is shown in Figure 2.1.

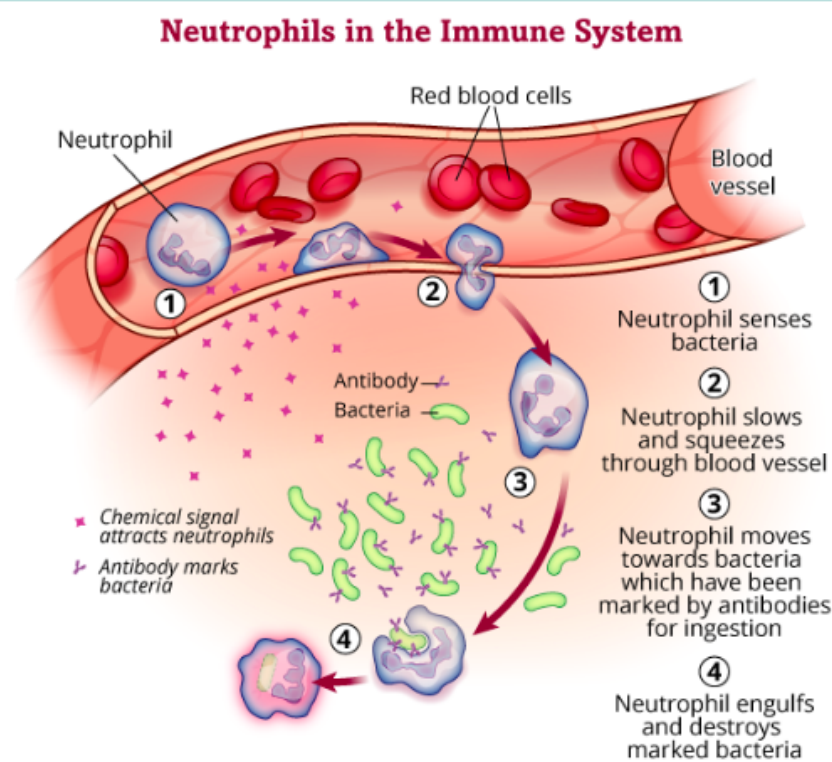


FIGURE 2.1: Schematic of the neutrophil's role in the human body. First, it migrates through the blood stream till it senses bacteria. Then, it will undergo trans-endothelial migration to reach the site of infections. There, it continues migrating till it reaches the bacteria and can destroy it. This image is taken from Hopsital (2019).

Understanding the properties that regulate neutrophil migration along and between tissues is paramount to creating drug treatments which regulate the migration and recruitment of neutrophils to inflammation sites. One of these properties is the ability of neutrophils to rapidly deform their shape and internal structures, including their nucleus. The nucleus is the largest organelle found in eukaryotic cells. It stores the genetic information of the cell and is the site of DNA replication and RNA synthesis (Jevtić et al. 2014). The nucleus is typically stiff, and has shown to play a role in the cell development and migration. Most human cells have an oval shaped nucleus. Its shape is maintained by the nuclear lamina, a mesh-like structure within the nucleus which is made up of lamin proteins which span the nucleus and are held in place to the nuclear membrane by lamin receptor proteins (Manley et al. 2018, Dittmer & Misteli 2011).

Lamins also play a role in the positioning of the nucleus within the cell due to their connections to the cell cytoskeleton (Carvalho et al. 2015, Calero-Cuenca et al. 2018). The cytoskeleton is the

network of different protein filaments, such as actin microfilaments and microtubules, that connect the nucleus membrane to the cell membrane. Like the nuclear lamina, it helps the cell maintain its shape and has functions in cell mobility (Calero-Cuenca et al. 2018). An image of the location and basic structure of the lamina and cytoskeleton within the neutrophil and its nucleus is shown in Figure 2.2.

Neutrophil nuclei exhibit a very different morphology than most cells. They have a highly lobulated (segmented) structure which is theorized to help in deformation to allow the neutrophil to squeeze between blood vessel cells (Schnipper et al. 2017). The role of the neutrophil's nucleus in its migration capacity has attracted much research, as the nucleus seems to be the limiting factor of trans-endothelial migration (Calero-Cuenca et al. 2018, Fruleux & Hawkins 2016). The therapeutic need to understand a neutrophil's migration ability inspired the main research aim of this project to be investigating how the nucleus's shape and position within a cell can affect a neutrophil's mobility, and which factors regulate these dynamics.

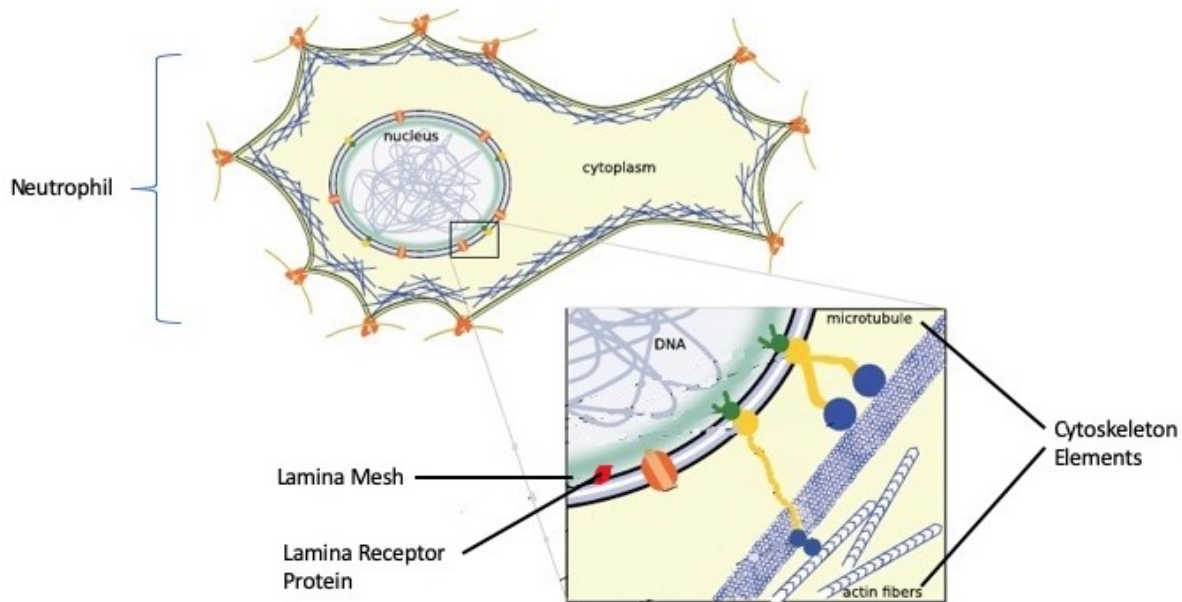


FIGURE 2.2: The neutrophil cytoskeleton elements, such as microtubules and actin fibers are shown in blue along the end of the neutrophil cell membrane. They are connected to the nucleus by the LINC complex, shown as yellow structures. The lamina mesh, shown as the green ring surround the nucleus membrane, supports the shape of the nucleus and is held in place by lamina receptor proteins, shown in red. This figure is taken and modified from Fruleux & Hawkins (2016).

2.3 Origins of the Data

The biological data analyzed during this project was generated by PhD candidate Harriet Manley from Monash University and the Australian Regenerative Medicine Institute. She used fluorescent light video microscopy to observe the motion of neutrophils in zebrafish larvae under different experimental conditions. These experiments seek to determine the physiological factors which induce morphological changes to the nucleus, what these changes were, and if they result in changes to the neutrophil's mobility.

The first experiment compared neutrophils in an injured zebrafish (Group 2) with neutrophils in an uninjured zebrafish (Group 1). This experiment sought to observe the difference between neutrophils in an "activate" and "inactive" state, as the inflammatory response is activated when there is an injury to the organism.

The second experiment analysed the role of the lamin B receptor (LBR) protein on the neutrophil's nucleus shape, nucleus position and mobility. This was done through genetic engineering of a zebrafish line to make its LBR gene non-functional (Group 5). These cells were then compared to neutrophils in a zebrafish with a functional LBR gene (Group 4). This experiment sought to verify that the lamin b receptor, which is embedded in the nuclear envelop and binds to lamins in the nuclear lamina mesh, plays a role in the lobulated shape of the nuclei (Jevtić et al. 2014). Deletion of the gene results in a rounder nucleus due to a decrease in the number of lobes. This is associated with impaired neutrophil migration and function as the nucleus can no longer deform for trans-endothelial migration (Davidson et al. 2014, Manley et al. 2018).

The third experimental group analysed the role of different cytoskeleton elements on the neutrophil's nucleus shape, nucleus position and mobility. This was done by exposing different zebrafish lines to drugs which inhibit different parts of the cytoskeleton. Group 3 neutrophils come from zebrafish lines exposed to a microtubule inhibitor drug called Nocodazole. Group 10 neutrophils come from zebrafish lines that were exposed to the drug LY294002, which is a phosphoinositide 3-kinase (PI3K) inhibitor, which impacts actin fibers. Group 7 neutrophils were the drug control model, and therefore come from zebrafish lines that have not been exposed to either of the drugs. These were studied because the cytoskeleton has been shown to play a role in the motility of cells by both generating and transferring forces through-out the cell

to propagate it forward, and by maintaining cell polarity (Cain & Ridley 2009, Rich & Hoffstein 1980, Qian et al. 2004). These cytoskeleton elements have also been shown to regulate the position of the nucleus and the nucleus shape, through interactions with the nuclear lamin mesh (Moreau et al. 2018, Calero-Cuenca et al. 2018, Yanakieva et al. 2019). Seeing what changes in nucleus shape each condition group exhibits, and then correlating them to changes in the cell's mobility, will generate a clearer model of the factors that regulate neutrophil migration.

3 Methods

3.1 Materials

The data analysed consisted of 468 videos, each representing a different cell which was segmented and tracked over time by Dr Reyes-Aldasoro. Figure 3.1 shows an example still of the videos generated by Dr Reyes-Aldasoro. The left-most frame is the raw microscopy image captured by Harriet Manley. The second frame from the left is a visualization of the cell's current location in yellow, its previous location in blue, and the areas of overlap in brown. The third frame is an outline of the segmented cell in yellow, its skeleton representation in blue, and an outline of the cell nucleus and its skeleton in red. The final two frames show changes in the number of branches and end points of the nucleus using the thinning technique (top right) and skeletonization technique (bottom right).

Each video has a corresponding MATLAB file containing two tables of metrics: one is 10 different metrics on the cell, the other is 10 different metrics on the nucleus. Using a modified script provided by Dr Reyes-Aldasoro, metrics of possible research interest were extracted from each video and combined into a table of 16,169 rows. Each row corresponds to a different image frame from the videos. Each row is labeled with the cell's experimental group number, which video it is from, and which frame number in that video so that the metrics can be linked back to the videos themselves. From this data set, new metrics were derived on the cell's movement and shape.

3.2 Cell Shape Image Classifier

One of the biological phenomena that Harriet Manley wanted to investigate was the unique Y and U shape that neutrophils can make. She had previously manually labeled a small sample

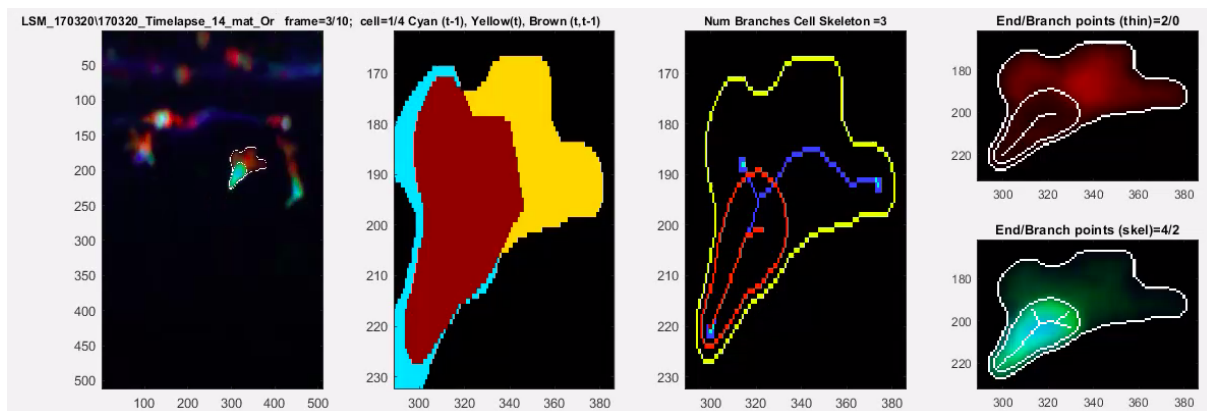


FIGURE 3.1: One frame from the processed videos generated by Dr Reyes Aldasoro. From left to right: The raw microscopy image of the neutrophil. A visualization of the movement of the cell showing its current location (yellow), its previous location (blue) and the overlap between the two areas (brown). The segmented neutrophil (yellow) and nucleus (red) with their corresponding skeletonized representations. Visualizing changes in the structure of the nucleus shape within the neutrophil using thinning (top right) and skeletonization (bottom right)

of videos ($n = 58$) and corresponding frames which showed clear examples of these shapes. A print-out of this labeling is attached in Appendix E. To aid in the analysis of these shapes, an image classifier was created to automate their detection and accelerate the preprocessing step of manually labeling the cells. The resulting classifier takes a video frame as its input and outputs a label of the cell shape.

3.2.1 Random Forest

The classification algorithm used was called random forests. A random forest is a supervised machine learning algorithm for classification and prediction tasks. It works by growing a “forest” of independent decision trees, each tree trained on a bootstrap sample (random sampling with replacement) of the data and the features. The algorithm’s output is either the mean (prediction) or mode (classification) decision of all the trees in the forest (Breiman 2001).

Random forest was selected as the classification algorithm because it is robust to noise, easy to train, and can inherently solve multi-classification problems without having to modify its structure, unlike another popular algorithms like support vector machines (SVMs) (Bosch et al. 2007). They have been used with high accuracy rates for classifying a variety of different tasks, including human pose-estimation and colon polyp-detection (Dantone et al. 2013, Iwahori et al.

2015, Ko et al. 2011, Zhang et al. 2003). Iwahori et al. (2015)'s work showing that using random forests with edge-based features, such as histogram of gradients (HoG), can out perform other algorithms such as SVMs with local binary pattern (LBR) features influenced this project's methods.

3.2.2 Extracting Features

In image classification, features are the characteristics of an object which both describe it and enable discrimination of it from others. This project tested two different feature extraction methods to discover which was most effective for cell shape classification. The two feature extraction methods were the histogram of gradients and the bag of visual SURF features.

The histogram of gradients feature extraction method works by calculating the gradient values of the object in the image of interest, which corresponds to its edges. Then, the gradient values are binned into orientations, which are then stored as a histogram. These histograms then become the feature vectors which are passed through the machine learning algorithm for classification (Dalal & Triggs 2005). Figure 3.2 shows an example of a video frame to be classified on the left, and a visualization of its corresponding oriented gradients on the right. The white lines are arrows showing the direction of the objects detected in the image. Looking closely, the arrows outline the edges of the cell.

The bag of visual SURF feature extraction method first extracts speed-up robust features (SURF) from an image. SURF are local feature detectors and descriptors based on summing the Haar-wavelets around an area of interest, using integral images to approximate the determinant of the Hessian matrix (Bay et al. 2006). Once the SURF points are extracted, they are converted into feature vectors using the "bag of words" method. This extracts the strongest features for each class and then performs k-means clustering to reduce them into groups which become the bag of visual words. Each image is then encoded by the bag into a histogram of which clusters they contain. The histograms are then used as the feature vectors in a classification model (Csurka et al. n.d.).

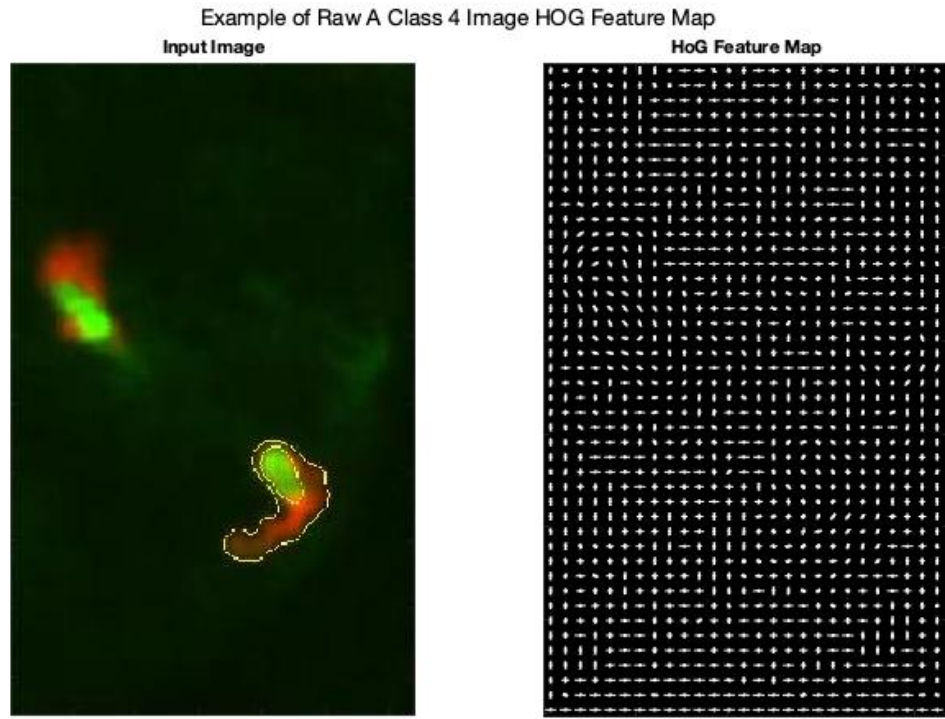


FIGURE 3.2: Example of a histogram of gradients feature vector for an image labeled Class 4 (U-shape) in the Raw A data set. On the left is the raw image, on the right is a visualization of the oriented gradients extracted from the image.

3.2.3 Building the models

Six different image classifiers were generated using different data-sets and different feature extraction methods in order to find the most accurate classifier. The first two initial data sets used were created by extracting and manually classifying the raw video microscopy frames (most left in Figure 3.1). There were a total of 280 frames extracted from the videos of the neutrophils from the list provided by Harriet Manley.

The first data set, Raw A, was composed of five classes: round, straight, pseudopodia, U-shape, and Y-shape. The second data set, Raw B, was composed of three classes: U-shape, Y-shape, and Other. Two different data sets were generated to see if a high accuracy could be maintained with more granular shape definitions or if the distinctions between them would be too subtle for the image classifier to pick up on. A third data set was created using the processed images of the cell generated by Dr. Reyes-Aldasoro, called Processed B. It followed the same classification pattern as the Raw B data set, but was slightly larger with 352 frames. The class composition

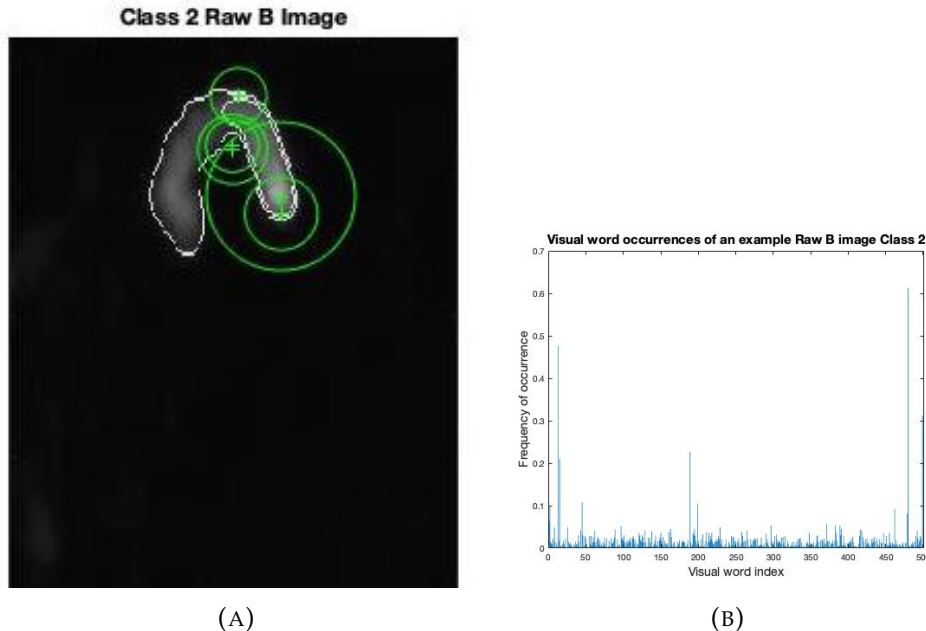


FIGURE 3.3: Example of the five strongest SURF features for an image labeled Class 2 (U-Shape) in the Raw B data set; Example of a bag of SURF features vector for an image labeled Class 2 (U-Shape) in the Raw B data set.

of each data set is shown in Table 3.4.

3.2.4 Training and Testing Data

To train and test the models, the data sets were split. To ensure class balance, the data was first reduced so that each class had the same number of images. This was set to the minimum image count found amongst all the classes. Then, the data was split 80% into a training set and 20% into a testing set. As random forests use a sub-sample of the data set to train each tree, the samples that are “out of the bag” were used as the validation data during model training.

3.2.5 Hyperparameter Tuning and Grid Search

Six different models were built from the combination of features and data sets: random forest with HOG features on Raw A images, random forest with BAG features on Raw A images, random forest with HOG features on Raw B images, random forest with BAG features on Raw B images, random forest with HOG features on Processed B images, and finally random forest with BAG features on Processed B images.

| Data Set | Class Number and Description | Number of Frames | Percentage Breakdown |
|-------------|------------------------------|------------------|----------------------|
| Raw A | Class 1: Straight | 50 | 17.85% |
| Raw A | Class 2: Round | 60 | 21.42% |
| Raw A | Class 3: Pseudopodia | 60 | 21.42% |
| Raw A | Class 4: U-shape | 67 | 23.92% |
| Raw A | Class 5: Y-Shape | 43 | 15.25% |
| Raw B | Class 1: Other Shape | 168 | 60% |
| Raw B | Class 2: U-shape | 68 | 24.2% |
| Raw B | Class 3: Y-Shape | 44 | 15.71% |
| Processed B | Class 1: Other Shape | 188 | 53.41% |
| Processed B | Class 2: U-shape | 103 | 29.26% |
| Processed B | Class 3: Y-Shape | 61 | 17.33% |

FIGURE 3.4: Table showing the number of image samples in each class for the three data sets. The last column contains the percentage that the class makes up of data set.

To build the models, hyperparameter tuning through a grid search was used. The hyperparameters that were tuned of the random forest were the minimum number of observations needed per leaf of the tree and the number of trees grown in the forest. The minimum number of observations tested was 1 through 10. The number of trees tested was 1 to 200, going in multiples of 20. All combinations of parameters were tested, resulting in 109 different hyperparameter combinations for each of the six models listed above. The models were trained using the training data. The out-of-the-bag validation error and accuracy rates were calculated for each model and stored in a table with the corresponding hyperparameters tuned.

The model with the highest accuracy and lowest error was then selected and its corresponding hyperparameters were stored and passed into a final model for training on the training data. The resulting model's accuracy was then calculated by testing its prediction ability on the testing data, which up to now has not been seen by the model. The final model's overall accuracy, error and single accuracy rates for each class were then stored.

Classification accuracy was the metric used to select the final model to classify cell shapes for all the data. Once the final model was selected, a new script was written to classify the frames of all the videos in the data set. The script first extracts the region of interest from the video frame. This region was then passed through the feature extractor to create the feature vector. This feature vector was then passed through the final model and the predicted cell shape was

stored in a matrix which also contained the video and frame number that corresponds to that label. Once all the frames had been classified, the resulting matrix was merged with the cell metrics table to create a new cell shape column.

3.3 Defining Nuclear Elongation

Typically, biological research on nuclear elongation may do a simple t-test to compare the mean lengths of the nucleus for each experimental group. However, this project sought to investigate the initial moment of nuclear elongation. To do this, the phenomenon of nuclear elongation was quantified and used as a classification system to label each cell as exhibiting nuclear elongation or not. To define nuclear elongation, the metric used was the percentage change of the major axis length (μM) of the nucleus between frames of a video. A nucleus would be considered elongated if this percentage change matched a certain threshold. To determine the correct threshold, four thresholds were tested. These were 10%, 15%, and 20%. The thresholds were then manually verified by comparing the frames labeled as elongation by the classifier against the frames labeled as elongation by Harriet Manley. It was found that 10% resulted in a high false positive classification rate and 15% resulted in a high false negative classification rate. A threshold value of 12% was then selected as it was the lowest percentage change value of the frames labeled as having nuclear elongation by Manley. The validation data set consisted of 24 videos, which had a combined total of 743 rows. The validation notes generated during this process can be seen in Appendix E.

After defining nuclear elongation as having a percentage change in the major axis length from the previous frame equal to or greater than 12%, each video was passed through the classification code to label its frames. A frame was labeled 0 if its major axis percentage change was less than 12, and it was labeled 1 if its percentage change was greater than or equal to 12. This generated a matrix which contained the video number, the frame number, the major axis percentage change, and the elongation classification label. As this was a percentage change exercise, it meant that the first frame of each video was not labeled and therefore removed from this data set.

3.4 Detecting and Defining Movement

Another cell behaviour of interest to be detected and defined was whether the cell was moving, and if so in which direction. The first step in detecting movement was calculating the vector magnitude between the x and the y coordinates for each frame of a video. This was carried out by running the public MathWorks function plot_dir3 (Kangwon 2010). Next, significant changes in movement were identified. This was done by first calculating the mean X-vector magnitude and mean Y-vector magnitude for each individual video. Each frame was then labeled as significant (1) if its value was greater than the mean. If it was less than the mean, the frame was labeled as non-significant (0). This classification system was manually validated using the same validation data set in 3.3. Frames highlighted as having significant changes in movement were compared to manually annotated frames. The manually annotated list was generated by watching the raw microscopy videos and by plotting the cell's x,y centroid locations over time. This determined if the classification system was robust and detected the kinds of movement we were interested in. The validation notes from this process can also be seen in Appendix E.

The number of 1s and 0s then determined in which axis the significant movement was occurring, and the sign of the corresponding vector magnitude determined the direction of that movement. Frames which only had significant movement in one of the axis were labeled with a cardinal direction (North, East, South, West). Frames with significant movement in both axis were labeled with an ordinal direction (North East, North West, South East, South West). If there was no significant movement detected in either axis, the frame was labeled as "no direction". Table 3.1 shows the classification process for labelling the cell's current direction of movement. This labeling process is based on the cell and object movement classification methods by Nishimoto et al. (2018) and Rosebrock (2015). The resulting five columns generated in this step were then added to the overall metrics table.

3.5 Biological Experiment Analysis

The final data set contained 15,318 rows and 31 columns of metrics on the cell and nuclei morphology and movement found in that frame. Rows with missing cell velocity, nucleus velocity,

| X-Vector Sign | Y-Vector Sign | X Greater than Mean | Y Greater than Mean | Direction |
|---------------|---------------|---------------------|---------------------|--------------|
| + | | 1 | 0 | East |
| - | | 1 | 0 | West |
| | + | 0 | 1 | South |
| | - | 0 | 1 | North |
| + | - | 1 | 1 | North East |
| - | - | 1 | 1 | North West |
| + | + | 1 | 1 | South East |
| - | + | 1 | 1 | South West |
| | | 0 | 0 | No Direction |

TABLE 3.1: To label the directions

and nucleus relative position were removed. This sample size, representing 468 individual cells, is much higher than many previous video microscopy studies which generally have sample sizes of approximately 25 neutrophils (Mathias et al. 2006)

Using this data set, statistical analysis was conducted to determine significant differences between experimental group features and the sizes of the differences. Then, the results were examined considering current biological research to determine the physiological reasons behind these differences and what these reasons reveal about neutrophil function and regulation.

3.5.1 Questions and Metrics

These tests sought to answer three primary questions:

- What effect does the experiment have on neutrophil nucleus shape?
- What effect does the experiment have on neutrophil nucleus position?
- What effect does the experiment have on neutrophil cell mobility and migration?

The metrics used to investigate nuclear shape were counts of elongation events, nuclear major axis length [μM], and nuclear eccentricity value. The metric used to investigate nuclear position was nuclear relative position. The metrics used to investigate cell mobility and migration were cell velocity [$\mu M/\text{second}$], change in direction counts, and cell path tortuosity. These metrics, except for elongation event count and change in direction count, were generated by Dr Reyes-Aldasoro.

Major axis length is the length of the longest diameter of the nuclei. The eccentricity value indicates how round the nuclei or cell is. It is calculated by dividing the minor axis length

(shortest diameter of the nuclei within the centre) over the major axis length (3.1). A value of 1 indicates a circular nucleus, while a value close to 0 indicates an oval shaped nucleus. Visualization of this feature, using images from the raw data, are shown in Figure 3.5.

$$\text{Eccentricity} = \frac{\text{Minor Axis Length } \mu\text{M}}{\text{Major Axis Length } \mu\text{M}} \quad (3.1)$$

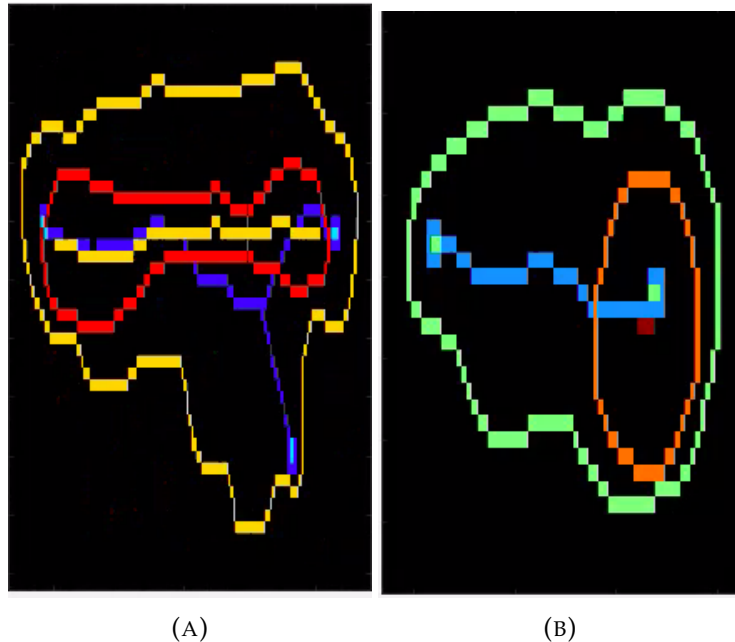


FIGURE 3.5: (A) Shows an example of a segmented cell with a nucleus (red) with an eccentricity value close to 0, indicating an ovoid shape. (B) Shows an example of a segmented cell with a nucleus (orange) with an eccentricity value close to 1, indicating a circular shape.

Relative position of the nuclei indicates where the nucleus's skeleton is in-respect to the cell's skeleton. It is calculated by finding the average distance of each pixel of the nucleus skeleton to the cell's skeleton and dividing it by the maximum distance between the skeletons. The value was then scaled between -1 and 1. A value of -1 indicates that the nucleus is positioned at the back of the cell, a value of 0 indicates that the nucleus is in the center of the cell, and a value of 1 indicates that the nucleus is in the front of the cell. Visualization of this feature, using images from the raw microscopy data, are shown in Figure 3.6.

Cell velocity is how fast the cell moves in the video calibrated as [$\mu\text{M}/\text{second}$]. Cell path tortuosity is defined as the total distance the cell moved in the video over the shortest distance between the cell's starting and end locations 3.2. A cell path tortuosity value close to one indicates that the cell moved in a straight line. A cell path tortuosity value above one indicates that

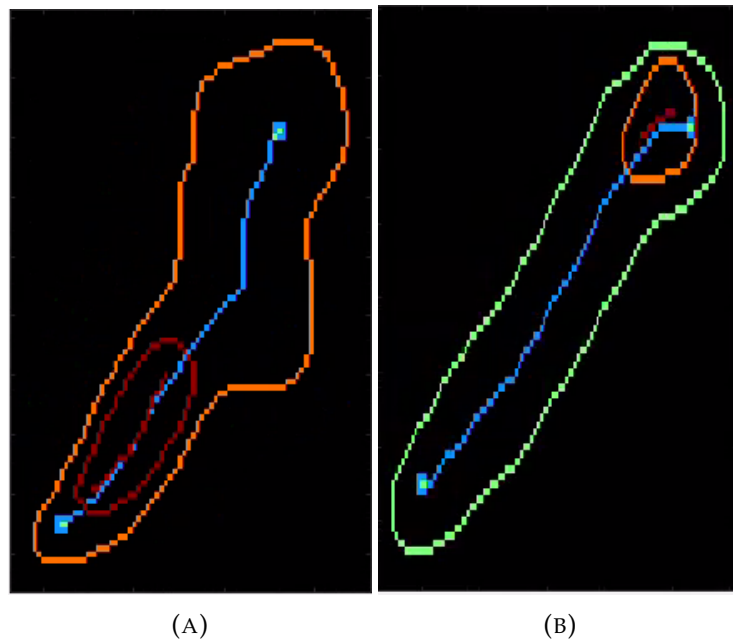
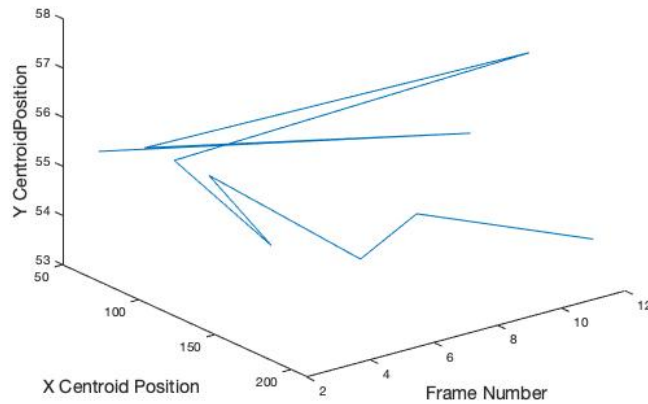


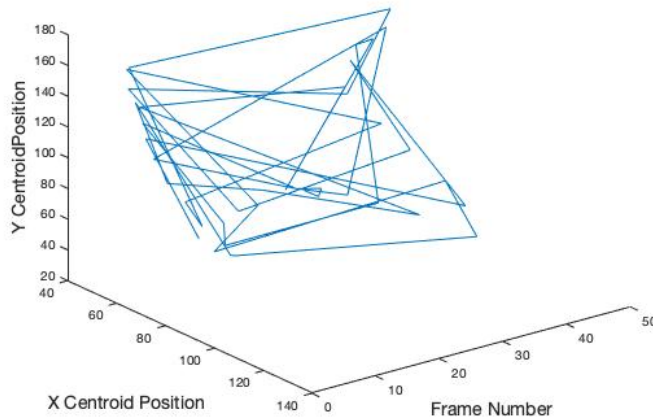
FIGURE 3.6: The same segmented cell is shown in both (A), in orange, and (B), in green. It is moving in the direction of the top right corner of the image. This means the front of the cell is at the top right corner and the back of the cell is at the bottom left corner. (A) Shows the cell when its nucleus (red) has a relative position of -0.426, meaning it is in the back of the cell. (B) Shows the cell when its nucleus (orange) has a relative position of 0.726, meaning it is in the front of the cell

it meandered between its start and end locations. The higher the value, the more winding the cell's path is. Figure 3.7a shows a visual representation of a cell's path whose path tortuosity value is 1 and Figure 3.7b shows a visual representation of a cell's path whose path tortuosity value is 22. Comparison of the plots shows how different the paths were taken by the cells between their starting and end points.

$$\text{Path Tortuosity} = \frac{\text{Distance between start and end point}}{\text{Total distance traveled}} \quad (3.2)$$

X/Y plot of cell centroid with path tortuosity value of 1

(A)

X/Y plot of cell centroid with path tortuosity value of 22

(B)

FIGURE 3.7: 3D plots of the x and y coordinates of a cell's centroid over time (frame number), showing the path the cell took in the video. (A) Shows the trajectory plot of a cell with a path tortuosity value of 1, indicating that it was very direct in its movement from its starting point to its end point. (B) Shows the trajectory plot of a cell with a path tortuosity value of 22, indicating that it meandered on its path between its start and end point.

3.5.2 T-Test, Anova, and Tukey Multicomparison Correction Tests

To determine if there is a significant difference between experimental groups, the two-sample t-test and the analysis of variance (ANOVA) test were used to compare the group means of different continuous metrics. The t-test was employed to compare just two experimental group

means using the function "ttest2()" in MATLAB. To compare more than two group means, the ANOVA test was employed using the function "anova1()" in MATLAB. Both tests calculate the difference of means of the groups, with their null hypothesis being that the means of the groups are the same (McDonald 2014*e,d*).

Both tests estimate a "p-value", which is the probability of obtaining the same results if the null hypothesis is true. If the p-value is below a certain threshold, then the null hypothesis can be rejected, this means that there is a difference between the mean values of the groups. The p-value also states the probability of a false positive in detecting a difference even if the null hypothesis (that there is no difference) is true. The p-value threshold for this study is 0.05, the standard value in biological studies, which means that the false positive rate of detecting a difference is less than 5% (McDonald 2014*a*). Alongside the p-value, this project will report effect sizes to quantify the difference discovered, and aid in understand the biology that is occurring. The effect size will be calculated by subtracting the absolute mean values of each group from each other, to get the absolute mean difference. The confidence interval will also be calculated to show the reliability of this mean difference estimate (McDonald 2014*b*).

When multiple groups are being compared, the ANOVA will produce only one p-value which states that there is a significant difference between at least one pair of groups. It does not tell you, however, which pair it is.

To determine this, individual pairwise t-tests could be conducted between the groups. However, increasing the number of tests conducted also increases the risk of detecting false positives. Therefore, to prevent this, various multicomparison post-hoc tests can be employed which adjust for the increased error rate (Lee & Lee 2018). This project uses the Tukey method, which calculates the minimum significant difference for each pair of means (McDonald 2014*d*). This is done using the "multcompare()" function in MATLAB, which reports the p-value for each pair of means, the estimated mean difference, and the 95% confidence interval of this estimate.

Both the t-test and ANOVA are parametric tests which assume that the data within each group is normally distributed. Studies have shown, however, that it is not too sensitive to deviate from this assumption. This means that even if the data is not normally distributed, it will not increase the rate of false positives being detected. This is especially true with groups with a

large sample size and when they have the same distribution (McDonald 2014*e*, Fagerland 2012). Therefore, even though most of the data in this project is not normally distributed, as shown in the histograms in Appendix B, these parametric tests were used over their non-parametric counterparts (Wilcoxon Rank Sum Test and the Kruskal Wallis Test) for biological understanding, it is more effective to understand the difference between the mean values versus comparing the distributions themselves (Ford 2017).

3.5.3 Fisher's Exact Test & Odd's Ratio

To determine if there is a non-random association between two categorical variables, the Fisher's exact test was employed in MATLAB through the function "fishertest()" (The MathWorks n.d.). The Fisher's exact test a non-parametric statistical hypothesis test that takes a 2 by 2 contingency table as its input, shown generically in Figure 3.8. It looks to see if the odds of a variable being in a particular row is influenced by being in a particular column (Freeman & Campbell n.d.). It outputs a p-value to determine if the null hypothesis can be rejected or not, and an odds ratio showing what the increased or decreased probability of having a particular outcome from being in a particular group (McDonald 2014*c*, The MathWorks n.d.). The odd's ratio is calculated as:

$$\text{Odds Ratio} = \frac{A11 * A22}{A21 * A12}$$

| | Condition 1 | Condition 2 |
|---------|-------------|-------------|
| Group 1 | A11 | A12 |
| Group 2 | A21 | A22 |

FIGURE 3.8: Example of a 2 by 2 contingency table used during a Fisher's exact test.

If the p-value of the Fisher's Exact test is less than 0.05, this means that there is a significant difference in the proportions of each category. Therefore, we can reject the null hypothesis that there is a random association between the two categories being studied. To determine the size of this difference, the odds ratio can be used. An odds ratio less than 1 shows a decreased probability of the condition occurring for the second group, while a ratio greater than 1 shows an increased probability. An odds ratio of one indicates that there is no difference in probability and therefore the null hypothesis cannot be rejected (Szumilas 2010, McDonald 2014*c*). An example interpretation of an odds ratio of 1.5 for Figure 3.8 is that it is 1.5 times more likely for

members of Group 2 to have Condition 2 than it is for members of Group 1. The Fisher's exact test was used over a Chi-square test because it does not make assumptions about the sample distributions of the data and it calculates an exact p-value versus making an estimate.

4 Results

4.1 Final data set

The final data set contains 31 columns and 15,318 rows. Of these 31 columns, 9 were generated throughout this project. These columns are: percentage change of nucleus major axis length, elongation classification, vector magnitude change of x centroid, vector magnitude change of y centroid, classification of the x vector magnitude being greater than the mean, classification of the y vector magnitude being greater than the mean, the direction of movement of the cell, classification of if the cell-changed direction, and the shape of the cell. Table 4.1 shows counts of many elongation events, direction paths, direction changes, and shapes which were labeled in the final data set. The first 24 rows of this data set for columns 1 - 12 and columns 18 - 31 can be found in Appendix F.1 and F.2 respectively.

| Metric Column Name | Metric Value | Frequency |
|--------------------|-----------------------|-----------|
| PvX_Mean | 0 (PvX < mean) | 5,123 |
| | 1 (PvX > mean) | 10,195 |
| PvY_Mean | 0 (PvY < mean) | 5,036 |
| | 1 (PvY > mean) | 10,282 |
| Elongation | 0 (no Elongation) | 12,548 |
| | 1 (Elongation) | 2,770 |
| Change Direction | 0 (No Change) | 8,017 |
| | 1 (Change) | 7,301 |
| Direction | East | 1,195 |
| | North | 1,243 |
| | North East | 2,134 |
| | North West | 1,888 |
| | South | 1,161 |
| | South East | 1,961 |
| | South West | 1,895 |
| | West | 1,122 |
| | No Direction Detected | 2,719 |
| Shapes | Other (1) | 3,472 |
| | U-Shape (2) | 9,879 |
| | Y-Shape (3) | 2,082 |

FIGURE 4.1: Table of the metrics derived during this project, the metric values, and the frequency of each of these metric values.

4.2 Cell Image Classifier

The hyperparameter tuning grid search for the six cell shape classifiers sought to determine which hyperparameters produce the highest accuracy model. These parameters and their corresponding validation classification accuracy and error rates are shown in Table 4.2. Using these parameters, final models were trained and their classification accuracy were tested using the unseen testing data set. The testing results for each model are shown in Table 4.3, which contains the model's overall classification accuracy rate, classification error rate, and the accuracy rates for each individual class. The corresponding testing confusion matrices for each model can be found in Appendix B. The final model selected to be used as the image classifier was the model with the highest overall accuracy rate.

| Parameter Tuning: Best Model Results | | | | | | |
|--------------------------------------|--------------|-------------|-----------------|--------------|----------------------|---------------------------------|
| Model | Feature Type | DataSet | Number of Trees | Minimum Leaf | Out of the bag Error | Out of the Bag Predict Accuracy |
| Random Forest | HOG | Raw_B | 180 | 1 | 31.43 | 68.57 |
| Random Forest | Bag SURF | Raw_B | 100 | 3 | 32.38 | 67.62 |
| Random Forest | Bag SURF | Raw_B | 140 | 3 | 32.38 | 67.62 |
| Random Forest | Bag SURF | Raw_B | 160 | 1 | 32.38 | 67.62 |
| Random Forest | Bag SURF | Raw_B | 160 | 4 | 32.38 | 67.62 |
| Random Forest | Bag SURF | Raw_B | 200 | 5 | 32.38 | 67.62 |
| Random Forest | Hog | Raw_A | 180 | 9 | 44.11 | 55.88 |
| Random Forest | Bag of SURF | Raw_A | 120 | 3 | 44.71 | 55.29 |
| Random Forest | Bag of SURF | Raw_A | 200 | 2 | 44.71 | 55.29 |
| Random Forest | BAG of SURF | Processed B | 140 | 3 | 24.44 | 75.56 |
| Random Forest | HOG | Processed B | 180 | 1 | 26.67 | 73.34 |
| Random Forest | HOG | Processed B | 180 | 4 | 26.67 | 73.34 |

FIGURE 4.2: Model parameter tuning results

Initially, only the Raw image data sets were used for model training. In this method, the highest accuracy model was the random forest model using histogram of gradients as features on the Raw B image data set. It had a testing accuracy of 77.78%. However, the classification breakdown by the model on the remainder of the data showed that the random forest model may have undetected errors. Of the 15,433 samples classified, 1,691 frames were labelled as Class 1 (11%), 12,057 samples were labeled as Class 2 (78%), and 1,685 samples were labeled as Class 3 (11%). This breakdown does not match the training data set class balance, shown in 3.4, implying errors in the classifier that were not detected in the testing phase. To investigate this,

| Final Model Testing Results - Raw_A Images | | | | | | | | |
|--|--------------|------------------|---------------|--------------------|--------------------|--------------------|--------------------|--------------------|
| Model | Feature Type | Overall Accuracy | Overall Error | Accuracy - Class 1 | Accuracy - Class 2 | Accuracy - Class 3 | Accuracy - Class 4 | Accuracy - Class 5 |
| Random Forest | HOG | 64.44 | 35.56 | 66.67 | 66.67 | 55.56 | 66.67 | 66.67 |
| Random Forest | Bag SURF | 62.22 | 37.78 | 77.78 | 55.56 | 33.34 | 66.67 | 77.78 |
| Final Model Testing Results - Raw_B Images | | | | | | | | |
| Model | Feature Type | Overall Accuracy | Overall Error | Accuracy - Class 1 | Accuracy - Class 2 | Accuracy - Class 3 | | |
| Random Forest | HOG | 77.78 | 22.22 | 88.89 | 77.78 | 66.67 | | |
| Random Forest | Bag SURF | 59.62 | 40.74 | 66.67 | 55.56 | 55.56 | | |
| Final Model Testing Results - Processed B Images | | | | | | | | |
| Model | Feature Type | Overall Accuracy | Overall Error | Accuracy - Class 1 | Accuracy - Class 2 | Accuracy - Class 3 | | |
| Random Forest | HOG | 81.82 | 18.18 | 1.00 | 63.63 | 81.81 | | |
| Random Forest | Bag SURF | 60.61 | 39.39 | 45.46 | 72.72 | 63.36 | | |

FIGURE 4.3: The testing results for the

I manually examined one of the videos labelled entirely as Class 2. This showed that the video frames contained florescent artifacts of other cells, shown in Figure 4.4a, as the methodology for extracting the image to be classified does not specifically detect the cell within the frame but passes the whole image through.

In attempting to rectify this, modifications of the code were made to see whether the specific cell of interest could be segmented out of the image. The method used was to generate a bounding box, using the "regionprops()" method from MATLAB (MathWorks n.d.). This was not an effective solution, as it revealed too many bounding boxes, none of which were in the right areas. Figure 4.4 shows a visualization of these bounding boxes for the image in both colour 4.4b and grayscale 4.4c. Next, a modification was added to make the method more precise by trying to detect MSER regions before applying region properties, however no MSER regions could be detected and consequently this method was abandoned.

The next method used to improve the shape classifier was to train the classifier using the processed cell outline images that Dr Carlos Constantios Reyes-Aldasoro generated during segmentation of the cells. This in turn generated the Processed B Image data set which was trained and tested in the same fashion as the Raw A and Raw B image models. After hyper-parameter tuning, the model with the highest accuracy was the random forest using histogram of gradient

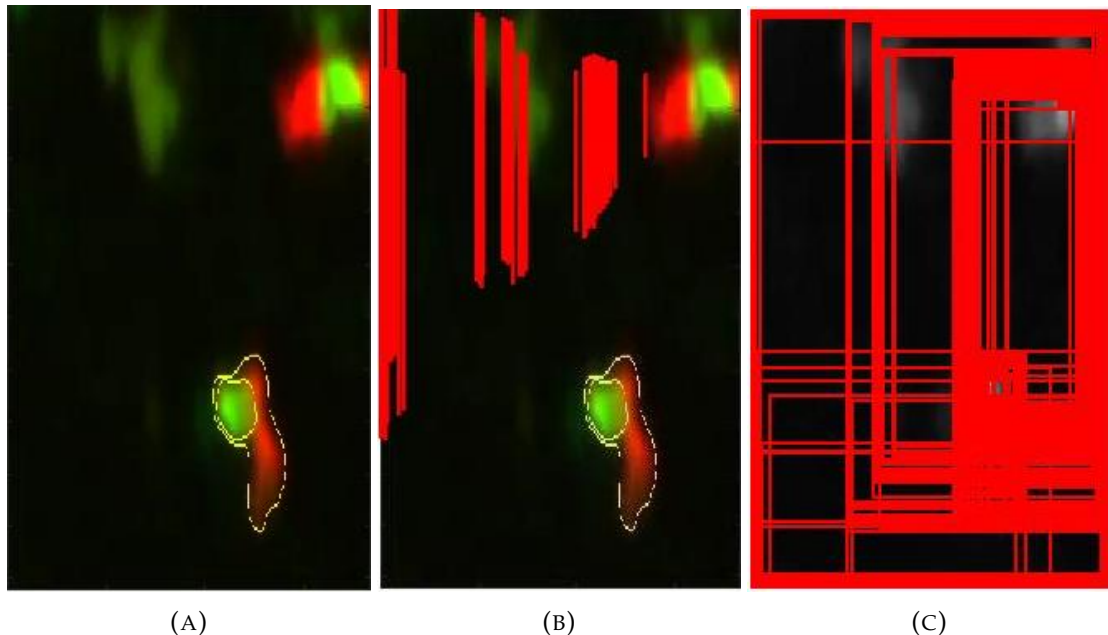


FIGURE 4.4: Trying to improve the cell shape classifier. The still image taken from the raw video of a cell (A). The bounding boxes found using MATLAB’s region proprieties on a colour version of the image (B) and a grayscale version of the image (C).

features with an overall testing accuracy of 81.82%.

After passing all the videos through the Processed B image classifier, the resulting matrix was 15,433 rows. There were 3,472 frames labeled as Class 1, or “Other”, 9,879 frames labeled as Class 2, or “U-shape”, and 2,082 frames labeled as Class 3, or “Y-shape”. This represents a proportional breakdown of 22.5%, 64.01%, and 13.49% respectively. However, this still does not match the breakdown of images labeled, where Class 1 was 53% of the data, Class 2 was 30% and Class 3 was 17%. This heavy weighting onto Class 2 will require further investigation. If the classification is accurate, it could be evidence of a shape preference of neutrophils not previously known. Despite the variance, this breakdown was more accurate than using the Raw B classifier which had a class breakdown of 11%, 78% and 11%. These results show how widely variable classifiers can perform with “real world” data which has not been curated for training purposes. It also highlights the need for human intervention in image processing of biological data where the differences between shapes may be indistinct to a machine.

4.3 Elongation Event Analysis

To understand what is happening to neutrophils when their nucleus elongates, two-sample t-tests were used to compare features of the cells when the nucleus is elongated and when it is not. The features tested were cell velocity, frequency of directional change, the relative position of the nucleus within the cell, the cell's skeleton tortuosity, and the cell's eccentricity. The research questions investigated are listed in 3.5.1.

Impacts on neutrophil mobility during nuclear elongation were found. First, there is a significant increase in the mean velocity of the cell when the nucleus undergoes elongation ($p = 1.7487e - 283$). During elongation, the cell's velocity increases on average by $0.0671 \mu\text{M}/\text{second}$, shown in boxplot 4.5a. This represents a shift in an average velocity of $0.0979 \mu\text{M}/\text{second}$ to $0.1650 \mu\text{M}/\text{second}$ (Confidence Interval = [0.0635 0.0706]). Boxplots of the groups cell velocity values are shown in Figure 4.5a. Second, a non-random association was detected between the odds of a cell changing direction and its nucleus elongating ($p = 1.7194e - 19$). The odds ratio of the Fisher's Exact Test indicates that the odds of a cell changing direction is more probable when the nucleus is not elongating (Odds Ratio = 1.4671, Confidence Interval = [1.3493 1.5952]).

The corresponding contingency table is shown in 4.1.

| | No Change | Change |
|---------------|-----------|--------|
| Elongated | 1664 | 1106 |
| Non-Elongated | 6353 | 6195 |

TABLE 4.1: Contingency Table of Nucleus Elongation versus Cell Changing Direction used in a Fisher's Exact Test.

Analysis of the impacts of nuclear elongation on the relative position of the nucleus revealed a significant shift backward of the nucleus within the cell ($p = 0.0015$). It moves from an average position of -0.2080 when the nucleus is not elongating, to a position of -0.2255 during elongation (Confidence Interval = [-0.0283 -0.0067]). Boxplots of the groups neucleus relation position are shown in Figure 4.5b.

Differences between the cell's average skeleton tortuosity and the cell's eccentricity were analysed to determine whether nuclear elongation effects the cell's shape. No significant difference was found between the average tortuosity of the cell's skeleton when the nucleus is elongated versus when it is not ($p = 0.0871$) (Figure 4.5d). However, a significant difference was found

between the cell eccentricity between the groups ($p = 1.2549e - 36$). Cell's undergoing nucleus elongation have a decreased cell eccentricity, going from an average value of 0.5135 when the nucleus is static to 0.4700 during elongation (Confidence Interval = [-0.0502 -0.0368]) (Figure 4.5c). This means the cell shape is less round and more oval.

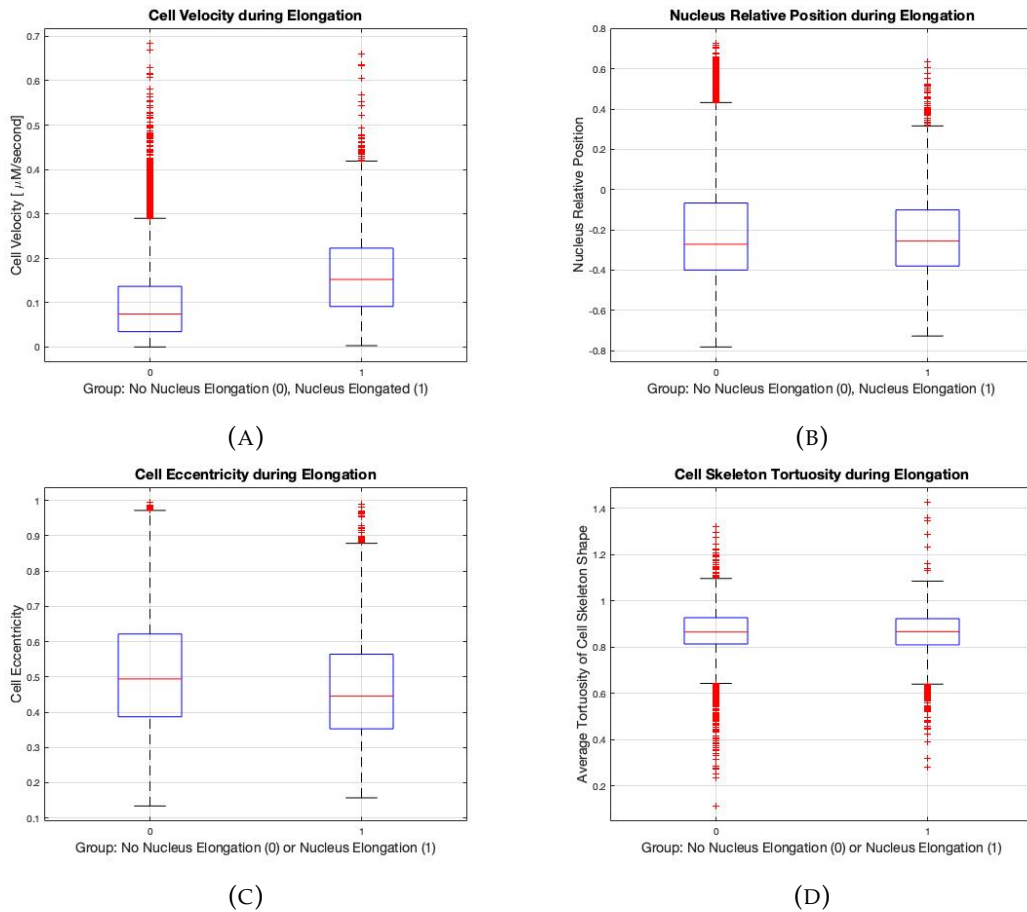


FIGURE 4.5: Boxplots comparing different metric values of cells without nuclear elongation (0) and with nuclear elongation (1). (A) Boxplot of the cell velocity. (B) Boxplot of the nucleus relative position. (C) Boxplot of the cell eccentricity value. (D) Boxplot of the cell skeleton tortuosity value.

4.4 Directional Change Analysis

A significant difference between the mean velocity of the cell when it is changing direction and when it is not was found ($p = 2.1161e - 131$). Changing direction decreases the average cell velocity on average by $0.0345 \mu\text{M}/\text{second}$. This represents a decrease from an average velocity of $0.1269 \mu\text{M}/\text{second}$ to $0.0915 \mu\text{M}/\text{second}$ when the cell changes direction (Confidence Interval: [0.0326 0.0383]).

Analysis of the effects of changing direction on the nucleus's relative position showed that there is a significant shift of the nucleus forward within the cell when it is changing direction ($p = 1.2805e - 06$). The nucleus goes from a relative position of -0.2209 in non-direction changing cells to -0.2004 in direction changing cells (Confidence Interval = [-0.0288 -0.0122]). Boxplots showing both of these results are in Figure 4.6.

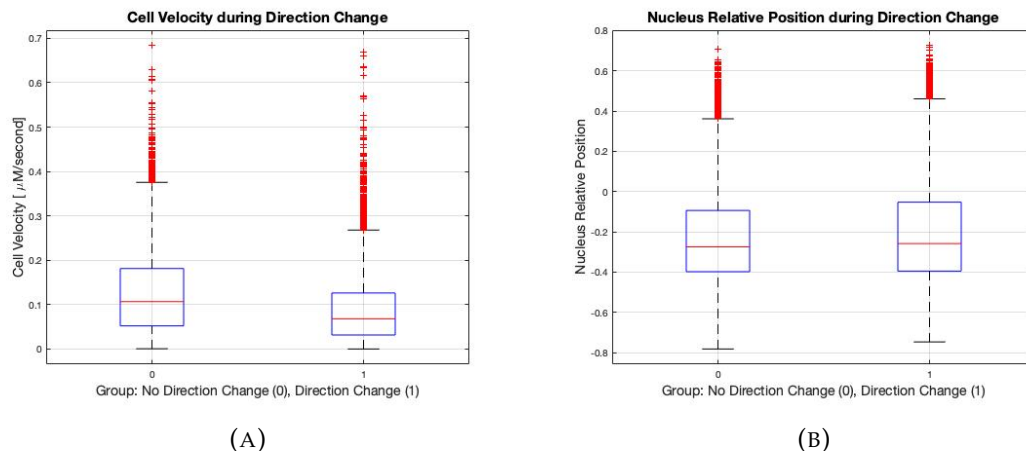


FIGURE 4.6: Boxplots comparing different metric values of cells not changing direction (0) and cells changing direction (1). (A) Boxplot of the cell velocity. (B) Boxplot of the nucleus relative position.

4.5 Biological Experimental Group Analysis

Three different experiments were conducted by Harriet Manley to try to discover the biological process which regulate plasticity in nuclear shape, nuclear position, and cell mobility. The first experiment compared neutrophils in uninjured zebrafish (Group 1) with neutrophils in injured zebrafish (Group 2). The second experiment compared neutrophils with the lamin B receptor (LBR) gene deleted, called lamin mutants (Group 5), and neutrophils without any genetic mutation, called wildtype cells (Group 4). The third experiment investigated inhibition of the cytoskeleton by exposing neutrophils to various inhibitory drugs. Group 7 cells were the drug control group, Group 3 cells were given a microtubule inhibitor and Group 10 cells were given a phosphokinase (PI3K) inhibitor.

To examine the effects of these experiments on shape, the features of nucleus elongation classification, nucleus major axis length, nucleus eccentricity, and cell eccentricity were all analysed. To examine the effect on nuclear position, the nucleus relative position was analysed. To examine the effect on cell mobility, the features cell velocity, change in direction classification, and

cell path tortuosity were analysed. The analysis tools used were two sample t-tests, ANOVA, and Fisher's Exact Test.

4.5.1 Tissue Injury: Non-injured (Group 1) versus Injured (Group 2)

The first test conducted was a Fisher's Exact Test which compared the occurrence of nucleus elongation between the groups, seen in Table 4.2. The result was not significant ($p = 0.7553$). However, a significant difference was found in the extent of nuclei elongation, with the mean nucleus major axis length decreasing $1.2139 \mu M$ during nuclei elongation in Group 2 cells (Confidence Interval: [0.3963 2.0314]). This is in opposition to the finding that overall, Group 2 neutrophils have significantly longer nuclei major axis lengths than Group 1 neutrophils by $0.6450 \mu M$ (Confidence Interval: [-0.9249 -0.3651]). These differences can be visualized in the boxplots in Figure 4.7b and Figure 4.7a .

Tissue injury induced morphological changes of both the cell and its nucleus. There was a significant decrease in the nucleus eccentricity value of Group 2 cells, going from a mean value of 0.4976 in Group 1 cells to 0.4584 ($p = 1.487e - 10$, Confidence Interval = [0.0273 0.0513]). This means that tissue injury cause the nucleus to become less round. A significant increase in cell eccentricity was found, however, in Group 2 cells by 0.0274 ($p = 1.82623e - 06$, Confidence Interval: [-0.0387 -0.0162]). They become rounder, going from a mean value of 0.4729 in Group 1 cells to 0.5004 in Group 2 cells. These differences can be visualized in the boxplots in Figure 4.7c and Figure 4.7d .

| Group | No Elongation | Elongation |
|---------|---------------|------------|
| Group 1 | 1609 | 266 |
| Group 2 | 1124 | 179 |

TABLE 4.2: Contingency Table of Group 1 and 2 versus the nucleus elongating used in a Fisher's Exact Test.

To understand changes in nuclear position, a t-test was conducted comparing the relative nuclear position of Group 1 and Group 2. It showed a significant difference between locations ($p = 7.1775e - 22$). On average, the nuclei of Group 2 cells are positioned further back in the nucleus than Group 1 cells, going from an average relative position value of -0.2463 in Group 1 cells to -0.1533 in Group 2 cells (Confidence Interval = [0.0741 0.1118]). The differences can be seen in Figure 4.8a.

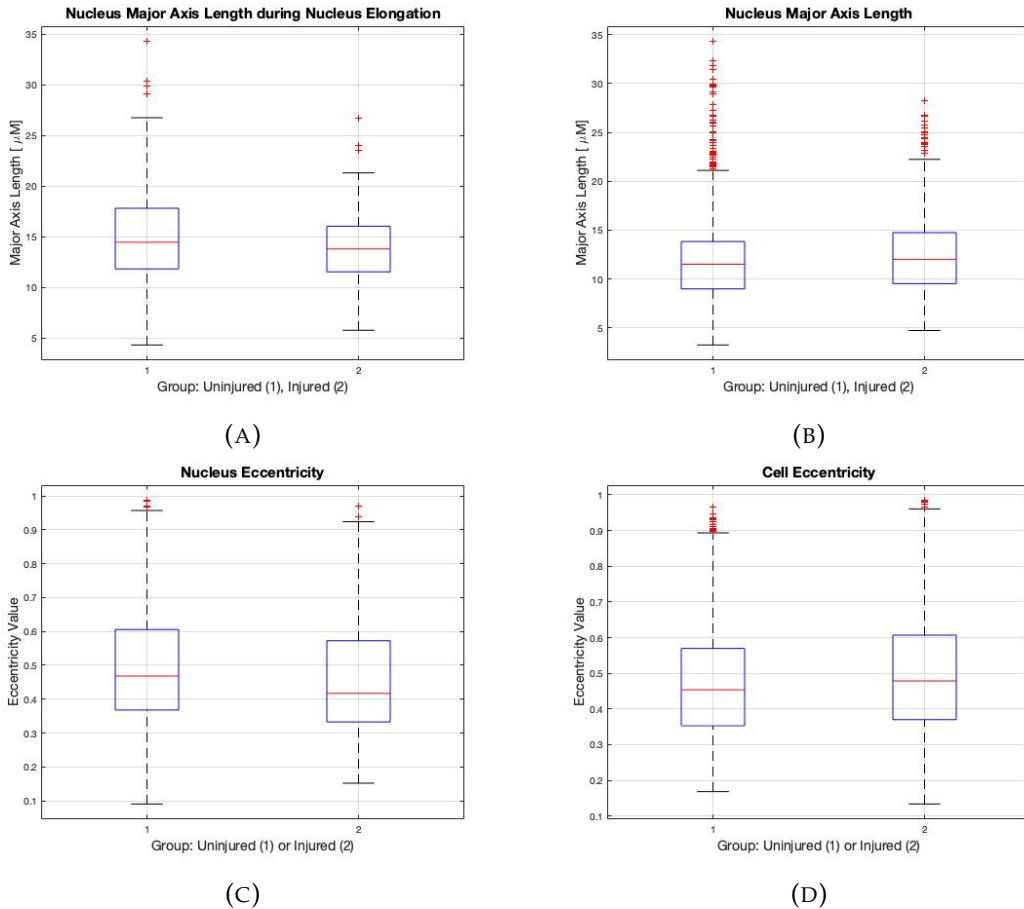


FIGURE 4.7: Boxplots comparing different metric values of Group 1 and Group 2. (A) Boxplot of the nucleus major axis length during nucleus elongation. (B) Boxplot of the nucleus major axis length for all the cells in the groups. (C) Boxplot of the nucleus eccentricity values. (D) Boxplot of the cell eccentricity values.

Cell velocity increased in Group 2 neutrophils ($p = 0.0247$) on average by $0.0065 \mu\text{M}/\text{second}$, increasing from an average velocity of $0.0832 \mu\text{M}/\text{second}$ to $0.0897 \mu\text{M}/\text{second}$ (Confidence Interval = [-0.0121 -0.0008]). The differences can be seen in Figure 4.8b. There was no significant difference found in the odds of the neutrophils changing direction between Group 1 or Group 2, with a Fisher's exact test resulting in a p-value of 0.4931 (4.3). There was also no significant difference found in the path tortuosity levels between the groups ($p = 0.8153$, 4.8c).

| Group | No Change | Change Direction |
|---------|-----------|------------------|
| Group 1 | 900 | 975 |
| Group 2 | 642 | 661 |

TABLE 4.3: Contingency Table of Group 1 and 2 versus the cell changing direction used in a Fisher's Exact Test.

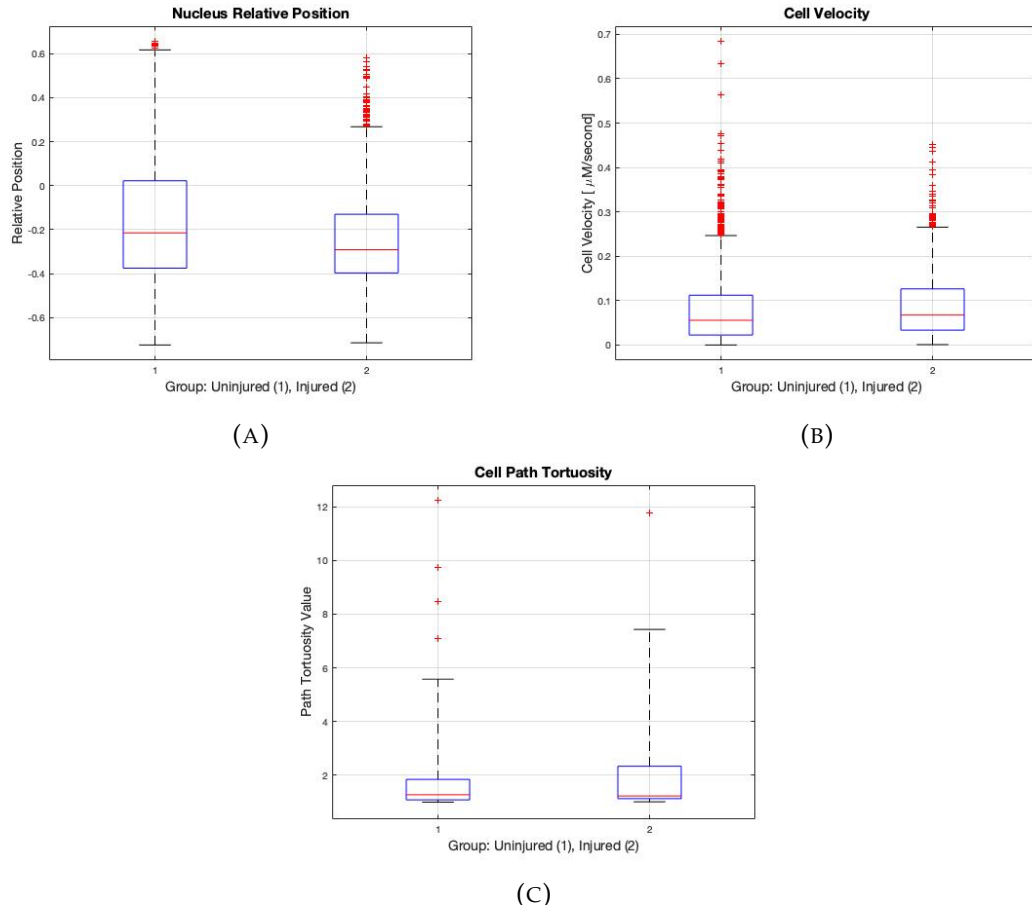


FIGURE 4.8: Boxplots comparing different metric values of Group 1 and Group 2. (A) Boxplot of the nucleus relative position. (B) Boxplot of the cell velocity. (C) Boxplot of the cell path tortuosity.

4.5.2 LBR Mutation: Wildtype (Group 4) versus LBR Mutant (Group 5)

As previously found, no difference in the occurrence of nuclear elongation between Group 4 and Group 5 cells was detected ($p = 0.7552, 4.4$). A significant difference was detected in the extent of elongation between groups ($p = 1.5047e - 13$), with LBR deletion resulting in a decreased nucleus major axis length of $1.1408 \mu\text{M}$ during nucleus elongation (Confidence Interval = [0.7686 1.3189]). This result is consistent overall, as the nucleus major axis length of all LBR mutant cells was found to be significantly shorter (by $1.0438 \mu\text{M}$) than wildtype cells ($p = 1.5047e - 13$; Confidence Interval = [0.7686 1.3189]). These differences are shown in Figures 4.9a and 4.9b.

LBR mutants have significantly rounder nuclei than LBR wildtype cells ($p = 4.0205e - 12$), with an average increase in nucleus eccentricity value of 0.0565 (Confidence Interval = [-0.0723 -0.0406]). No significant difference was found between the mean cell eccentricity of Group 4

| Group | No Elongation | Elongation |
|---------|---------------|------------|
| Group 4 | 596 | 140 |
| Group 5 | 947 | 262 |

TABLE 4.4: Contingency Table of Group 4 and 5 versus the nucleus elongating used in a Fisher's Exact Test.

and Group 5 neutrophils ($p = 0.2030$). The corresponding boxplots are Figures 4.9c and 4.9d.

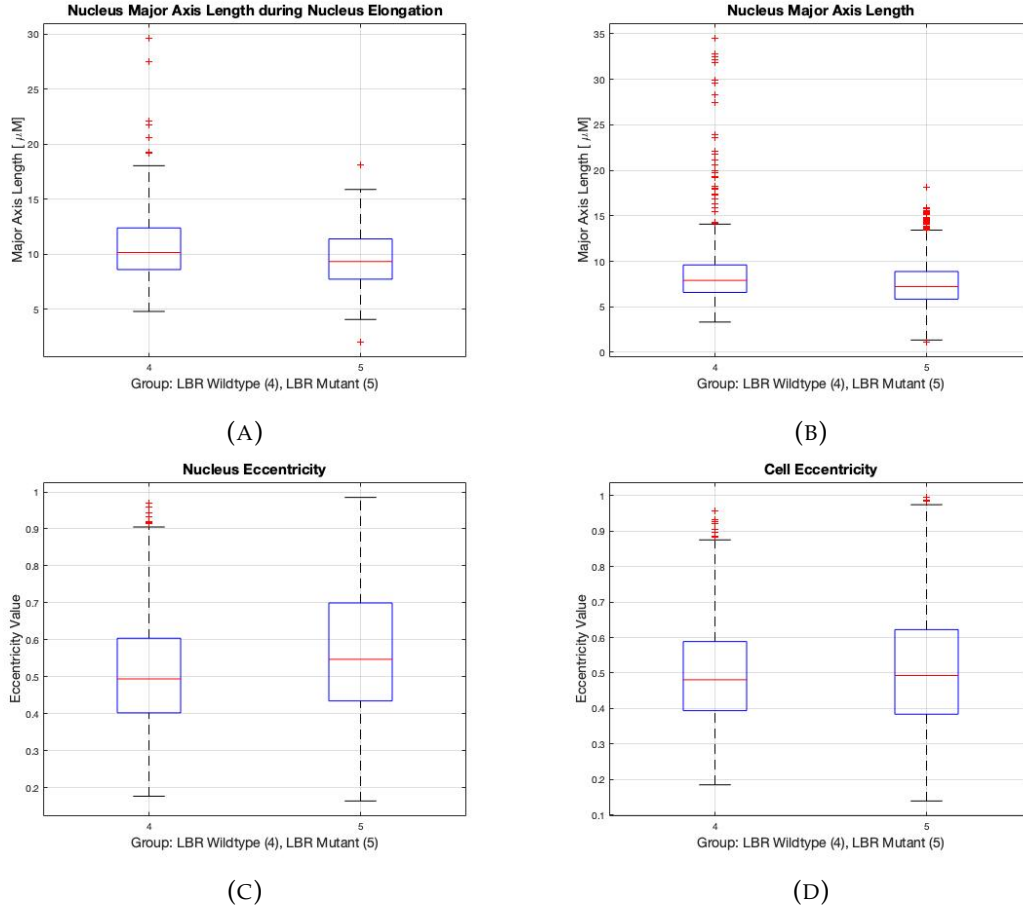


FIGURE 4.9: Boxplots comparing different metric values of Group 4 and Group 5. (A) Boxplot of the nucleus major axis length during nucleus elongation. (B) Boxplot of the nucleus major axis length for all the cells in the groups. (C) Boxplot of the nucleus eccentricity values. (D) Boxplot of the cell eccentricity values.

The relative position of the nucleus in LBR mutant neutrophils was found to be further forward than in wildtype cells ($p = 0.0195$). Wildtype cells were found to have a relative nuclear position of -0.2149 while LBR mutants were found to have a mean relative nuclear position of -0.1840, representing a forward shift of 0.0308 (Confidence Interval = [-0.0567 -0.0050]). This can be seen in Figure 4.10a.

The LBR mutant neutrophils were found to have significantly decreased cell velocity, with

the mean reduction being $0.0166 \mu\text{M}/\text{second}$ ($p = 4.5141e - 04$, Confidence Interval = [0.0073 0.0258]). This represents a shift from a mean velocity of $0.1351 \mu\text{M}/\text{second}$ in Group 4 cells to $0.1186 \mu\text{M}/\text{second}$ in Group 5 cells, shown in Figure 4.10b. There is also a significant decrease in the odds of LBR mutant cells changing direction ($p = 0.0020$; Odds Ratio = 0.7459; Confidence Interval = [0.6207 0.8964]), shown in Table 4.5. No significant difference was found between the average cell path tortuosity of the groups ($p = 0.8660$), seen in Figure 4.10c.

| Group | No Change | Change Direction |
|---------|-----------|------------------|
| Group 4 | 362 | 375 |
| Group 5 | 682 | 527 |

TABLE 4.5: Contingency Table of Group 4 and 5 versus the cell changing direction used in a Fisher's Exact Test.

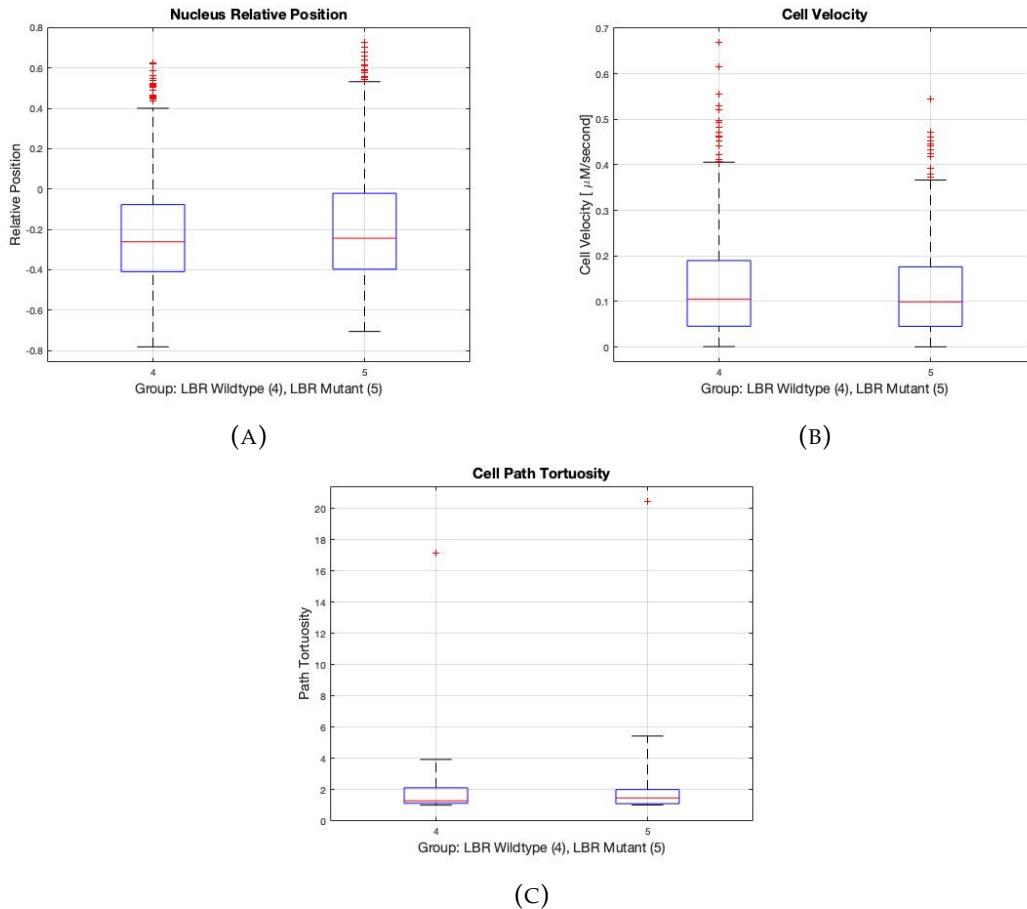


FIGURE 4.10: Boxplots comparing different metric values of Group 1 and Group 2. (A) Boxplot of the nucleus relative position. (B) Boxplot of the cell velocity. (C) Boxplot of the cell path tortuosity.

4.5.3 Drug Groups: Group 7 (Control) vs Group 3 and Group 10

To investigate the cell's cytoskeleton role in neutrophil plasticity, two different experiments were conducted. The first exposed zebrafish to a microtubule inhibitor (Group 3 cells) and the second exposed zebrafish to a phosphokinase inhibitor (Group 10 cells). The behaviours of Group 3 cells and Group 10 cells were then compared to Group 7 cells, which were not exposed to any inhibitory drugs. Boxplot visualizations of the differences between groups are shown in Figure 4.11 and 4.12. The contingency tables for the Fisher's Exact Tests are shown Table 4.6 and Table 4.7.

Microtubule inhibition did not result in a significant difference in the number of times the neutrophil's nucleus elongates as compared to Group 7 cells ($p = 0.1799$). It did, however, result in a significant decrease in the nucleus major axis length during elongation, decreasing the average length by $3.97 \mu M$ ($p = 0.0000$; Confidence Interval = [-4.9753 -2.9589]). This result is seen again when studying the difference in nucleus major axis length between all the cells in each group, as the nucleus in Group 3 cells was found to be on average $3.58 \mu M$ shorter than in Group 7 cells ($p = 0.0000$; Confidence Interval = [-3.5766 -3.1286]).

Microtubule inhibition results in a rounder cell shape and nucleus shape. Group 3 nuclei eccentricity significantly increased from a mean value of 0.4323 in Group 7 cells to 0.6181 ($p = 0.000$, Confidence Interval = [0.1639 0.2077]). Microtubule inhibition also significantly increased the eccentricity value of the neutrophils themselves, on average increasing from a value of 0.4870 to 0.5641 (($p = 0.0000$), Confidence Interval = [0.0541 0.1000]).

Phosphokinase inhibited cells had a decreased odds of their nucleus elongating, as compared to control cells, as found by a Fisher's exact test odd's ratio value of 0.6772 ($p == 0.0033$, Confidence Interval = [0.5240 0.8710]). The nucleus major axis length of Group 10 cell's during nucleus elongation was also significantly decreased as compared to Group 7 cells, with an average shortening in length by $0.9224 \mu M$ ($p = 0.0000$, Confidence Interval = [-0.400 1.8847]). The nucleus major axis length of all Group 10 cells was also shorter on average by $1.1897 \mu M$, as compared to Group 7 cells ($p = 0.0000$; Confidence Interval = [0.8066 1.1897]).

Phosphokinase inhibition resulted in rounder cell shape and nucleus shape as well. Group 10 cells had a significant increase in their nucleus eccentricity value, going from an average value of 0.4870 in Group 7 cells to an average value of 0.5332 when exposed to the phosphokinase

inhibitor ($p = 0.0000$, Confidence Interval = [-0.1052 -0.0678]). Group 10 cell's also had a significant increase in their eccentricity value, going from average cell eccentricity value of 0.4870 in Group 7 cells to 0.5332 ($p = 0.0000$, Confidence Interval = [-0.0658 -0.0266]).

The relative position of the nucleus in the cell was found to have changed significantly for both Group 3 and Group 10 cells ($p = 0.0000$). The nucleus relative position shifted forward in both groups. Group 3 cells saw their nuclei shift forward by a mean value of 0.2149 (Confidence Interval = [0.2516 0.3208]) while Group 10 nuclei saw their nuclei shift forward by a mean value of 0.1840 (Confidence Interval = [-0.1539 -0.0948]).

There was a significant decrease in the cell velocity of Group 10 cells as compared to Group 7 cells ($p = 0.0000$). Group 10 cells had a mean decrease in their velocity by $0.0301 \mu\text{M}/\text{second}$ (Confidence Interval = [0.0205 0.0396]). There was no significant difference found between the cell velocity of Group 3 cells and Group 7 cells ($p = 0.267$).

No significant difference was detected in the average cell path tortuosity for either Group 3 or Group 10 cells ($p = 0.4514$). However, a significant increase was detected in the odds of Group 10 cells changing direction in comparison to Group 7 cells ($p = 6.8004e - 06$; Odds Ratio = 1.5683; Confidence Interval = [1.2904 1.9061]). No significant difference in the odds of the cell changing direction was found between Group 3 and Group 7 cells ($p = 0.1597$).

| Group | No Elongation | Elongation | Group | No Elongation | Elongation |
|---------|---------------|------------|----------|---------------|------------|
| Group 7 | 538 | 133 | Group 7 | 538 | 133 |
| Group 3 | 416 | 125 | Group 10 | 416 | 125 |

(A)

(B)

TABLE 4.6: Contingency Table of (A) Group 7 and Group 3 and (B) Group 7 and Group 10 versus nucleus elongation used in a Fisher's Exact Test.

| Group | No Change | Change | Group | No Change | Change |
|---------|-----------|--------|----------|-----------|--------|
| Group 7 | 381 | 290 | Group 7 | 381 | 290 |
| Group 3 | 329 | 212 | Group 10 | 480 | 573 |

(A)

(B)

TABLE 4.7: Contingency Table of (A) Group 7 and Group 3 and (B) Group 7 and Group 10 versus directional change used in a Fisher's Exact Test.

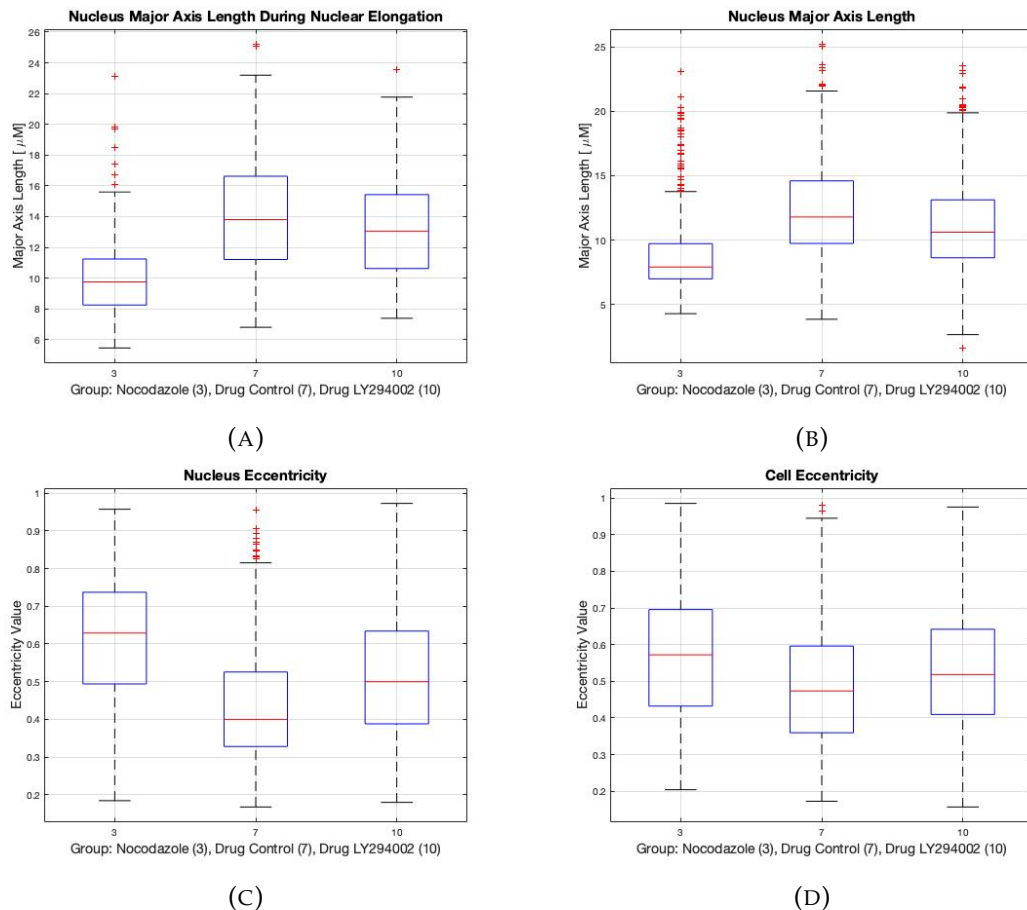


FIGURE 4.11: Boxplots comparing different metric values of Group 3, Group 7 and Group 10. (A) Boxplot of the nucleus major axis length during nucleus elongation. (B) Boxplot of the nucleus major axis length for all the cells in the groups. (C) Boxplot of the nucleus eccentricity values. (D) Boxplot of the cell eccentricity values.

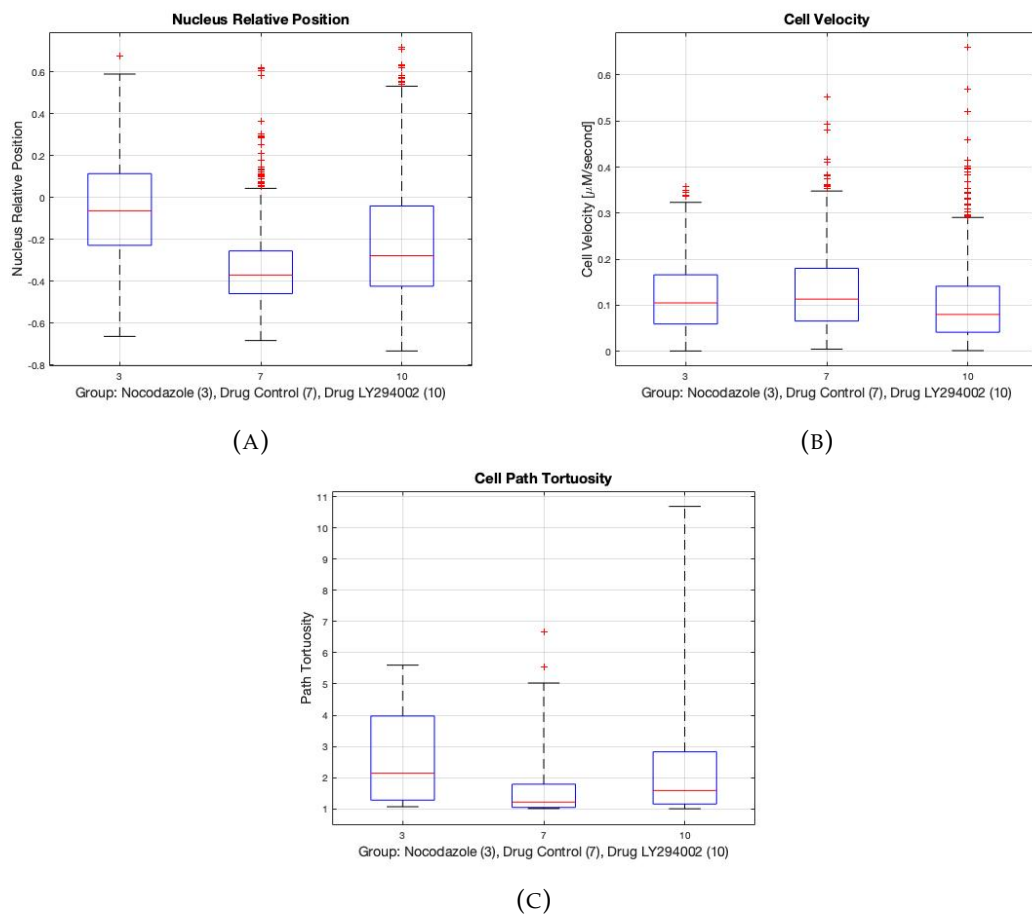


FIGURE 4.12: Boxplots comparing different metric values of Group 3, Group 7 and Group 10. (A) Boxplot of the nucleus relative position. (B) Boxplot of the cell velocity. (C) Boxplot of the cell path tortuosity.

5 Discussion

As stated in 1.2, the aim of this project was to determine patterns in neutrophil nucleus shape and movement under different experimental conditions by automating the generation of quantitative metrics that have been detected qualitatively by the biologists' eye. The objectives of this project were to:

- Generate metrics that reflect biological characteristics of the cells including shape and movement
- Analyse the cells' behavior using these metrics and determine if there are patterns unique to each condition group
- Investigate whether there is a statistical difference between the different condition groups' metrics
- If there is significance, quantify the effect of each condition on the metrics of interest

In meeting these objectives, previously unconsidered cell metrics were generated, including the identification of moments of nucleus elongation, the detection of cell directional change, the classification of cell shapes, and the determination of the direction of cell movement. These were then used in conjunction with other features to determine which properties are unique to cells under various conditions. These include moments of nuclear elongation, moments of cell directional change, whether the neutrophil is in an injured tissue environment, and moments when the neutrophil experiences changes to its molecular and genetic structure. The differences and effects of these conditions were analysed and reported to generate hypotheses on how neutrophils move and function within the body. Many of the results seen are supported by previous research, but this study also reveals new insights which demonstrate the need for future work to determine the biological significance of this study's findings (Manley et al. 2018, Jevtić et al. 2014, Carvalho et al. 2015).

The cell shape image classifier created during this project demonstrates the scope for automating the labeling of cell shapes which would otherwise be classified manually by a biologist. The testing accuracy of the best image classifier was 81% on the testing data, however, using the full data-set resulted in class distribution which differed from the training data set. If we are to assume that the training data set is representative of the actual class balance then the corresponding classification output should have been the same. However, they were flipped for Class 1 and Class 2. This demonstrates the need for further investigation into what is the true distribution of neutrophil shapes, and why the classifier was outputting different results. This project's focus was to examine changes in the neutrophil's nucleus, and therefore offered little scope for investigating the true shape classification balance of the neutrophils. The disjoint between the Class 1 and Class 2 results of this image classifier could be because the training data set used was not representative of real-world behaviors, such that neutrophils may exhibit a "U-shape" more frequently than believed during migration. Therefore, this paper recommends further research into the typical neutrophil shapes under different conditions.

Overall, this project demonstrates how data science tools can allow biological researchers to examine their data at different scales by quantitatively classifying behaviours seen by eye but not detected in cell segmentation and tracking algorithms. The behaviours identified and classified in this project were nucleus elongation and directional movement of the cell. These behaviours were not originally intended to be the focus of this study, therefore Manley's experimental set-up was not conducive to direct analysis of them. However, using computational analysis techniques to build classification systems allowed for the analysis of nuclear elongation and changes in cell directionality. For example, as the videos were not calibrated to have the same tissue injury orientation, directional persistence of the cells could not be directly calculated. However, the persistent movement of the cell could be inferred by examining the number of directional changes made by the cell. Fewer changes indicate a greater persistence of directional movement. Another example is that upon initial viewing of the videos, Manley noted that the neutrophils' nuclei would exhibit elongation behaviours and thought this worthy of investigation. In a typical immunological research setting, this would require establishing a new wet lab experiment to specifically study this behaviour under different conditions. However, thanks to the ability of data science toolkits to rapidly analyse thousands of data points and develop classification systems, nuclear elongation event analysis was conducted without the need for a

new wet lab.

The results of the biological experiment analysis revealed many insights into the regulatory mechanisms behind neutrophil plasticity. Firstly, the nucleus appears to elongate in moments of increased directional persistence of movement, as the cell's velocity increases and the odds of the cell changing direction decreases. This supports the hypothesis that the nucleus plays a role in driving the nucleus forward (Manley et al. 2018). Further supporting this conclusion is the nucleus' position at the back of the cell during these moments. This matches Calero-Cuenca et al. (2018)'s finding that the nucleus positions itself at the back of the cell during neutrophil migration. Further supporting this theory is the difference observed between neutrophils in an injured tissue environment (Group 2) and uninjured environment (Group 1). Group 2 neutrophils had their nuclei positioned further back in the cell and as their cell velocity increased. This suggests that there is a relationship between neutrophil cell velocity and nucleus position.

When the neutrophils were in an injured tissue environment, the corresponding morphology changes found were in-line with activated neutrophil morphology. This includes a rounder cell shape and an increase in cell velocity (Henry et al. 2013, Ritter et al. 1998, Mathias et al. 2006). However, we would expect to see a corresponding decrease in the occurrence of the cell directional changes or a decrease in cell path tortuosity, as neutrophils tend to migrate towards sites of inflammation with increased directional persistence and along the "path of least resistance" (Renkawitz et al. 2019). That this was not observed (as there was no significant difference in the odds of changing direction or path tortuosity between Group 1 and Group 2 cells) could be due to the type of data collected, which was single-cell and short term. It also did not track the behaviour of movement towards a wound specifically.

The LBR mutation experiment was conducted to verify the lamin b receptors role in increasing the roundness of the nucleus and examine any impacts on neutrophil plasticity it may have had (Schnipper et al. 2017, Manley et al. 2018). While a significant increase in nucleus eccentricity of LBR mutants was detected, there was no observed difference in the cell eccentricity between LBR mutants and LBR wildtype cells. This suggests that the nucleus is round because of the mutation itself, rather than being influenced by corresponding changes in the cell shape. The experimental results also corroborate previous findings that LBR mutants have impaired wound response functions, because there was both a decrease in cell velocity and the odds of the cell changing direction (Salvermoser et al. 2018, Davidson et al. 2014). This suggests that

cells do not move or exhibit directional persistence as they should in an injured tissue environment.

A noteworthy observation is that the LBR mutation resulted in decreased cell velocity, and is correlated with the nucleus shifting forward in the cell. As this is the opposite result seen in this project, where cell velocity increases as the nucleus shifts back, it supports the hypothesis that there is a relationship between cell velocity and the position of the nucleus in the cell.

Microtubule inhibition resulted in the largest changes to the neutrophil's morphology. However, these changes did not result in changes to the cell's movement, as no significant difference in cell velocity and the odds of changing direction between Group 3 cells and Group 7 cells was observed. The effects of microtubule inhibition on the neutrophil's morphology were much larger than in other experimental changes. Group 3 cells experienced a decrease in nucleus major axis length by almost $3 \mu M$ on average, while the second largest change is seen Group 10 cells with a mean decrease of only $1.2 \mu M$. Microtubule inhibition also resulted in the largest change in nucleus position, with a shift forward of almost 0.3 points compared with a shift of less than 0.1 in points in the other experiments. Lastly, microtubule inhibition resulted in nucleus eccentricity to increase in value by 0.186 points, while the other experiments only resulted in a change less than 0.087 points. This suggests a central role of the cytoskeleton microtubules in maintaining nucleus integrity, but does not corroborate their role in regulating cell mobility (Rich & Hoffstein 1980).

Group 10 cells, which experienced inhibition of the cytoskeletal element phosphokinase, saw changes in cell mobility in addition to morphological changes. Group 10 cells had a decreased velocity and decreased odds of changing direction. This differs from the project's previous results that a decreased velocity is linked with increased odds of changing direction. This implies that phosphokinase may have a role in regulating the cell's ability to migrate properly (Cain & Ridley 2009). Group 10 cells also saw the nucleus position shift forward, further supporting the finding that there may be a relationship between cell velocity and nucleus position.

6 Evaluation, Reflections and Conclusions

This project demonstrated the impact that data science analytical tools, such as cell tracking algorithms, image classifiers, and behaviour classifiers, can have on determining patterns in cell shape and movement. By defining specific behaviours quantitatively, and then classifying cells based on that definition, complicated behaviours can be defined and analysed in aggregate. This includes identifying the exact moment of nucleus elongation and moments of cell directional change, versus studying the length of the nucleus or the movement vector as absolute values. This creates new areas for analysis while also allowing for the re-purposing of data to study a range of biological phenomena without the need to run new biological experimental protocols. This project also outlined the scope for automating image labelling tasks using image classifiers to reduce the need for manual preprocessing of biological data, leaving more time for analysis. Lastly, this project demonstrated how studying cells at specific moments under different conditions allows for identification of cell behaviours not previously observed, such as a relationship between cell velocity and the position of the nucleus.

There were a few limitations to the methods used in this project. The first limitation was that the classification system used to identify nuclear elongation events could only detect the initial moment of nuclear elongation, not the persistence of the nucleus in that state. This is because the classification system is based on a percentage change of the nucleus major axis length between frames. If the nucleus maintains the longer length in the next frame, the classifier will not detect it because the percentage change will be 0. Future analysis of nuclear elongation should focus on creating a classifier that can identify the persistence of the nucleus in an elongated state. Analysis can then be conducted to see cell behaviour during the initial stages of nuclear elongation is consistent as the nucleus remains stretched. Another limitation of the analysis method was the use of the Tukey multi-comparison test instead of the Dunnett's

Multi-Comparison Test after the initial ANOVA analysis for comparing the experimental drug groups. Dunnett's Multi-Comparison Test only does pair-wise comparison of the groups to a specified control, while Tukey conducts all pair-wise comparisons. This reduces the power of the Tukey Multiple-Comparison Test and may make it more susceptible to false negatives, however as MATLAB does not implement Dunnett's, this test could not be implemented in the scope of this project.

Over the course of this project, I have learnt the importance of consistently engaging with research questions and objectives to ensure that work conducted is conducive and aligned towards the final objective. While divergence is needed to explore new techniques, too much divergence can lead to wasted effort and time delays. If this project were to be conducted again, more time would be given to validating and analysing errors behind the cell shape classifier, as this element of the project was added after the project planning phase as discussed in 1.3.1.

The contributions of this project to the field of immunology include the identification of a relationship between cell velocity and nucleus positioning. The project's findings corroborate existing literature surrounding the regulators of neutrophil nucleus morphology, and provide deeper insights through the demonstration that microtubules play a role in cell morphology but not cell mobility, whereas phosphokinase can modulate both behaviours.

These contributions show that data science research should not only be about improving analytical methods, but about applying them effectively to other research fields. This is because data science can automate tasks and discover hidden features of data. For the field of biology, this project shows the benefit of data science techniques in allowing for rapid hypothesis testing by generating new cell features and conducting broad analysis without the need for traditional wet-lab experiments. This shows the power of data science to improve the pace and quality of scientific research.

Bibliography

- Bay, H., Tuytelaars, T. & Van Gool, L. (2006), SURF: Speeded Up Robust Features, *in* A. Leonardis, H. Bischof & A. Pinz, eds, ‘Computer Vision – ECCV 2006’, Vol. 3951, Springer Berlin Heidelberg, Berlin, Heidelberg, pp. 404–417.
- Bosch, A., Zisserman, A. & Munoz, X. (2007), Image Classification using Random Forests and Ferns, *in* ‘2007 IEEE 11th International Conference on Computer Vision’, pp. 1–8.
- Breiman, L. (2001), ‘Random Forests’, *Machine Learning* **45**(1), 5–32.
- Cain, R. J. & Ridley, A. J. (2009), ‘Phosphoinositide 3-kinases in cell migration’, *Biology of the Cell* **101**(1), 13–29.
- Calero-Cuenca, F. J., Janota, C. S. & Gomes, E. R. (2018), ‘Dealing with the nucleus during cell migration’, *Current Opinion in Cell Biology* **50**, 35–41.
- Carvalho, L. O., Aquino, E. N., Neves, A. C. D. & Fontes, W. (2015), ‘The Neutrophil Nucleus and Its Role in Neutrophilic Function’, *Journal of Cellular Biochemistry* **116**(9), 1831–1836.
- Castro, M., Lythe, G., Molina-París, C. & Ribeiro, R. M. (2016), ‘Mathematics in modern immunology’, *Interface Focus* **6**(2).
- Csurka, G., Dance, C. R., Fan, L., Willamowski, J. & Bray, C. (n.d.), ‘Visual Categorization with Bags of Keypoints’, p. 16.
- Dalal, N. & Triggs, B. (2005), Histograms of Oriented Gradients for Human Detection, *in* ‘2005 IEEE Computer Society Conference on Computer Vision and Pattern Recognition (CVPR’05)’, Vol. 1, IEEE, San Diego, CA, USA, pp. 886–893.
- Dantone, M., Gall, J., Leistner, C. & Van Gool, L. (2013), Human Pose Estimation Using Body Parts Dependent Joint Regressors, *in* ‘2013 IEEE Conference on Computer Vision and Pattern Recognition’, IEEE, Portland, OR, USA, pp. 3041–3048.

- Danuser, G. (2011), 'Computer Vision in Cell Biology', *Cell* **147**(5), 973–978.
- Davidson, P. M., Denais, C., Bakshi, M. C. & Lammerding, J. (2014), 'Nuclear deformability constitutes a rate-limiting step during cell migration in 3-D environments', *Cellular and molecular bioengineering* **7**(3), 293–306.
- de Oliveira, S., Reyes-Aldasoro, C. C., Candel, S., Renshaw, S. A., Mulero, V. & Calado, Â. (2013), 'Cxcl8 (IL-8) Mediates Neutrophil Recruitment and Behavior in the Zebrafish Inflammatory Response', *The Journal of Immunology* **190**(8), 4349–4359.
- Dittmer, T. A. & Misteli, T. (2011), 'The lamin protein family', *Genome Biology* **12**(5), 222.
- Elks, P. M., van Eeden, F. J., Dixon, G., Wang, X., Reyes-Aldasoro, C. C., Ingham, P. W., Whyte, M. K. B., Walmsley, S. R. & Renshaw, S. A. (2011), 'Activation of hypoxia-inducible factor-1 (Hif-1) delays inflammation resolution by reducing neutrophil apoptosis and reverse migration in a zebrafish inflammation model', *Blood* **118**(3), 712–722.
- Fagerland, M. W. (2012), 'T-tests, non-parametric tests, and large studies—a paradox of statistical practice?', *BMC Medical Research Methodology* **12**, 78.
- Féletalou, M. (2011), *The Endothelium: Part 1: Multiple Functions of the Endothelial Cells—Focus on Endothelium-Derived Vasoactive Mediators*, Integrated Systems Physiology: From Molecule to Function to Disease, Morgan & Claypool Life Sciences, San Rafael (CA).
- Ford, C. (2017), 'The Wilcoxon Rank Sum Test', <https://data.library.virginia.edu/the-wilcoxon-rank-sum-test/>.
- Freeman, J. V. & Campbell, M. J. (n.d.), 'The Analysis of Categorical Data: Fisher's Exact Test', p. 2.
- Fruleux, A. & Hawkins, R. J. (2016), 'Physical role for the nucleus in cell migration', *Journal of Physics: Condensed Matter* **28**(36), 363002.
- Gaudreau, P.-O., Stagg, J., Soulières, D. & Saad, F. (2016), 'The Present and Future of Biomarkers in Prostate Cancer: Proteomics, Genomics, and Immunology Advancements: Supplementary Issue: Biomarkers and their Essential Role in the Development of Personalised Therapies (A)', *Biomarkers in Cancer* **8s2**, BIC.S31802.

- Hamilton, N. A., Pantelic, R. S., Hanson, K. & Teasdale, R. D. (2007), 'Fast automated cell phenotype image classification', *BMC Bioinformatics* **8**(1), 110.
- Henry, K. M., Pase, L., Ramos-Lopez, C. F., Lieschke, G. J., Renshaw, S. A. & Reyes-Aldasoro, C. C. (2013), 'PhagoSight: An Open-Source MATLAB Package for the Analysis of Fluorescent Neutrophil and Macrophage Migration in a Zebrafish Model', *PLOS ONE* **8**(8), 11.
- Hopsital, S. J. C. R. (2019), 'ANC and Neutropenia in Childhood Cancer', <https://together.stjude.org/en-us/diagnosis-treatment/side-effects/absolute-neutrophil-count-anc-neutropenia.html>.
- Iwahori, Y., Hattori, A., Adachi, Y., Bhuyan, M., Woodham, R. J. & Kasugai, K. (2015), 'Automatic Detection of Polyp Using Hessian Filter and HOG Features', *Procedia Computer Science* **60**, 730–739.
- Jevtić, P., Edens, L. J., Vuković, L. D. & Levy, D. L. (2014), 'Sizing and shaping the nucleus: Mechanisms and significance', *Current opinion in cell biology* **0**, 16–27.
- Kadirkamanathan, V., Anderson, S. R., Billings, S. A., Zhang, X. L., Holmes, G. R., Reyes Aldasoro, C. C., Elks, P. M. & Renshaw, S. A. (2012), 'The neutrophil's eye-view: Inference and visualisation of the chemoattractant field driving cell chemotaxis in vivo'.
- Kan, A. (2017), 'Machine learning applications in cell image analysis', *Immunology & Cell Biology* **95**(6), 525–530.
- Kangwon, L. (2010), 'Plot With Direction 3D - File Exchange - MATLAB Central', <https://www.mathworks.com/matlabcentral/fileexchange/29307>.
- Ko, B. C., Kim, S. H. & Nam, J.-Y. (2011), 'X-ray Image Classification Using Random Forests with Local Wavelet-Based CS-Local Binary Patterns', *Journal of Digital Imaging* **24**(6), 1141–1151.
- Kusumoto, D. & Yuasa, S. (2019), 'The application of convolutional neural network to stem cell biology', *Inflammation and Regeneration* **39**(1), 14.
- Lee, S. & Lee, D. K. (2018), 'What is the proper way to apply the multiple comparison test?', *Korean Journal of Anesthesiology* **71**(5), 353–360.

- Liepe, J., Taylor, H., Barnes, C. P., Huvet, M., Bugeon, L., Thorne, T., Lamb, J. R., Dallman, M. J. & Stumpf, M. P. H. (2012), 'Calibrating spatio-temporal models of leukocyte dynamics against in vivo live-imaging data using approximate Bayesian computation', *Integrative biology : quantitative biosciences from nano to macro* **4**(3), 335–345.
- Lin, L., Wang, W. & Chen, B. (2019), 'Leukocyte recognition with convolutional neural network', *Journal of Algorithms & Computational Technology* **13**, 174830181881332.
- Manley, H. R., Keightley, M. C. & Lieschke, G. J. (2018), 'The Neutrophil Nucleus: An Important Influence on Neutrophil Migration and Function', *Frontiers in Immunology* **9**.
- Marée, R., Geurts, P. & Wehenkel, L. (2007), 'Random subwindows and extremely randomized trees for image classification in cell biology', *BMC Cell Biology* **8**(S1), S2.
- Mathias, J. R., Perrin, B. J., Liu, T.-X., Kanki, J., Look, A. T. & Huttenlocher, A. (2006), 'Resolution of inflammation by retrograde chemotaxis of neutrophils in transgenic zebrafish', *Journal of Leukocyte Biology* **80**(6), 1281–1288.
- MathWorks, I. (n.d.), 'Measure properties of image regions - MATLAB regionprops', <https://www.mathworks.com/help/images/ref/regionprops.html>.
- McDonald, J. (2014a), *Handbook of Biological Statistics: Basic Concepts of Hypothesis Testing*, 3 edn, Sparky House Publishing, Baltimore, Maryland.
- McDonald, J. (2014b), *Handbook of Biological Statistics: Confidence Limits*, 3 edn, Sparky House Publishing, Baltimore, Maryland.
- McDonald, J. (2014c), *Handbook of Biological Statistics: Fisher's Exact Test of Independence*, 3 edn, Sparky House Publishing, Baltimore, Maryland.
- McDonald, J. (2014d), *Handbook of Biological Statistics: One-Way ANOVA*, 3 edn, Sparky House Publishing, Baltimore, Maryland.
- McDonald, J. (2014e), *Handbook of Biological Statistics: Student's t-Test for Two Samples*, 3 edn, Sparky House Publishing, Baltimore, Maryland.
- Moreau, H. D., Piel, M., Voituriez, R. & Lennon-Duménil, A.-M. (2018), 'Integrating Physical and Molecular Insights on Immune Cell Migration', *Trends in Immunology* **39**(8), 632–643.

- Nishimoto, S., Tokuoka, Y., Yamada, T. G., Hiroi, N. F. & Funahashi, A. (2018), Predicting the future direction of cell movement with convolutional neural networks, Preprint, Systems Biology.
- Putzu, L., Caocci, G. & Di Ruberto, C. (2014), 'Leucocyte classification for leukaemia detection using image processing techniques', *Artificial Intelligence in Medicine* **62**(3), 179–191.
- Qian, Y., Corum, L., Meng, Q., Blenis, J., Zheng, J. Z., Shi, X., Flynn, D. C. & Jiang, B.-H. (2004), 'PI3K induced actin filament remodeling through Akt and p70S6K1: Implication of essential role in cell migration', *American Journal of Physiology. Cell Physiology* **286**(1), C153–163.
- Rawat, W. & Wang, Z. (2017), 'Deep Convolutional Neural Networks for Image Classification: A Comprehensive Review', *Neural Computation* **29**(9), 2352–2449.
- Renkawitz, J., Kopf, A., Stopp, J., de Vries, I., Driscoll, M. K., Merrin, J., Hauschild, R., Welf, E. S., Danuser, G., Fiolka, R. & Sixt, M. (2019), 'Nuclear positioning facilitates amoeboid migration along the path of least resistance', *Nature* **568**(7753), 546.
- Reyes-Aldasoro, C. C., Zhao, Y., Coca, D., Billings, S. A., Kadirkamanathan, V., Tozer, G. M. & Renshaw, S. A. (2009), Analysis of immune cell function using in vivo cell shape analysis and tracking, in '4th IAPR International Conference on Pattern Recognition in Bioinformatics'.
- Rich, A. M. & Hoffstein, S. T. (1980), 'Inverse Correlation Between Neutrophil Microtubule Numbers and Enhanced Random Migration', (48), 181–191.
- Ritter, M., Schratzberger, P., Rossmann, H., Wöll, E., Seiler, K., Seidler, U., Reinisch, N., Kähler, C. M., Zwierzina, H., Lang, H. J., Lang, F., Paulmichl, M. & Wiedermann, C. J. (1998), 'Effect of inhibitors of Na⁺/H⁺-exchange and gastric H⁺/K⁺ ATPase on cell volume, intracellular pH and migration of human polymorphonuclear leucocytes', *British Journal of Pharmacology* **124**(4), 627–638.
- Rosales, C. (2018), 'Neutrophil: A Cell with Many Roles in Inflammation or Several Cell Types?', *Frontiers in Physiology* **9**.
- Rosebrock, A. (2015), 'OpenCV Track Object Movement'.
- Salvermoser, M., Begandt, D., Alon, R. & Walzog, B. (2018), 'Nuclear Deformation During Neutrophil Migration at Sites of Inflammation', *Frontiers in Immunology* **9**.

- Schnipper, N., Stassen, H. H., Kallinich, T., Sperling, K. & Hoffmann, K. (2017), 'Image analysis of neutrophil nuclear morphology: Learning about phenotypic range and its reliable analysis from patients with pelger-Huët-anomaly and treated with colchicine', *Cytometry Part B: Clinical Cytometry* **92**(6), 541–549.
- Shifat-E-Rabbi, M., Yin, X., Fitzgerald, C. E. & Rohde, G. K. (2019), 'Cell image classification: A comparative overview', *arXiv:1906.03316 [q-bio]*.
- Solís-Lemus, J. A., Stramer, B., Slabaugh, G. & Reyes-Aldasoro, C. C. (2018), Analysis of the Interactions of Migrating Macrophages, in M. Nixon, S. Mahmoodi & R. Zwiggelaar, eds, 'Medical Image Understanding and Analysis', Vol. 894, Springer International Publishing, Cham, pp. 262–273.
- Szumilas, M. (2010), 'Explaining Odds Ratios', *Journal of the Canadian Academy of Child and Adolescent Psychiatry* **19**(3), 227–229.
- The MathWorks, I. (n.d.), 'Fisher's exact test - MATLAB fishertest', <https://www.mathworks.com/help/stats/fishertest.html>.
- Thomas, R. M. & John, J. (2017), A review on cell detection and segmentation in microscopic images, in '2017 International Conference on Circuit ,Power and Computing Technologies (ICCPCT)', pp. 1–5.
- Tranquillo, R. T., Lauffenburger, D. A. & Zigmond, S. H. (1988), 'A stochastic model for leukocyte random motility and chemotaxis based on receptor binding fluctuations', *The Journal of Cell Biology* **106**(2), 303–309.
- Yanakieva, I., Erzberger, A., Matejčić, M., Modes, C. D. & Norden, C. (2019), 'Cell and tissue morphology determine actin-dependent nuclear migration mechanisms in neuroepithelia', *bioRxiv* p. 536698.
- Zhang, H., Yu, C.-Y. & Singer, B. (2003), 'Cell and tumor classification using gene expression data: Construction of forests', *Proceedings of the National Academy of Sciences* **100**(7), 4168–4172.

A RMPI Project Proposal

Determining patterns in immune cell shape and movement using biological models and tracking algorithms

Lara Chammas

1. Introduction

Immunology is the study of the immune system to understand its physiological function in both healthy and diseased states. It covers all aspects of the immune system, from physical barriers such as the skin to bacterial killer cells such as neutrophils, with the end goal of developing a complete model of how each part works in different conditions. Immunology has applications in the treatment of cancer, autoimmune disease, and bacterial infections and the creation of vaccines. Developing an accurate understanding of immune cell functions and interactions is paramount to advancing medical treatments.

Immunological experiments include capillary (Lewus and Ford, 2001) and video microscopy assays (Sheng *et al.*, 2009), where either the cells' genetic code or their environment is changed. Comparison of the experimental groups to a control group using statistical hypothesis testing and correlation analysis shows the significance extent of the change's impact. This analysis is then assessed in the context of known immunological research, allowing for a model to be generated (Castro *et al.*, 2016).

With advances in image processing, video microscopy is becoming a preferred way to study immune cells as it allows for in-vitro, within organism, analysis. This involves conducting segmentation and then tracking of individual immune cells from images and videos generated through microscopy (Henry *et al.*, 2013; Thomas and John, 2017). There can be hundreds of cells to track just within one image, and a time lapse leads to many images being generated. Having an automated way to process these images and then analyze them for biological patterns is paramount to making biology a more quantitative science versus using human eye processing to see changes in cells.

This project aims to address this quantitative gap and advance the integration of modeling into immunological research by answering the question **to what extent can outputs of cell tracking algorithms be used to determine patterns in immune cell shape and movement?** The project will build upon current understanding of different movement patterns immune cells exhibit and the shape of the cells during these movements (Reyes-Aldasoro *et al.*, 2009; Holmes *et al.*, 2012). It will also integrate mathematical models and coefficients created to quantify these behaviors (Mathias *et al.*, 2006; Codling Edward A, Plank Michael J and Benhamou Simon, 2008; Holmes *et al.*, 2012).

1.1 Aims and Objectives

The main aim of this project is to analyze the behavior of immune cells observed within zebrafish using fluorescent microscopy and determine any patterns in cell shape and movement seen under different conditions. To meet this aim, the objects are:

- Generate metrics that reflect biological characteristics of the cells including shape and movement
- Analyze the cell's behavior overtime using these metrics and determine if there are patterns unique to each condition group

- Investigate if there is a statistical difference between the different condition groups' results
- If there is significance, quantify the effect of each condition on the metrics of interest

Beneficiaries: The main beneficiaries are immunologists and other biological researchers as understanding how a cell is moving, automatically and quantitatively, will help researchers to understand the underlying effects of their experiments. The knock-off effect is that it will help patients as a greater understanding of how the immune system works will improve treatments. Lastly, this will help others in the field of cell image processing as it will show the potential to relate image processing to biological function.

2. Critical Context

2.1 Immunology and Data Science

The foundation of most immunological understanding are in-vitro studies, which are conducted outside of the cell's natural environment, such as a test tube cell analysis. The cells are placed under different conditions (genetic and environmental) and then various techniques, such as microscopy and assays, are used to compare the cells and infer biological understanding. Due to many advances in technology, immunological research can now be done in-vivo, or within an organism, using zebrafish. This is because zebrafish larvae are transparent, allowing to directly see structures deep within the fish. They are also easy to genetically alter, allowing for fluorescent labeling of their immune cells, which are homologs of mammalian immune cells. This makes it easy to track different cells and allows for their direct imaging using microscopy techniques (Reyes-Aldasoro *et al.*, 2009; Liepe *et al.*, 2012).

Data science is applied to the analysis of microscopy images and videos through image processing, which involves cell segmentation and tracking. After tracking, statistics and metrics of the cell's movement, shape and interactions in zebrafish can be generated. Segmentation and tracking methods can be broadly classified as “model-based, feature-based and learning-based” (Thomas and John, 2017). An example of a feature-based method is Fiole *et al.* (2012), who used the feature “roundness”, determined by edge detection, to track dendritic cells (DC). This was an advancement as DCs cannot be discriminated based on fluorescent tags from other immune cells but can be by shape they do not have the same characteristic “round” shape. This highlights the importance of including biological knowledge into modelling and analysis methodologies to improve accuracy and leverage their effectiveness.

Most work in microscopy image and video analysis has gone to improving tracking and segmentation algorithms by making them adaptable to situations such as cells touching and cells moving out of the field of the camera (Thomas and John, 2017; Solís-Lemus *et al.*, 2018). More work, however, needs to be done on how these algorithms can be used to understand the biological processes underpinning the cells and automate these findings (Kadirkamanathan *et al.*, 2012). This includes moving beyond the generation of measurements such as velocity and cell count to include measurements such as directionality persistence and shape type. From these metrics and their analysis, including differences between groups, biological function and pathology can be deduced.

An example of a cell tracking algorithm that is working to understand biological processes is Solís-Lemus et al.'s (2018). Their algorithm worked on studying macrophage migration patterns as an effect of inter-cell interactions. However, while it shows that there is a change in direction, we do not know if this change is intentional, or simply due to the effect of bumping. This could be determined by figuring out if the path is stochastic before and after the interaction or just before. Therefore, more work needs to be done to fully describe the biological processes occurring.

2.2 Biostatistics and Modeling

Biostatistics and mathematical biology are rapidly growing fields born from the integration of mathematics and data science into analysis of wet biological laboratory results (Liepe *et al.*, 2012; Castro *et al.*, 2016). One area which has advanced with mathematical modeling is cell movement analysis. Chemotaxis, the movement towards a chemical, is the most well-defined patterns, as many cells from bacteria to immune cells exhibit it. There are a few other well defined movement patterns including retrograde chemotaxis and random motility (Tranquillo, Lauffenburger and Zigmond, 1988; Mathias *et al.*, 2006; Sheng *et al.*, 2009; James and Vauchelet, 2013) Research in the past has used various techniques to model these movements, including partial derivatives, stochastic methods, fractional order signal processing, and Bayesian computation (Tranquillo, Lauffenburger and Zigmond, 1988; Sheng *et al.*, 2009; Liepe *et al.*, 2012). One of the most commonly used model for chemotaxis is the Keller-Segel model, which models movement as a function of cell density variation and chemical attractant concentration over time (Kadirkamanathan *et al.*, 2012). Most of these models however are developed by mathematicians or physicists and can be hard for many biologists to use in-practice when analyzing their data.

2.3 Inferring function from quantitative metrics

Quantitative metrics of cells generated by image processing include volume, area, number of branches of the skeleton, velocity of movement, distance moved, and angle of movement. Research has shown that from these measurements, the function of cells can be inferred. Mathias et al. (2006) discussed that there is evidence for neutrophils to develop rounded morphologies with reduced pseudopod extensions once they reach a wound site. Using metrics that determine how round the cell is and if there are any arm-like extensions can be used to see if the cell has reached its destination such as a wound site or a site of inflammation. These findings match observations that neutrophils reduce their pseudopod extensions once reaching the wound but will keep them during migration. They have also been found to maintain the extensions in high gradient concentrations of chemoattractant and reduce their number in areas of low gradient concentrations of chemoattractant (Liepe *et al.*, 2012). The rounded morphology could be due to an increase in cell volume, found by Henry et al. (2013) and Ritter et al. (Ritter *et al.*, 1998). These are all examples of how quantitative metrics about the cell's morphology and movement can easily relate to function and pathology of disease progression.

3. Approaches

This project will fill the gaps presented in Section 2 by developing metrics and models that infer biological function from quantitative measurements and can be used and analyzed by biologists directly. This project will work to build upon and expand the ideas in Solís-Lemus et al. (2018), which worked to analyze how interactions between cells affect their

movement and will use, as well as expand upon, its shape parameters. This will be done within the software package Phagosight, developed by Henry et al. (2013), which also looked into the relationship between cell changes and movement and found that cell volume increases as the cell moves towards a wounded area.

3.1 Data and preprocessing

The data used in this project are videos from fluorescent microscopy of GFP-labelled neutrophils in zebrafish. This data has been generated by biologists in a lab and the resulting fluorescent microscopy videos have already undergone pre-processing by Dr. Constantino Carlos Reyes-Aldasoro from City, University. The initial processing includes the segmentation and tracking of individual cells and their nuclei. Once the tracks were generated, each cell and its corresponding nucleus are analyzed, and their metrics are recorded. Currently 29 metrics have been generated for each time frame for both the cell and the nucleus for each of the 11 experimental groups and 1 control group. As the cells are not from specific human populations and the data collection does not involve human participants, there are no ethical obligations to consider around the data collection or analysis.

3.2 Metrics

The 29 initial metrics are: area, Centroid, bounding box, major axis length, minor axis length, eccentricity, orientation, extrema, new area, old area, distance, angle, extent, number branches, number of end points, average tortuosity, touch border, rows, columns, number slices, forkness, skeleton alignment, skeleton perimeter, ratio skeletons, and then the re-scaled measurements for distance (um_s), area (um_2), major axis length (um), minor axis length (um), and minimum major axis length.

I will try to extend these initial metrics by generating new statistics around the type of shape the cell is exhibiting. This will include how round the cell is and how the number of skeleton branches is changing within each time frame. These metrics will be created because an increase in a rounded morphology and reduction in pseudopod extensions have been shown to be linked to arrival of a neutrophil at a wound site (Mathias *et al.*, 2006). Further metrics on describing the cell's movement will also be generated, as further discussed in Section 3.4.

3.3 Analysis

First, I will analyze these initial metrics through simple descriptive and summary statistics to compare the groups and gain an understanding of the differences between them. This will be done without knowing what the biological and experimental differences are between them, so as to not bias the analysis or result in “confirmation bias”.

Then, using statistical hypothesis testing methods such as t-tests and Anova, I will compare the control group to each experimental group, and then all other combinations that make biological sense, to determine if there are statistical differences between the different groups. If there is a correlation between two groups, linear regression may be employed to understand the function and degree of correlation. The combination of these analysis tools alongside our current biological understanding, will help to create models of how changes

in genetics or environment result in differences in the function, shape, or movement of the neutrophils.

3.4 Movement modeling

To generate an estimate of what movement pattern the cell is exhibiting, I will focus on two main movement patterns: chemotaxis and random motility. Using the methods from Liepe et al. (2012) and Mathias et al. (2006) different metrics and equations will be generated which will indicate which type of movement is occurring. The equations used from Liepe et al. (2012) allow the application or “calibration” of the typical mathematical models of leukocyte movement to trajectories observed from live imaging data.

The statistics from Mathias et al. (2006) that will be used are velocity, persistence, and directionality index. Directionality index (D/T) is calculated as the division of the shortest linear distance between the start and end point of the cell’s path (D) by the total distance traveled by the cell (T). To determine if chemotaxis or random motility is occurring, each of these parameters and coefficients of the equations will need to be monitored for their changes over time. An increase in persistence, velocity, and directionality index indicates directional migration, or chemotaxis, and thus a loss of random motility.

3.5 Visualization and Evaluation

Another element of this work will be to generate insightful plots which can be interpreted by biologists to determine significance and help aid in relation of the metrics to biological function. They will include boxplots, line graphs, histograms, trajectory graphs and 3D volume analysis.

Evaluation of biological research and modeling is not as straight forward as calculating an accuracy. Verification of biological research is typically done through repeat experiments and peer-review. Cell segmentation and tracking algorithms are validated either through comparison to ground-truth samples or they are manually verified by an expert. For this project, evaluation will be done through collaboration with the biologist in the team to see if the results of the metrics and movement models correspond and fit into current biological understanding. If possible, I could explore trying to find data from an in-vitro experiment where there is confirmed chemotaxis or random motility and analyze the data using my experimental methodology to see if the results are consistent.

4. Workplan

5. Risks

| Risk | Likelihood (1-3) | Impact (1-5) | Risk Impact (LxC) | Mitigation |
|--|---------------------|-----------------|----------------------|--|
| Too much data to process | 3 | 4 | 12 | Determine early-on a feasible amount of data to analysis and conduct a subsampling process to ensure this number |
| Movement models selected do not work with the data | 2 | 5 | 10 | Determine many different models that can be used to increase likelihood that one works |
| Computer is lost/stolen or crashes | 2 | 5 | 10 | Back up hourly and automatically data and results to the City University OneDrive |
| In-sufficient time to complete all planned steps | 2 | 5 | 10 | Add 10% time to each stage to ensure plenty of time to complete project |

References:

- Castro, M. *et al.* (2016) ‘Mathematics in modern immunology’, *Interface Focus*, 6(2). doi: 10.1098/rsfs.2015.0093.
- Codling Edward A, Plank Michael J and Benhamou Simon (2008) ‘Random walk models in biology’, *Journal of The Royal Society Interface*, 5(25), pp. 813–834. doi: 10.1098/rsif.2008.0014.
- Fiole, D. *et al.* (2012) ‘Shape-Based Tracking Allows Functional Discrimination of Two Immune Cell Subsets Expressing the Same Fluorescent Tag in Mouse Lung Explant’, *PLoS ONE*, 7(6). doi: 10.1371/journal.pone.0039831.
- Henry, K. M. *et al.* (2013) ‘PhagoSight: An Open-Source MATLAB Package for the Analysis of Fluorescent Neutrophil and Macrophage Migration in a Zebrafish Model’, *PLOS ONE*, 8(8), p. 11.
- Holmes, G. R. *et al.* (2012) ‘Repelled from the wound, or randomly dispersed? Reverse migration behaviour of neutrophils characterized by dynamic modelling’, *Journal of The Royal Society Interface*, 9(77), pp. 3229–3239. doi: 10.1098/rsif.2012.0542.
- James, F. and Vauchelet, N. (2013) ‘Chemotaxis: from kinetic equations to aggregate dynamics’, *Nonlinear Differential Equations and Applications NoDEA*, 20(1), pp. 101–127. doi: 10.1007/s00030-012-0155-4.
- Kadirkamanathan, V. *et al.* (2012) ‘The neutrophil’s eye-view: inference and visualisation of the chemoattractant field driving cell chemotaxis in vivo’. Available at: <https://core.ac.uk/reader/9551796> (Accessed: 17 April 2019).
- Lewus, P. and Ford, R. M. (2001) ‘Quantification of random motility and chemotaxis bacterial transport coefficients using individual-cell and population-scale assays’, *Biotechnology and Bioengineering*, 75(3), pp. 292–304. doi: 10.1002/bit.10021.
- Liepe, J. *et al.* (2012) ‘Calibrating spatio-temporal models of leukocyte dynamics against in vivo live-imaging data using approximate Bayesian computation’, *Integrative biology : quantitative biosciences from nano to macro*, 4(3), pp. 335–345. doi: 10.1039/c2ib00175f.
- Mathias, J. R. *et al.* (2006) ‘Resolution of inflammation by retrograde chemotaxis of neutrophils in transgenic zebrafish’, *Journal of Leukocyte Biology*, 80(6), pp. 1281–1288. doi: 10.1189/jlb.0506346.
- Reyes-Aldasoro, C. C. *et al.* (2009) ‘Analysis of immune cell function using in vivo cell shape analysis and tracking’. *4th IAPR International Conference on Pattern Recognition in Bioinformatics*, Sheffield, UK. Available at: <http://ml.dcs.shef.ac.uk/prib2009/> (Accessed: 13 April 2019).
- Ritter, M. *et al.* (1998) ‘Effect of inhibitors of Na+/H+-exchange and gastric H+/K+ ATPase on cell volume, intracellular pH and migration of human polymorphonuclear leucocytes’, *British Journal of Pharmacology*, 124(4), pp. 627–638. doi: 10.1038/sj.bjp.0701864.
- Sheng, H. *et al.* (2009) ‘A Fractional Order Signal Processing (FOSP) Technique for Chemotaxis Quantification Using Video Microscopy’, pp. 1293–1299. doi: 10.1115/DETC2009-87472.
- Solís-Lemus, J. A. *et al.* (2018) ‘Analysis of the Interactions of Migrating Macrophages’, in Nixon, M., Mahmoodi, S., and Zwiggelaar, R. (eds) *Medical Image Understanding and Analysis*. Cham: Springer International Publishing, pp. 262–273. doi: 10.1007/978-3-319-95921-4_25.
- Thomas, R. M. and John, J. (2017) ‘A review on cell detection and segmentation in microscopic images’, in *2017 International Conference on Circuit ,Power and Computing Technologies (ICCPCT)*. *2017 International Conference on Circuit ,Power and Computing Technologies (ICCPCT)*, pp. 1–5. doi: 10.1109/ICCPCT.2017.8074189.
- Tranquillo, R. T., Lauffenburger, D. A. and Zigmond, S. H. (1988) ‘A stochastic model for leukocyte random motility and chemotaxis based on receptor binding fluctuations’, *The Journal of Cell Biology*, 106(2), pp. 303–309. doi: 10.1083/jcb.106.2.303.

Research Ethics Review Form: BSc, MSc and MA Projects

Computer Science Research Ethics Committee (CSREC)

Undergraduate and postgraduate students undertaking their final project in the Department of Computer Science are required to consider the ethics of their project work and to ensure that it complies with research ethics guidelines. In some cases, a project will need approval from an ethics committee before it can proceed. Usually, but not always, this will be because the student is involving other people ("participants") in the project.

In order to ensure that appropriate consideration is given to ethical issues, all students must complete this form and attach it to their project proposal document. There are two parts:

PART A: Ethics Checklist. All students must complete this part. The checklist identifies whether the project requires ethical approval and, if so, where to apply for approval.

| A.1 If you answer YES to any of the questions in this block, you must apply to an appropriate external ethics committee for approval and log this approval as an External Application through Research Ethics Online - https://ethics.city.ac.uk/ | | <i>Delete as appropriate</i> |
|---|--|------------------------------|
| 1.1 | Does your research require approval from the National Research Ethics Service (NRES)? <i>e.g. because you are recruiting current NHS patients or staff?</i> <i>If you are unsure try - https://www.hra.nhs.uk/approvals-amendments/what-approvals-do-i-need/</i> | NO |
| 1.2 | Will you recruit participants who fall under the auspices of the Mental Capacity Act? <i>Such research needs to be approved by an external ethics committee such as NRES or the Social Care Research Ethics Committee - http://www.scie.org.uk/research/ethics-committee/</i> | NO |
| 1.3 | Will you recruit any participants who are currently under the auspices of the Criminal Justice System, for example, but not limited to, people on remand, prisoners and those on probation? <i>Such research needs to be authorised by the ethics approval system of the National Offender Management Service.</i> | NO |
| A.2 If you answer YES to any of the questions in this block, then unless you are applying to an external ethics committee, you must apply for approval from the Senate Research Ethics Committee (SREC) through Research Ethics Online - https://ethics.city.ac.uk/ | | <i>Delete as appropriate</i> |
| 2.1 | Does your research involve participants who are unable to give informed consent? <i>For example, but not limited to, people who may have a degree of learning disability or mental health problem, that means they are unable to make an informed decision on their own behalf.</i> | NO |
| 2.2 | Is there a risk that your research might lead to disclosures from participants concerning their involvement in illegal activities? | NO |
| 2.3 | Is there a risk that obscene and or illegal material may need to be accessed for your research study (including online content and other material)? | NO |
| 2.4 | Does your project involve participants disclosing information about special category or sensitive subjects? <i>For example, but not limited to: racial or ethnic origin; political opinions; religious beliefs; trade union membership; physical or mental health; sexual life; criminal offences and proceedings</i> | NO |

| | | |
|---|--|------------------------------|
| 2.5 | Does your research involve you travelling to another country outside of the UK, where the Foreign & Commonwealth Office has issued a travel warning that affects the area in which you will study? <i>Please check the latest guidance from the FCO - http://www.fco.gov.uk/en/</i> | NO |
| 2.6 | Does your research involve invasive or intrusive procedures? <i>These may include, but are not limited to, electrical stimulation, heat, cold or bruising.</i> | NO |
| 2.7 | Does your research involve animals? | NO |
| 2.8 | Does your research involve the administration of drugs, placebos or other substances to study participants? | NO |
| A.3 If you answer YES to any of the questions in this block, then unless you are applying to an external ethics committee or the SREC, you must apply for approval from the Computer Science Research Ethics Committee (CSREC) through Research Ethics Online - https://ethics.city.ac.uk/ Depending on the level of risk associated with your application, it may be referred to the Senate Research Ethics Committee. | | <i>Delete as appropriate</i> |
| 3.1 | Does your research involve participants who are under the age of 18? | NO |
| 3.2 | Does your research involve adults who are vulnerable because of their social, psychological or medical circumstances (vulnerable adults)? <i>This includes adults with cognitive and / or learning disabilities, adults with physical disabilities and older people.</i> | NO |
| 3.3 | Are participants recruited because they are staff or students of City, University of London? <i>For example, students studying on a particular course or module. If yes, then approval is also required from the Head of Department or Programme Director.</i> | NO |
| 3.4 | Does your research involve intentional deception of participants? | NO |
| 3.5 | Does your research involve participants taking part without their informed consent? | NO |
| 3.5 | Is the risk posed to participants greater than that in normal working life? | NO |
| 3.7 | Is the risk posed to you, the researcher(s), greater than that in normal working life? | NO |
| A.4 If you answer YES to the following question and your answers to all other questions in sections A1, A2 and A3 are NO, then your project is deemed to be of MINIMAL RISK. If this is the case, then you can apply for approval through your supervisor under PROPORTIONATE REVIEW. You do so by completing PART B of this form. If you have answered NO to all questions on this form, then your project does not require ethical approval. You should submit and retain this form as evidence of this. | | <i>Delete as appropriate</i> |
| 4 | Does your project involve human participants or their identifiable personal data? <i>For example, as interviewees, respondents to a survey or participants in testing.</i> | NO |

B Model Training Figures

B.1 Out of the bag classification error plots

Below are line plots showing the out of the bag classification error over the number of trees grown in the random forest, calculated during hyperparameter model training.

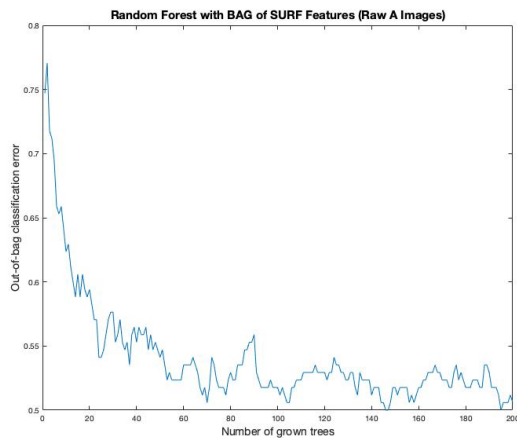


FIGURE B.1: Random forest with bag of SURF features classification error for different numbers of trees in the forest, training on the Raw A data set.

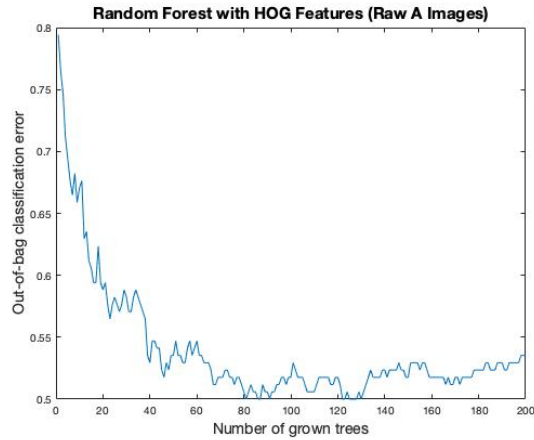


FIGURE B.2: Random forest with histogram of gradient features classification error for different numbers of trees in the forest, training on the Raw A data set.

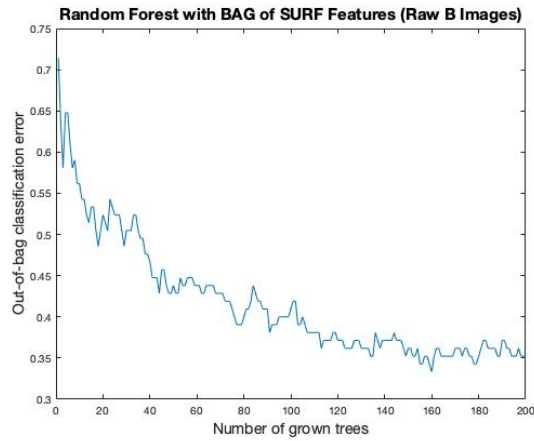


FIGURE B.3: Random forest with bag of SURF features classification error for different numbers of trees in the forest, training on the Raw B data set.

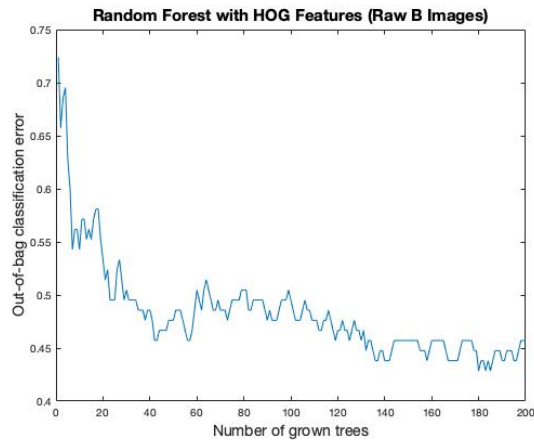


FIGURE B.4: Random forest with histogram of gradient features classification error for different numbers of trees in the forest, training on the Raw B data set.

B.2 Confusion matrices

The confusion matrices of they hyperparameter tuned model on the unseen testing data set.

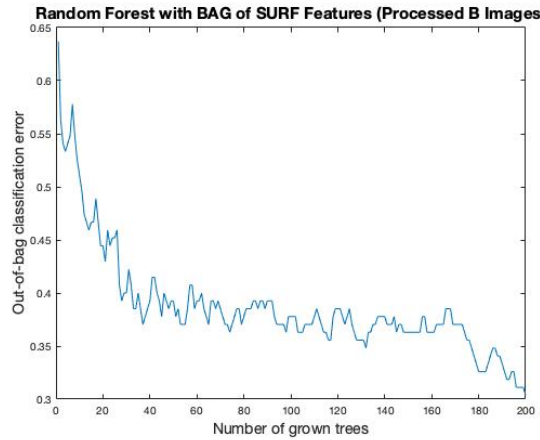


FIGURE B.5: Random forest with bag of SURF features classification error for different numbers of trees in the forest, training on the Processed B data set.

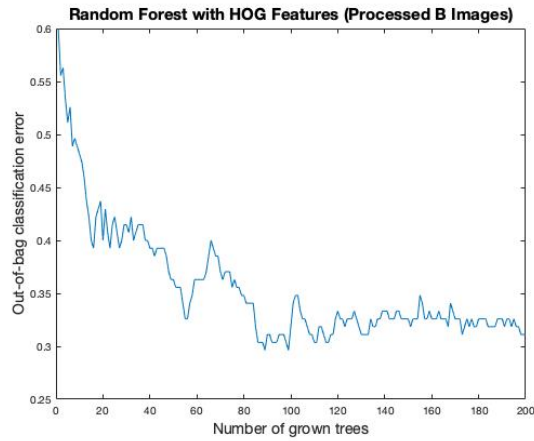


FIGURE B.6: Random forest with histogram of gradient features classification error for different numbers of trees in the forest, training on the Processed B data set.



FIGURE B.7: Random forest with bag of SURF features classification predictions on the testing Raw A data set.

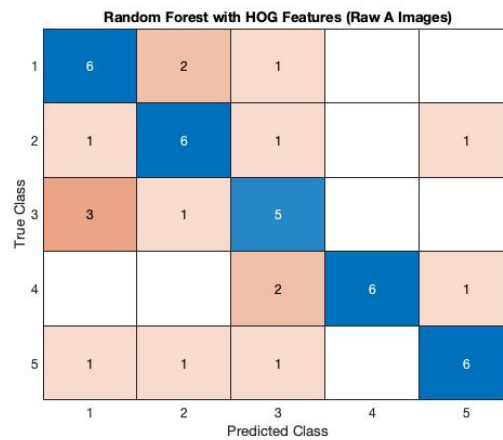


FIGURE B.8: Random forest with HoG features classification predictions on the testing Raw A data set.

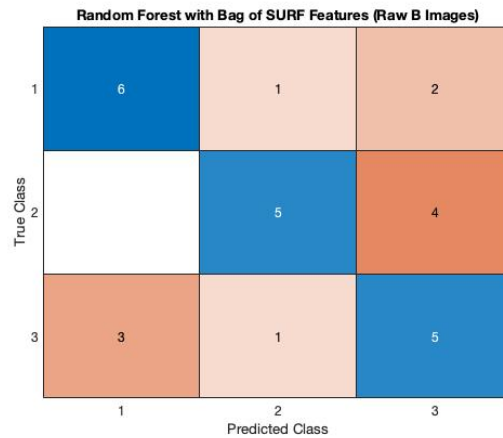


FIGURE B.9: Random forest with bag of SURF features classification predictions on the testing Raw B data set.

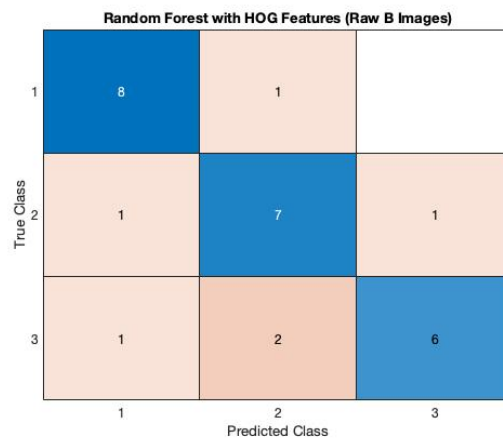


FIGURE B.10: Random forest with HoG features classification predictions on the testing Raw B data set.

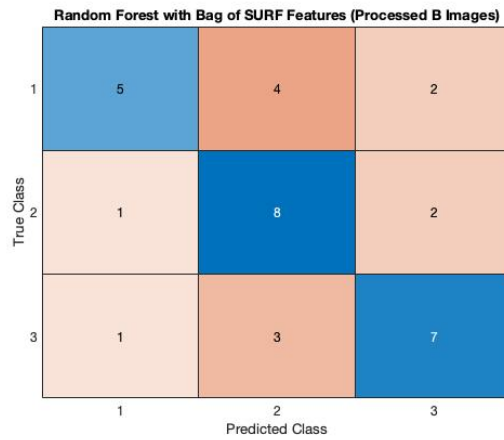


FIGURE B.11: Random forest with bag of SURF features classification predictions on the testing Processed B data set.

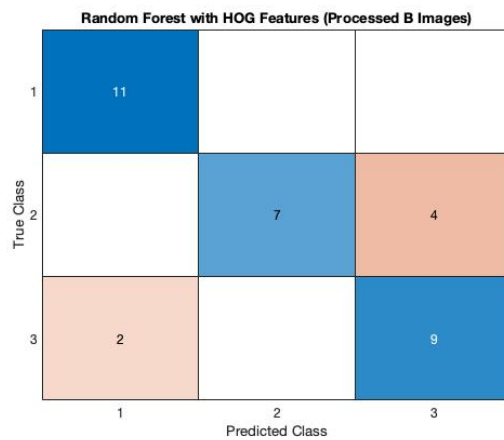


FIGURE B.12: Random forest with HoG features classification predictions on the testing Processed B data set.

C Image Classifier Hyperparameter Tuning Results

| Random Forest Bag Raw A Images | | | |
|--------------------------------|----------------------|----------------------|------------------------------------|
| Number Trees | Number Obs on Leaves | Out of the Bag Error | Out of the Bag Prediction Accuracy |
| 1.00 | 1.00 | 0.82 | 18.24 |
| 1.00 | 2.00 | 0.76 | 23.53 |
| 1.00 | 3.00 | 0.75 | 24.71 |
| 1.00 | 4.00 | 0.76 | 24.12 |
| 1.00 | 5.00 | 0.74 | 25.88 |
| 1.00 | 6.00 | 0.72 | 27.65 |
| 1.00 | 7.00 | 0.72 | 27.65 |
| 1.00 | 8.00 | 0.77 | 22.94 |
| 1.00 | 9.00 | 0.75 | 25.29 |
| 1.00 | 10.00 | 0.78 | 22.35 |
| 20.00 | 1.00 | 0.54 | 45.88 |
| 20.00 | 2.00 | 0.61 | 39.41 |
| 20.00 | 3.00 | 0.60 | 40.00 |
| 20.00 | 4.00 | 0.58 | 42.35 |
| 20.00 | 5.00 | 0.58 | 42.35 |
| 20.00 | 6.00 | 0.59 | 41.18 |
| 20.00 | 7.00 | 0.59 | 41.18 |
| 20.00 | 8.00 | 0.61 | 39.41 |
| 20.00 | 9.00 | 0.55 | 44.71 |
| 20.00 | 10.00 | 0.63 | 37.06 |
| 40.00 | 1.00 | 0.54 | 45.88 |
| 40.00 | 2.00 | 0.48 | 52.35 |
| 40.00 | 3.00 | 0.46 | 53.53 |
| 40.00 | 4.00 | 0.48 | 51.76 |
| 40.00 | 5.00 | 0.52 | 47.65 |
| 40.00 | 6.00 | 0.54 | 46.47 |
| 40.00 | 7.00 | 0.58 | 41.76 |
| 40.00 | 8.00 | 0.52 | 47.65 |
| 40.00 | 9.00 | 0.60 | 40.00 |
| 40.00 | 10.00 | 0.56 | 43.53 |
| 60.00 | 1.00 | 0.55 | 45.29 |
| 60.00 | 2.00 | 0.53 | 47.06 |
| 60.00 | 3.00 | 0.49 | 50.59 |
| 60.00 | 4.00 | 0.55 | 45.29 |
| 60.00 | 5.00 | 0.55 | 45.29 |
| 60.00 | 6.00 | 0.53 | 47.06 |
| 60.00 | 7.00 | 0.52 | 48.24 |
| 60.00 | 8.00 | 0.53 | 47.06 |
| 60.00 | 9.00 | 0.58 | 42.35 |
| 60.00 | 10.00 | 0.55 | 45.29 |
| 80.00 | 1.00 | 0.53 | 47.06 |
| 80.00 | 2.00 | 0.51 | 49.41 |

| | | | |
|--------|-------|------|-------|
| 80.00 | 3.00 | 0.52 | 48.24 |
| 80.00 | 4.00 | 0.56 | 44.12 |
| 80.00 | 5.00 | 0.54 | 45.88 |
| 80.00 | 6.00 | 0.51 | 48.82 |
| 80.00 | 7.00 | 0.54 | 45.88 |
| 80.00 | 8.00 | 0.54 | 45.88 |
| 80.00 | 9.00 | 0.48 | 52.35 |
| 80.00 | 10.00 | 0.54 | 45.88 |
| 100.00 | 1.00 | 0.48 | 51.76 |
| 100.00 | 2.00 | 0.51 | 49.41 |
| 100.00 | 3.00 | 0.49 | 51.18 |
| 100.00 | 4.00 | 0.50 | 50.00 |
| 100.00 | 5.00 | 0.53 | 47.06 |
| 100.00 | 6.00 | 0.49 | 50.59 |
| 100.00 | 7.00 | 0.49 | 50.59 |
| 100.00 | 8.00 | 0.51 | 48.82 |
| 100.00 | 9.00 | 0.52 | 48.24 |
| 100.00 | 10.00 | 0.55 | 44.71 |
| 120.00 | 1.00 | 0.53 | 47.06 |
| 120.00 | 2.00 | 0.45 | 54.71 |
| 120.00 | 3.00 | 0.45 | 55.29 |
| 120.00 | 4.00 | 0.48 | 52.35 |
| 120.00 | 5.00 | 0.53 | 47.06 |
| 120.00 | 6.00 | 0.52 | 48.24 |
| 120.00 | 7.00 | 0.56 | 44.12 |
| 120.00 | 8.00 | 0.54 | 46.47 |
| 120.00 | 9.00 | 0.52 | 48.24 |
| 120.00 | 10.00 | 0.49 | 51.18 |
| 140.00 | 1.00 | 0.48 | 51.76 |
| 140.00 | 2.00 | 0.46 | 53.53 |
| 140.00 | 3.00 | 0.47 | 52.94 |
| 140.00 | 4.00 | 0.52 | 48.24 |
| 140.00 | 5.00 | 0.52 | 47.65 |
| 140.00 | 6.00 | 0.52 | 47.65 |
| 140.00 | 7.00 | 0.48 | 51.76 |
| 140.00 | 8.00 | 0.50 | 50.00 |
| 140.00 | 9.00 | 0.54 | 45.88 |
| 140.00 | 10.00 | 0.53 | 47.06 |
| 160.00 | 1.00 | 0.48 | 52.35 |
| 160.00 | 2.00 | 0.48 | 51.76 |
| 160.00 | 3.00 | 0.49 | 50.59 |
| 160.00 | 4.00 | 0.52 | 47.65 |
| 160.00 | 5.00 | 0.52 | 48.24 |
| 160.00 | 6.00 | 0.51 | 48.82 |
| 160.00 | 7.00 | 0.54 | 45.88 |

| | | | |
|--------|-------|------|-------|
| 160.00 | 8.00 | 0.50 | 50.00 |
| 160.00 | 9.00 | 0.48 | 51.76 |
| 160.00 | 10.00 | 0.50 | 50.00 |
| 180.00 | 1.00 | 0.48 | 51.76 |
| 180.00 | 2.00 | 0.50 | 50.00 |
| 180.00 | 3.00 | 0.49 | 51.18 |
| 180.00 | 4.00 | 0.51 | 48.82 |
| 180.00 | 5.00 | 0.49 | 51.18 |
| 180.00 | 6.00 | 0.51 | 49.41 |
| 180.00 | 7.00 | 0.50 | 50.00 |
| 180.00 | 8.00 | 0.56 | 44.12 |
| 180.00 | 9.00 | 0.48 | 52.35 |
| 180.00 | 10.00 | 0.52 | 47.65 |
| 200.00 | 1.00 | 0.48 | 51.76 |
| 200.00 | 2.00 | 0.45 | 55.29 |
| 200.00 | 3.00 | 0.48 | 51.76 |
| 200.00 | 4.00 | 0.48 | 51.76 |
| 200.00 | 5.00 | 0.46 | 54.12 |
| 200.00 | 6.00 | 0.52 | 47.65 |
| 200.00 | 7.00 | 0.55 | 44.71 |
| 200.00 | 8.00 | 0.52 | 47.65 |
| 200.00 | 9.00 | 0.52 | 47.65 |
| 200.00 | 10.00 | 0.51 | 49.41 |

Random Forest HOG Raw A

| Number Trees | NumberObs on Leaves | Out of the Bag Error | Out of the Bag Prediction Accuracy |
|--------------|---------------------|----------------------|------------------------------------|
| 1.00 | 1.00 | 0.72 | 28.24 |
| 1.00 | 2.00 | 0.77 | 22.94 |
| 1.00 | 3.00 | 0.76 | 23.53 |
| 1.00 | 4.00 | 0.76 | 23.53 |
| 1.00 | 5.00 | 0.77 | 22.94 |
| 1.00 | 6.00 | 0.74 | 25.88 |
| 1.00 | 7.00 | 0.75 | 25.29 |
| 1.00 | 8.00 | 0.75 | 24.71 |
| 1.00 | 9.00 | 0.77 | 22.94 |
| 1.00 | 10.00 | 0.75 | 25.29 |
| 20.00 | 1.00 | 0.55 | 44.71 |
| 20.00 | 2.00 | 0.64 | 36.47 |
| 20.00 | 3.00 | 0.62 | 38.24 |
| 20.00 | 4.00 | 0.56 | 44.12 |
| 20.00 | 5.00 | 0.59 | 41.18 |
| 20.00 | 6.00 | 0.64 | 35.88 |
| 20.00 | 7.00 | 0.65 | 34.71 |

| | | | |
|--------|-------|------|-------|
| 20.00 | 8.00 | 0.57 | 42.94 |
| 20.00 | 9.00 | 0.61 | 38.82 |
| 20.00 | 10.00 | 0.63 | 37.06 |
| 40.00 | 1.00 | 0.55 | 45.29 |
| 40.00 | 2.00 | 0.54 | 46.47 |
| 40.00 | 3.00 | 0.54 | 45.88 |
| 40.00 | 4.00 | 0.49 | 50.59 |
| 40.00 | 5.00 | 0.56 | 44.12 |
| 40.00 | 6.00 | 0.55 | 45.29 |
| 40.00 | 7.00 | 0.59 | 41.18 |
| 40.00 | 8.00 | 0.52 | 47.65 |
| 40.00 | 9.00 | 0.54 | 45.88 |
| 40.00 | 10.00 | 0.56 | 43.53 |
| 60.00 | 1.00 | 0.56 | 44.12 |
| 60.00 | 2.00 | 0.55 | 45.29 |
| 60.00 | 3.00 | 0.51 | 49.41 |
| 60.00 | 4.00 | 0.53 | 47.06 |
| 60.00 | 5.00 | 0.55 | 45.29 |
| 60.00 | 6.00 | 0.52 | 48.24 |
| 60.00 | 7.00 | 0.54 | 45.88 |
| 60.00 | 8.00 | 0.54 | 45.88 |
| 60.00 | 9.00 | 0.53 | 47.06 |
| 60.00 | 10.00 | 0.55 | 45.29 |
| 80.00 | 1.00 | 0.51 | 49.41 |
| 80.00 | 2.00 | 0.52 | 47.65 |
| 80.00 | 3.00 | 0.53 | 47.06 |
| 80.00 | 4.00 | 0.54 | 46.47 |
| 80.00 | 5.00 | 0.49 | 50.59 |
| 80.00 | 6.00 | 0.48 | 52.35 |
| 80.00 | 7.00 | 0.56 | 44.12 |
| 80.00 | 8.00 | 0.49 | 51.18 |
| 80.00 | 9.00 | 0.51 | 49.41 |
| 80.00 | 10.00 | 0.57 | 42.94 |
| 100.00 | 1.00 | 0.48 | 52.35 |
| 100.00 | 2.00 | 0.48 | 52.35 |
| 100.00 | 3.00 | 0.49 | 51.18 |
| 100.00 | 4.00 | 0.51 | 48.82 |
| 100.00 | 5.00 | 0.51 | 48.82 |
| 100.00 | 6.00 | 0.52 | 47.65 |
| 100.00 | 7.00 | 0.52 | 47.65 |
| 100.00 | 8.00 | 0.54 | 46.47 |
| 100.00 | 9.00 | 0.54 | 45.88 |
| 100.00 | 10.00 | 0.52 | 48.24 |
| 120.00 | 1.00 | 0.49 | 51.18 |
| 120.00 | 2.00 | 0.49 | 50.59 |

| | | | |
|--------|-------|------|-------|
| 120.00 | 3.00 | 0.50 | 50.00 |
| 120.00 | 4.00 | 0.52 | 47.65 |
| 120.00 | 5.00 | 0.52 | 48.24 |
| 120.00 | 6.00 | 0.53 | 47.06 |
| 120.00 | 7.00 | 0.51 | 48.82 |
| 120.00 | 8.00 | 0.56 | 43.53 |
| 120.00 | 9.00 | 0.55 | 45.29 |
| 120.00 | 10.00 | 0.51 | 48.82 |
| 140.00 | 1.00 | 0.52 | 47.65 |
| 140.00 | 2.00 | 0.52 | 48.24 |
| 140.00 | 3.00 | 0.52 | 47.65 |
| 140.00 | 4.00 | 0.52 | 47.65 |
| 140.00 | 5.00 | 0.54 | 45.88 |
| 140.00 | 6.00 | 0.50 | 50.00 |
| 140.00 | 7.00 | 0.51 | 48.82 |
| 140.00 | 8.00 | 0.52 | 48.24 |
| 140.00 | 9.00 | 0.52 | 48.24 |
| 140.00 | 10.00 | 0.53 | 47.06 |
| 160.00 | 1.00 | 0.51 | 48.82 |
| 160.00 | 2.00 | 0.51 | 49.41 |
| 160.00 | 3.00 | 0.52 | 47.65 |
| 160.00 | 4.00 | 0.54 | 46.47 |
| 160.00 | 5.00 | 0.49 | 50.59 |
| 160.00 | 6.00 | 0.52 | 48.24 |
| 160.00 | 7.00 | 0.51 | 48.82 |
| 160.00 | 8.00 | 0.52 | 47.65 |
| 160.00 | 9.00 | 0.51 | 48.82 |
| 160.00 | 10.00 | 0.54 | 45.88 |
| 180.00 | 1.00 | 0.46 | 54.12 |
| 180.00 | 2.00 | 0.49 | 51.18 |
| 180.00 | 3.00 | 0.50 | 50.00 |
| 180.00 | 4.00 | 0.48 | 51.76 |
| 180.00 | 5.00 | 0.48 | 52.35 |
| 180.00 | 6.00 | 0.50 | 50.00 |
| 180.00 | 7.00 | 0.52 | 48.24 |
| 180.00 | 8.00 | 0.50 | 50.00 |
| 180.00 | 9.00 | 0.44 | 55.88 |
| 180.00 | 10.00 | 0.56 | 43.53 |
| 200.00 | 1.00 | 0.50 | 50.00 |
| 200.00 | 2.00 | 0.50 | 50.00 |
| 200.00 | 3.00 | 0.53 | 47.06 |
| 200.00 | 4.00 | 0.49 | 51.18 |
| 200.00 | 5.00 | 0.54 | 46.47 |
| 200.00 | 6.00 | 0.53 | 47.06 |
| 200.00 | 7.00 | 0.54 | 46.47 |

| | | | |
|--------|-------|------|-------|
| 200.00 | 8.00 | 0.53 | 47.06 |
| 200.00 | 9.00 | 0.49 | 51.18 |
| 200.00 | 10.00 | 0.52 | 48.24 |

| Random Forest Bag Raw B Images | | | |
|--------------------------------|----------------------|----------------------|------------------------------------|
| Number Trees | Number Obs on Leaves | Out of the Bag Error | Out of the Bag Prediction Accuracy |
| 1.00 | 1.00 | 0.65 | 35.24 |
| 1.00 | 2.00 | 0.61 | 39.05 |
| 1.00 | 3.00 | 0.58 | 41.90 |
| 1.00 | 4.00 | 0.68 | 32.38 |
| 1.00 | 5.00 | 0.55 | 44.76 |
| 1.00 | 6.00 | 0.63 | 37.14 |
| 1.00 | 7.00 | 0.62 | 38.10 |
| 1.00 | 8.00 | 0.62 | 38.10 |
| 1.00 | 9.00 | 0.55 | 44.76 |
| 1.00 | 10.00 | 0.62 | 38.10 |
| 20.00 | 1.00 | 0.45 | 55.24 |
| 20.00 | 2.00 | 0.43 | 57.14 |
| 20.00 | 3.00 | 0.40 | 60.00 |
| 20.00 | 4.00 | 0.41 | 59.05 |
| 20.00 | 5.00 | 0.46 | 54.29 |
| 20.00 | 6.00 | 0.48 | 52.38 |
| 20.00 | 7.00 | 0.49 | 51.43 |
| 20.00 | 8.00 | 0.44 | 56.19 |
| 20.00 | 9.00 | 0.50 | 49.52 |
| 20.00 | 10.00 | 0.41 | 59.05 |
| 40.00 | 1.00 | 0.45 | 55.24 |
| 40.00 | 2.00 | 0.39 | 60.95 |
| 40.00 | 3.00 | 0.39 | 60.95 |
| 40.00 | 4.00 | 0.38 | 61.90 |
| 40.00 | 5.00 | 0.47 | 53.33 |
| 40.00 | 6.00 | 0.46 | 54.29 |
| 40.00 | 7.00 | 0.42 | 58.10 |
| 40.00 | 8.00 | 0.42 | 58.10 |
| 40.00 | 9.00 | 0.46 | 54.29 |
| 40.00 | 10.00 | 0.36 | 63.81 |
| 60.00 | 1.00 | 0.35 | 64.76 |
| 60.00 | 2.00 | 0.40 | 60.00 |
| 60.00 | 3.00 | 0.37 | 62.86 |
| 60.00 | 4.00 | 0.43 | 57.14 |
| 60.00 | 5.00 | 0.36 | 63.81 |
| 60.00 | 6.00 | 0.45 | 55.24 |
| 60.00 | 7.00 | 0.42 | 58.10 |

| | | | |
|--------|-------|------|-------|
| 60.00 | 8.00 | 0.38 | 61.90 |
| 60.00 | 9.00 | 0.45 | 55.24 |
| 60.00 | 10.00 | 0.43 | 57.14 |
| 80.00 | 1.00 | 0.36 | 63.81 |
| 80.00 | 2.00 | 0.36 | 63.81 |
| 80.00 | 3.00 | 0.35 | 64.76 |
| 80.00 | 4.00 | 0.37 | 62.86 |
| 80.00 | 5.00 | 0.39 | 60.95 |
| 80.00 | 6.00 | 0.37 | 62.86 |
| 80.00 | 7.00 | 0.36 | 63.81 |
| 80.00 | 8.00 | 0.46 | 54.29 |
| 80.00 | 9.00 | 0.41 | 59.05 |
| 80.00 | 10.00 | 0.39 | 60.95 |
| 100.00 | 1.00 | 0.40 | 60.00 |
| 100.00 | 2.00 | 0.36 | 63.81 |
| 100.00 | 3.00 | 0.32 | 67.62 |
| 100.00 | 4.00 | 0.36 | 63.81 |
| 100.00 | 5.00 | 0.40 | 60.00 |
| 100.00 | 6.00 | 0.39 | 60.95 |
| 100.00 | 7.00 | 0.37 | 62.86 |
| 100.00 | 8.00 | 0.38 | 61.90 |
| 100.00 | 9.00 | 0.36 | 63.81 |
| 100.00 | 10.00 | 0.43 | 57.14 |
| 120.00 | 1.00 | 0.37 | 62.86 |
| 120.00 | 2.00 | 0.33 | 66.67 |
| 120.00 | 3.00 | 0.39 | 60.95 |
| 120.00 | 4.00 | 0.41 | 59.05 |
| 120.00 | 5.00 | 0.39 | 60.95 |
| 120.00 | 6.00 | 0.38 | 61.90 |
| 120.00 | 7.00 | 0.35 | 64.76 |
| 120.00 | 8.00 | 0.43 | 57.14 |
| 120.00 | 9.00 | 0.35 | 64.76 |
| 120.00 | 10.00 | 0.39 | 60.95 |
| 140.00 | 1.00 | 0.41 | 59.05 |
| 140.00 | 2.00 | 0.38 | 61.90 |
| 140.00 | 3.00 | 0.32 | 67.62 |
| 140.00 | 4.00 | 0.38 | 61.90 |
| 140.00 | 5.00 | 0.35 | 64.76 |
| 140.00 | 6.00 | 0.38 | 61.90 |
| 140.00 | 7.00 | 0.40 | 60.00 |
| 140.00 | 8.00 | 0.43 | 57.14 |
| 140.00 | 9.00 | 0.40 | 60.00 |
| 140.00 | 10.00 | 0.38 | 61.90 |
| 160.00 | 1.00 | 0.32 | 67.62 |
| 160.00 | 2.00 | 0.39 | 60.95 |

| | | | |
|--------|-------|------|-------|
| 160.00 | 3.00 | 0.35 | 64.76 |
| 160.00 | 4.00 | 0.32 | 67.62 |
| 160.00 | 5.00 | 0.35 | 64.76 |
| 160.00 | 6.00 | 0.39 | 60.95 |
| 160.00 | 7.00 | 0.33 | 66.67 |
| 160.00 | 8.00 | 0.39 | 60.95 |
| 160.00 | 9.00 | 0.43 | 57.14 |
| 160.00 | 10.00 | 0.39 | 60.95 |
| 180.00 | 1.00 | 0.33 | 66.67 |
| 180.00 | 2.00 | 0.33 | 66.67 |
| 180.00 | 3.00 | 0.35 | 64.76 |
| 180.00 | 4.00 | 0.37 | 62.86 |
| 180.00 | 5.00 | 0.35 | 64.76 |
| 180.00 | 6.00 | 0.38 | 61.90 |
| 180.00 | 7.00 | 0.35 | 64.76 |
| 180.00 | 8.00 | 0.38 | 61.90 |
| 180.00 | 9.00 | 0.37 | 62.86 |
| 180.00 | 10.00 | 0.41 | 59.05 |
| 200.00 | 1.00 | 0.35 | 64.76 |
| 200.00 | 2.00 | 0.35 | 64.76 |
| 200.00 | 3.00 | 0.35 | 64.76 |
| 200.00 | 4.00 | 0.39 | 60.95 |
| 200.00 | 5.00 | 0.32 | 67.62 |
| 200.00 | 6.00 | 0.40 | 60.00 |
| 200.00 | 7.00 | 0.36 | 63.81 |
| 200.00 | 8.00 | 0.36 | 63.81 |
| 200.00 | 9.00 | 0.43 | 57.14 |
| 200.00 | 10.00 | 0.35 | 64.76 |

Random Forest HOG Raw B

| Number Trees | Number Obs on Leaves | Out of the Bag Error | Out of the Bag Prediction Accuracy |
|--------------|----------------------|----------------------|------------------------------------|
| 1.00 | 1.00 | 0.64 | 36.19 |
| 1.00 | 2.00 | 0.65 | 35.24 |
| 1.00 | 3.00 | 0.66 | 34.29 |
| 1.00 | 4.00 | 0.61 | 39.05 |
| 1.00 | 5.00 | 0.56 | 43.81 |
| 1.00 | 6.00 | 0.63 | 37.14 |
| 1.00 | 7.00 | 0.65 | 35.24 |
| 1.00 | 8.00 | 0.63 | 37.14 |
| 1.00 | 9.00 | 0.68 | 32.38 |
| 1.00 | 10.00 | 0.65 | 35.24 |
| 20.00 | 1.00 | 0.49 | 51.43 |
| 20.00 | 2.00 | 0.51 | 48.57 |
| 20.00 | 3.00 | 0.44 | 56.19 |

| | | | |
|--------|-------|------|-------|
| 20.00 | 4.00 | 0.49 | 51.43 |
| 20.00 | 5.00 | 0.51 | 48.57 |
| 20.00 | 6.00 | 0.43 | 57.14 |
| 20.00 | 7.00 | 0.55 | 44.76 |
| 20.00 | 8.00 | 0.50 | 50.48 |
| 20.00 | 9.00 | 0.50 | 49.52 |
| 20.00 | 10.00 | 0.53 | 46.67 |
| 40.00 | 1.00 | 0.42 | 58.10 |
| 40.00 | 2.00 | 0.51 | 48.57 |
| 40.00 | 3.00 | 0.42 | 58.10 |
| 40.00 | 4.00 | 0.48 | 52.38 |
| 40.00 | 5.00 | 0.41 | 59.05 |
| 40.00 | 6.00 | 0.39 | 60.95 |
| 40.00 | 7.00 | 0.49 | 51.43 |
| 40.00 | 8.00 | 0.41 | 59.05 |
| 40.00 | 9.00 | 0.48 | 52.38 |
| 40.00 | 10.00 | 0.44 | 56.19 |
| 60.00 | 1.00 | 0.38 | 61.90 |
| 60.00 | 2.00 | 0.42 | 58.10 |
| 60.00 | 3.00 | 0.43 | 57.14 |
| 60.00 | 4.00 | 0.47 | 53.33 |
| 60.00 | 5.00 | 0.45 | 55.24 |
| 60.00 | 6.00 | 0.41 | 59.05 |
| 60.00 | 7.00 | 0.40 | 60.00 |
| 60.00 | 8.00 | 0.40 | 60.00 |
| 60.00 | 9.00 | 0.48 | 52.38 |
| 60.00 | 10.00 | 0.46 | 54.29 |
| 80.00 | 1.00 | 0.39 | 60.95 |
| 80.00 | 2.00 | 0.38 | 61.90 |
| 80.00 | 3.00 | 0.39 | 60.95 |
| 80.00 | 4.00 | 0.39 | 60.95 |
| 80.00 | 5.00 | 0.40 | 60.00 |
| 80.00 | 6.00 | 0.44 | 56.19 |
| 80.00 | 7.00 | 0.35 | 64.76 |
| 80.00 | 8.00 | 0.35 | 64.76 |
| 80.00 | 9.00 | 0.45 | 55.24 |
| 80.00 | 10.00 | 0.44 | 56.19 |
| 100.00 | 1.00 | 0.40 | 60.00 |
| 100.00 | 2.00 | 0.40 | 60.00 |
| 100.00 | 3.00 | 0.40 | 60.00 |
| 100.00 | 4.00 | 0.38 | 61.90 |
| 100.00 | 5.00 | 0.44 | 56.19 |
| 100.00 | 6.00 | 0.42 | 58.10 |
| 100.00 | 7.00 | 0.50 | 50.48 |
| 100.00 | 8.00 | 0.39 | 60.95 |

| | | | |
|--------|-------|------|-------|
| 100.00 | 9.00 | 0.41 | 59.05 |
| 100.00 | 10.00 | 0.40 | 60.00 |
| 120.00 | 1.00 | 0.45 | 55.24 |
| 120.00 | 2.00 | 0.41 | 59.05 |
| 120.00 | 3.00 | 0.40 | 60.00 |
| 120.00 | 4.00 | 0.37 | 62.86 |
| 120.00 | 5.00 | 0.37 | 62.86 |
| 120.00 | 6.00 | 0.39 | 60.95 |
| 120.00 | 7.00 | 0.36 | 63.81 |
| 120.00 | 8.00 | 0.37 | 62.86 |
| 120.00 | 9.00 | 0.39 | 60.95 |
| 120.00 | 10.00 | 0.50 | 50.48 |
| 140.00 | 1.00 | 0.40 | 60.00 |
| 140.00 | 2.00 | 0.40 | 60.00 |
| 140.00 | 3.00 | 0.43 | 57.14 |
| 140.00 | 4.00 | 0.37 | 62.86 |
| 140.00 | 5.00 | 0.36 | 63.81 |
| 140.00 | 6.00 | 0.42 | 58.10 |
| 140.00 | 7.00 | 0.36 | 63.81 |
| 140.00 | 8.00 | 0.36 | 63.81 |
| 140.00 | 9.00 | 0.40 | 60.00 |
| 140.00 | 10.00 | 0.41 | 59.05 |
| 160.00 | 1.00 | 0.35 | 64.76 |
| 160.00 | 2.00 | 0.36 | 63.81 |
| 160.00 | 3.00 | 0.44 | 56.19 |
| 160.00 | 4.00 | 0.36 | 63.81 |
| 160.00 | 5.00 | 0.38 | 61.90 |
| 160.00 | 6.00 | 0.37 | 62.86 |
| 160.00 | 7.00 | 0.45 | 55.24 |
| 160.00 | 8.00 | 0.43 | 57.14 |
| 160.00 | 9.00 | 0.39 | 60.95 |
| 160.00 | 10.00 | 0.37 | 62.86 |
| 180.00 | 1.00 | 0.31 | 68.57 |
| 180.00 | 2.00 | 0.38 | 61.90 |
| 180.00 | 3.00 | 0.38 | 61.90 |
| 180.00 | 4.00 | 0.40 | 60.00 |
| 180.00 | 5.00 | 0.40 | 60.00 |
| 180.00 | 6.00 | 0.44 | 56.19 |
| 180.00 | 7.00 | 0.36 | 63.81 |
| 180.00 | 8.00 | 0.43 | 57.14 |
| 180.00 | 9.00 | 0.41 | 59.05 |
| 180.00 | 10.00 | 0.35 | 64.76 |
| 200.00 | 1.00 | 0.45 | 55.24 |
| 200.00 | 2.00 | 0.38 | 61.90 |
| 200.00 | 3.00 | 0.35 | 64.76 |

| | | | |
|--------|-------|------|-------|
| 200.00 | 4.00 | 0.35 | 64.76 |
| 200.00 | 5.00 | 0.36 | 63.81 |
| 200.00 | 6.00 | 0.41 | 59.05 |
| 200.00 | 7.00 | 0.37 | 62.86 |
| 200.00 | 8.00 | 0.39 | 60.95 |
| 200.00 | 9.00 | 0.42 | 58.10 |
| 200.00 | 10.00 | 0.46 | 54.29 |

Random Forest HOG Processed B

| Number Trees | Number Obs on Leaves | Out of the Bag Error | Out of the Bag Prediction Accuracy |
|--------------|----------------------|----------------------|------------------------------------|
| 1.00 | 1.00 | 0.56 | 44.44 |
| 1.00 | 2.00 | 0.58 | 42.22 |
| 1.00 | 3.00 | 0.58 | 42.22 |
| 1.00 | 4.00 | 0.57 | 42.96 |
| 1.00 | 5.00 | 0.63 | 37.04 |
| 1.00 | 6.00 | 0.66 | 34.07 |
| 1.00 | 7.00 | 0.59 | 41.48 |
| 1.00 | 8.00 | 0.55 | 45.19 |
| 1.00 | 9.00 | 0.61 | 39.26 |
| 1.00 | 10.00 | 0.60 | 40.00 |
| 20.00 | 1.00 | 0.42 | 57.78 |
| 20.00 | 2.00 | 0.40 | 60.00 |
| 20.00 | 3.00 | 0.36 | 64.44 |
| 20.00 | 4.00 | 0.40 | 60.00 |
| 20.00 | 5.00 | 0.40 | 60.00 |
| 20.00 | 6.00 | 0.38 | 62.22 |
| 20.00 | 7.00 | 0.36 | 63.70 |
| 20.00 | 8.00 | 0.38 | 62.22 |
| 20.00 | 9.00 | 0.40 | 60.00 |
| 20.00 | 10.00 | 0.47 | 52.59 |
| 40.00 | 1.00 | 0.33 | 67.41 |
| 40.00 | 2.00 | 0.33 | 66.67 |
| 40.00 | 3.00 | 0.36 | 64.44 |
| 40.00 | 4.00 | 0.34 | 65.93 |
| 40.00 | 5.00 | 0.34 | 65.93 |
| 40.00 | 6.00 | 0.36 | 64.44 |
| 40.00 | 7.00 | 0.39 | 60.74 |
| 40.00 | 8.00 | 0.33 | 66.67 |
| 40.00 | 9.00 | 0.39 | 61.48 |
| 40.00 | 10.00 | 0.33 | 67.41 |
| 60.00 | 1.00 | 0.36 | 64.44 |
| 60.00 | 2.00 | 0.31 | 68.89 |
| 60.00 | 3.00 | 0.36 | 64.44 |

| | | | |
|--------|-------|------|-------|
| 60.00 | 4.00 | 0.30 | 69.63 |
| 60.00 | 5.00 | 0.37 | 62.96 |
| 60.00 | 6.00 | 0.33 | 66.67 |
| 60.00 | 7.00 | 0.35 | 65.19 |
| 60.00 | 8.00 | 0.33 | 66.67 |
| 60.00 | 9.00 | 0.30 | 70.37 |
| 60.00 | 10.00 | 0.35 | 65.19 |
| 80.00 | 1.00 | 0.31 | 68.89 |
| 80.00 | 2.00 | 0.30 | 70.37 |
| 80.00 | 3.00 | 0.30 | 70.37 |
| 80.00 | 4.00 | 0.31 | 68.89 |
| 80.00 | 5.00 | 0.33 | 66.67 |
| 80.00 | 6.00 | 0.35 | 65.19 |
| 80.00 | 7.00 | 0.27 | 72.59 |
| 80.00 | 8.00 | 0.30 | 69.63 |
| 80.00 | 9.00 | 0.36 | 64.44 |
| 80.00 | 10.00 | 0.30 | 70.37 |
| 100.00 | 1.00 | 0.29 | 71.11 |
| 100.00 | 2.00 | 0.36 | 63.70 |
| 100.00 | 3.00 | 0.37 | 62.96 |
| 100.00 | 4.00 | 0.29 | 71.11 |
| 100.00 | 5.00 | 0.36 | 63.70 |
| 100.00 | 6.00 | 0.33 | 67.41 |
| 100.00 | 7.00 | 0.33 | 67.41 |
| 100.00 | 8.00 | 0.34 | 65.93 |
| 100.00 | 9.00 | 0.32 | 68.15 |
| 100.00 | 10.00 | 0.33 | 67.41 |
| 120.00 | 1.00 | 0.29 | 71.11 |
| 120.00 | 2.00 | 0.30 | 69.63 |
| 120.00 | 3.00 | 0.32 | 68.15 |
| 120.00 | 4.00 | 0.34 | 65.93 |
| 120.00 | 5.00 | 0.33 | 67.41 |
| 120.00 | 6.00 | 0.31 | 68.89 |
| 120.00 | 7.00 | 0.29 | 71.11 |
| 120.00 | 8.00 | 0.34 | 65.93 |
| 120.00 | 9.00 | 0.33 | 67.41 |
| 120.00 | 10.00 | 0.33 | 66.67 |
| 140.00 | 1.00 | 0.33 | 67.41 |
| 140.00 | 2.00 | 0.31 | 68.89 |
| 140.00 | 3.00 | 0.27 | 72.59 |
| 140.00 | 4.00 | 0.30 | 69.63 |
| 140.00 | 5.00 | 0.30 | 70.37 |
| 140.00 | 6.00 | 0.33 | 67.41 |
| 140.00 | 7.00 | 0.31 | 68.89 |
| 140.00 | 8.00 | 0.27 | 72.59 |

| | | | |
|--------|-------|------|-------|
| 140.00 | 9.00 | 0.32 | 68.15 |
| 140.00 | 10.00 | 0.32 | 68.15 |
| 160.00 | 1.00 | 0.29 | 71.11 |
| 160.00 | 2.00 | 0.31 | 68.89 |
| 160.00 | 3.00 | 0.33 | 66.67 |
| 160.00 | 4.00 | 0.29 | 71.11 |
| 160.00 | 5.00 | 0.35 | 65.19 |
| 160.00 | 6.00 | 0.33 | 66.67 |
| 160.00 | 7.00 | 0.34 | 65.93 |
| 160.00 | 8.00 | 0.30 | 69.63 |
| 160.00 | 9.00 | 0.27 | 72.59 |
| 160.00 | 10.00 | 0.30 | 70.37 |
| 180.00 | 1.00 | 0.27 | 73.33 |
| 180.00 | 2.00 | 0.27 | 72.59 |
| 180.00 | 3.00 | 0.30 | 70.37 |
| 180.00 | 4.00 | 0.27 | 73.33 |
| 180.00 | 5.00 | 0.34 | 65.93 |
| 180.00 | 6.00 | 0.30 | 69.63 |
| 180.00 | 7.00 | 0.30 | 70.37 |
| 180.00 | 8.00 | 0.33 | 67.41 |
| 180.00 | 9.00 | 0.34 | 65.93 |
| 180.00 | 10.00 | 0.35 | 65.19 |
| 200.00 | 1.00 | 0.31 | 68.89 |
| 200.00 | 2.00 | 0.30 | 70.37 |
| 200.00 | 3.00 | 0.28 | 71.85 |
| 200.00 | 4.00 | 0.32 | 68.15 |
| 200.00 | 5.00 | 0.31 | 68.89 |
| 200.00 | 6.00 | 0.30 | 70.37 |
| 200.00 | 7.00 | 0.35 | 65.19 |
| 200.00 | 8.00 | 0.31 | 68.89 |
| 200.00 | 9.00 | 0.31 | 68.89 |
| 200.00 | 10.00 | 0.31 | 68.89 |

Random Forest BAG Processed B

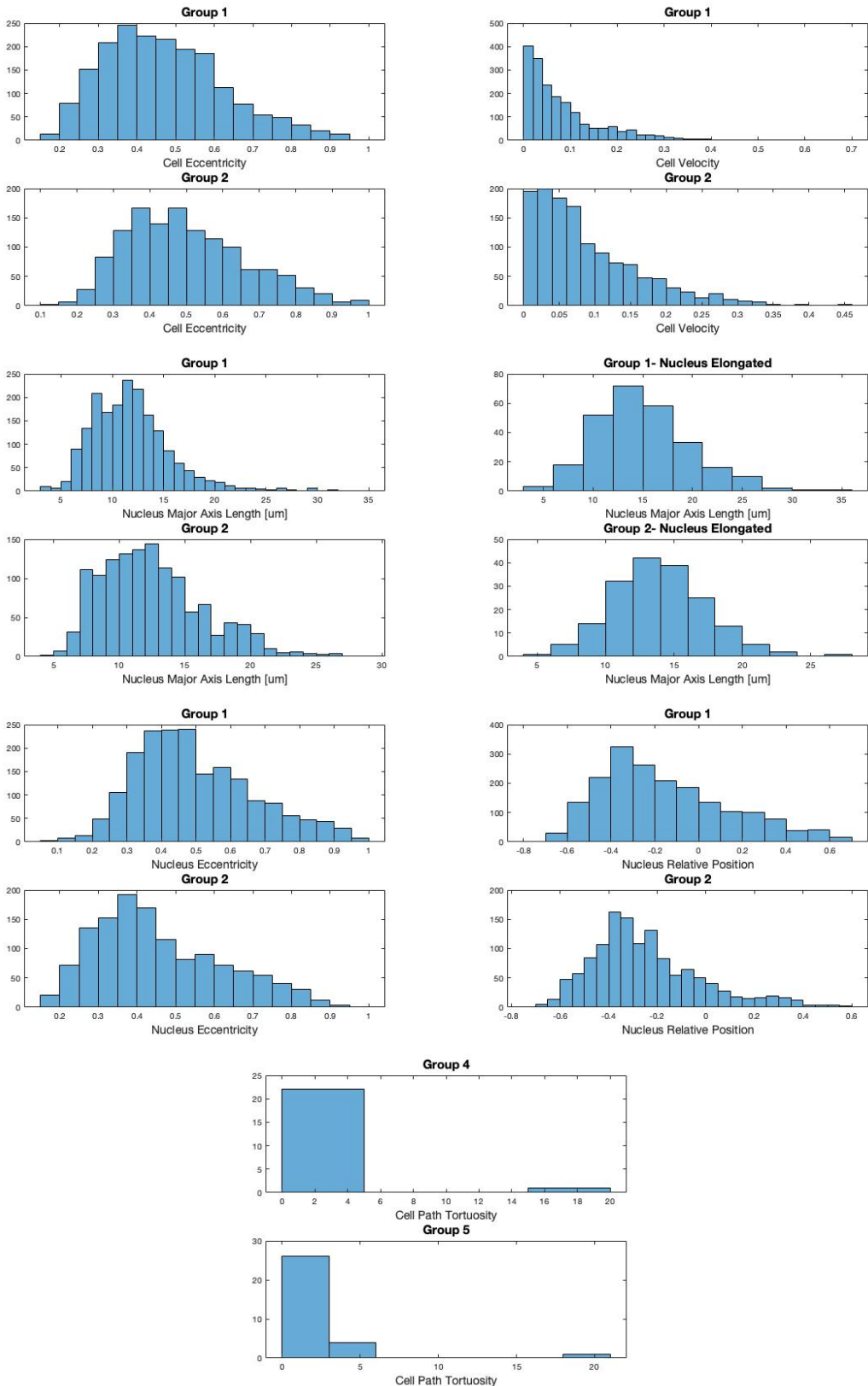
| Number Trees | Number Obs on Leaves | Out of the Bag Error | Out of the Bag Prediction Accuracy |
|--------------|----------------------|----------------------|------------------------------------|
| 1.00 | 1.00 | 0.56 | 43.70 |
| 1.00 | 2.00 | 0.61 | 38.52 |
| 1.00 | 3.00 | 0.57 | 42.96 |
| 1.00 | 4.00 | 0.64 | 36.30 |
| 1.00 | 5.00 | 0.57 | 42.96 |
| 1.00 | 6.00 | 0.61 | 38.52 |
| 1.00 | 7.00 | 0.64 | 36.30 |
| 1.00 | 8.00 | 0.67 | 32.59 |

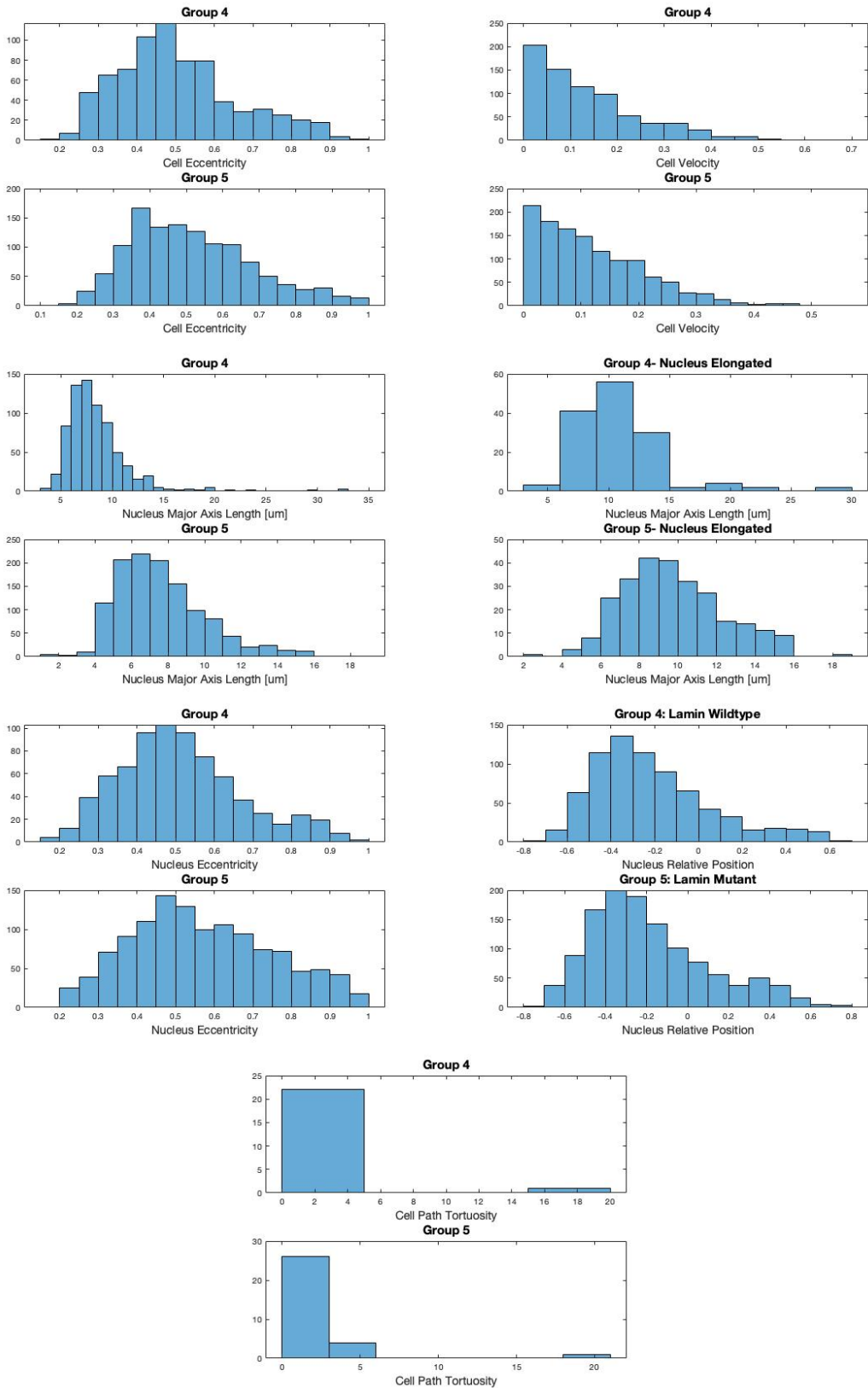
| | | | |
|--------|-------|------|-------|
| 1.00 | 9.00 | 0.61 | 38.52 |
| 1.00 | 10.00 | 0.56 | 44.44 |
| 20.00 | 1.00 | 0.47 | 53.33 |
| 20.00 | 2.00 | 0.31 | 68.89 |
| 20.00 | 3.00 | 0.40 | 60.00 |
| 20.00 | 4.00 | 0.34 | 65.93 |
| 20.00 | 5.00 | 0.41 | 59.26 |
| 20.00 | 6.00 | 0.41 | 59.26 |
| 20.00 | 7.00 | 0.40 | 60.00 |
| 20.00 | 8.00 | 0.39 | 60.74 |
| 20.00 | 9.00 | 0.38 | 62.22 |
| 20.00 | 10.00 | 0.42 | 57.78 |
| 40.00 | 1.00 | 0.33 | 66.67 |
| 40.00 | 2.00 | 0.35 | 65.19 |
| 40.00 | 3.00 | 0.34 | 65.93 |
| 40.00 | 4.00 | 0.35 | 65.19 |
| 40.00 | 5.00 | 0.37 | 62.96 |
| 40.00 | 6.00 | 0.32 | 68.15 |
| 40.00 | 7.00 | 0.35 | 65.19 |
| 40.00 | 8.00 | 0.38 | 62.22 |
| 40.00 | 9.00 | 0.33 | 66.67 |
| 40.00 | 10.00 | 0.39 | 61.48 |
| 60.00 | 1.00 | 0.30 | 69.63 |
| 60.00 | 2.00 | 0.29 | 71.11 |
| 60.00 | 3.00 | 0.34 | 65.93 |
| 60.00 | 4.00 | 0.25 | 74.81 |
| 60.00 | 5.00 | 0.37 | 62.96 |
| 60.00 | 6.00 | 0.37 | 62.96 |
| 60.00 | 7.00 | 0.36 | 64.44 |
| 60.00 | 8.00 | 0.31 | 68.89 |
| 60.00 | 9.00 | 0.36 | 63.70 |
| 60.00 | 10.00 | 0.38 | 62.22 |
| 80.00 | 1.00 | 0.31 | 68.89 |
| 80.00 | 2.00 | 0.36 | 63.70 |
| 80.00 | 3.00 | 0.34 | 65.93 |
| 80.00 | 4.00 | 0.30 | 69.63 |
| 80.00 | 5.00 | 0.33 | 66.67 |
| 80.00 | 6.00 | 0.32 | 68.15 |
| 80.00 | 7.00 | 0.33 | 67.41 |
| 80.00 | 8.00 | 0.35 | 65.19 |
| 80.00 | 9.00 | 0.31 | 68.89 |
| 80.00 | 10.00 | 0.33 | 67.41 |
| 100.00 | 1.00 | 0.32 | 68.15 |
| 100.00 | 2.00 | 0.35 | 65.19 |
| 100.00 | 3.00 | 0.32 | 68.15 |

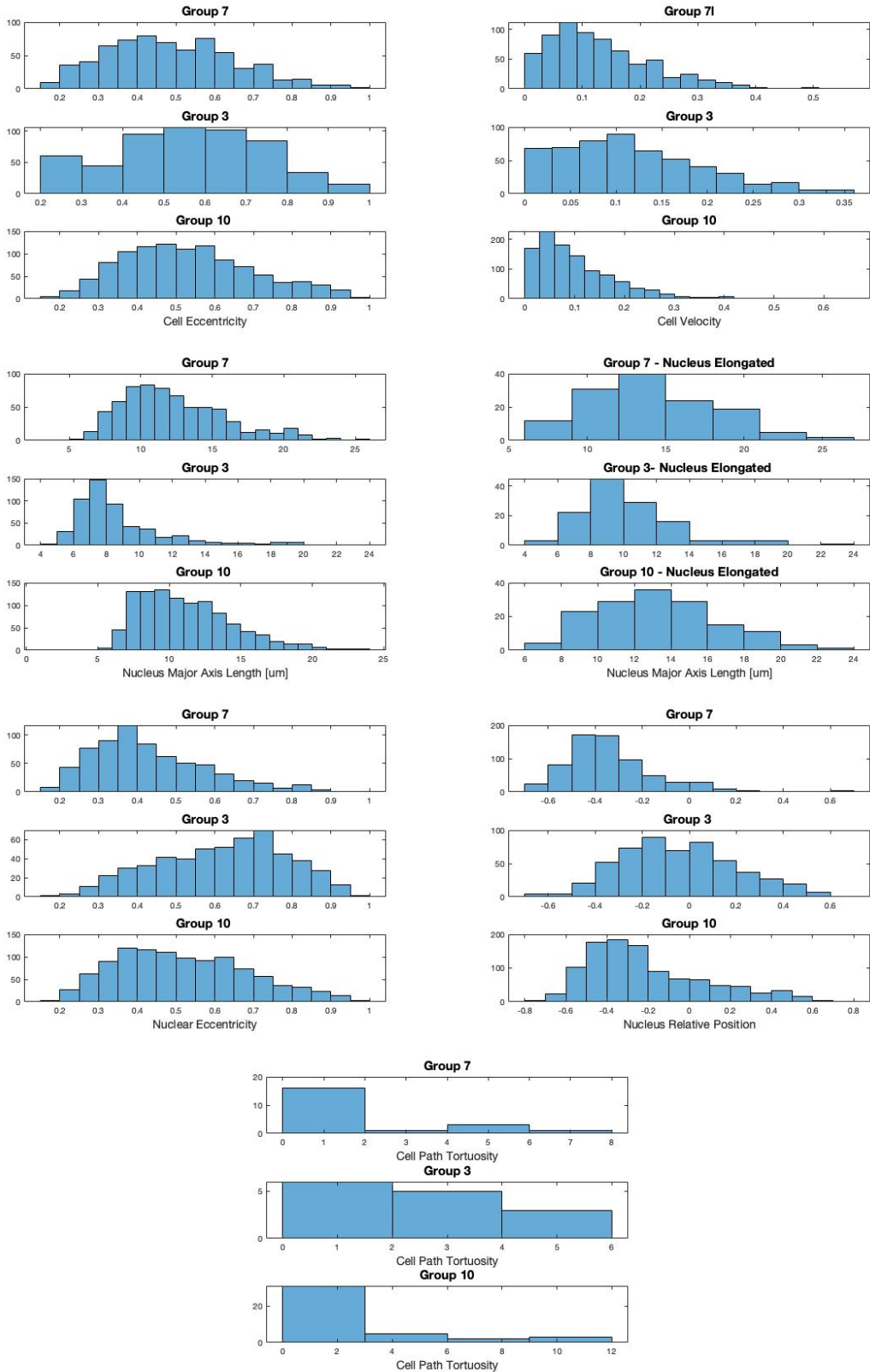
| | | | |
|--------|-------|------|-------|
| 100.00 | 4.00 | 0.27 | 72.59 |
| 100.00 | 5.00 | 0.33 | 66.67 |
| 100.00 | 6.00 | 0.30 | 69.63 |
| 100.00 | 7.00 | 0.34 | 65.93 |
| 100.00 | 8.00 | 0.30 | 70.37 |
| 100.00 | 9.00 | 0.33 | 66.67 |
| 100.00 | 10.00 | 0.34 | 65.93 |
| 120.00 | 1.00 | 0.28 | 71.85 |
| 120.00 | 2.00 | 0.25 | 74.81 |
| 120.00 | 3.00 | 0.31 | 68.89 |
| 120.00 | 4.00 | 0.31 | 68.89 |
| 120.00 | 5.00 | 0.31 | 68.89 |
| 120.00 | 6.00 | 0.31 | 68.89 |
| 120.00 | 7.00 | 0.31 | 68.89 |
| 120.00 | 8.00 | 0.33 | 66.67 |
| 120.00 | 9.00 | 0.33 | 67.41 |
| 120.00 | 10.00 | 0.31 | 68.89 |
| 140.00 | 1.00 | 0.28 | 71.85 |
| 140.00 | 2.00 | 0.29 | 71.11 |
| 140.00 | 3.00 | 0.24 | 75.56 |
| 140.00 | 4.00 | 0.31 | 68.89 |
| 140.00 | 5.00 | 0.33 | 67.41 |
| 140.00 | 6.00 | 0.25 | 74.81 |
| 140.00 | 7.00 | 0.30 | 69.63 |
| 140.00 | 8.00 | 0.30 | 69.63 |
| 140.00 | 9.00 | 0.36 | 64.44 |
| 140.00 | 10.00 | 0.33 | 67.41 |
| 160.00 | 1.00 | 0.28 | 71.85 |
| 160.00 | 2.00 | 0.29 | 71.11 |
| 160.00 | 3.00 | 0.33 | 67.41 |
| 160.00 | 4.00 | 0.30 | 69.63 |
| 160.00 | 5.00 | 0.25 | 74.81 |
| 160.00 | 6.00 | 0.36 | 64.44 |
| 160.00 | 7.00 | 0.33 | 67.41 |
| 160.00 | 8.00 | 0.34 | 65.93 |
| 160.00 | 9.00 | 0.31 | 68.89 |
| 160.00 | 10.00 | 0.35 | 65.19 |
| 180.00 | 1.00 | 0.25 | 74.81 |
| 180.00 | 2.00 | 0.28 | 71.85 |
| 180.00 | 3.00 | 0.32 | 68.15 |
| 180.00 | 4.00 | 0.29 | 71.11 |
| 180.00 | 5.00 | 0.32 | 68.15 |
| 180.00 | 6.00 | 0.30 | 69.63 |
| 180.00 | 7.00 | 0.32 | 68.15 |
| 180.00 | 8.00 | 0.32 | 68.15 |

| | | | |
|--------|-------|------|-------|
| 180.00 | 9.00 | 0.36 | 64.44 |
| 180.00 | 10.00 | 0.32 | 68.15 |
| 200.00 | 1.00 | 0.27 | 72.59 |
| 200.00 | 2.00 | 0.27 | 72.59 |
| 200.00 | 3.00 | 0.28 | 71.85 |
| 200.00 | 4.00 | 0.27 | 72.59 |
| 200.00 | 5.00 | 0.33 | 66.67 |
| 200.00 | 6.00 | 0.30 | 69.63 |
| 200.00 | 7.00 | 0.27 | 72.59 |
| 200.00 | 8.00 | 0.30 | 69.63 |
| 200.00 | 9.00 | 0.35 | 65.19 |
| 200.00 | 10.00 | 0.30 | 69.63 |

D Histograms of Metrics







E Behaviour Classifier Validation Notes

08/22/19

- frame = interested (label)
- name = labeled

| case | 'frame' | 'PvX>Mean' | 'PvY>Mean' | 'InterestedFrame' | Elongation % | Elongation? | Shape descr notes |
|------|---------|------------|------------|-------------------|--------------|-------------|-------------------------------------|
| 1 | 2 | 1 | 0 | 0 | 31.3393186 | 1 | along |
| 1 | 3 | 1 | 0 | 0 | 14.2364495 | 1 | along |
| 1 | 4 | 1 | 0 | 0 | -3.8310424 | 0 | |
| 1 | 5 | 1 | 1 | 1 | -10.534414 | 0 | cell moving |
| 1 | 6 | 0 | 1 | 0 | -17.500288 | 0 | |
| 1 | 7 | 0 | 1 | 0 | -13.525951 | 0 | |
| 1 | 8 | 1 | 1 | 1 | 6.01110817 | 0 | move up |
| 1 | 9 | 1 | 1 | 1 | 3.71029135 | 0 | cell moving |
| 1 | 10 | 1 | 0 | 0 | 18.6002429 | 1 | extend pseudopod |
| 1 | 11 | 1 | 0 | 0 | 32.8629512 | 1 | nucleus elong |
| 1 | 12 | 1 | 0 | 0 | 4.19404916 | 0 | M-shape |
| 1 | 13 | 1 | 1 | 1 | -17.252568 | 0 | M-shape |
| 1 | 14 | 1 | 1 | 1 | -15.652053 | 0 | Y shape |
| 1 | 15 | 0 | 1 | 0 | -2.1878678 | 0 | Y-shape |
| 1 | 16 | 0 | 1 | 0 | -0.4329884 | 0 | |
| 1 | 17 | 0 | 1 | 0 | 7.47372282 | 0 | |
| 1 | 18 | 1 | 0 | 0 | 15.4937925 | 1 | nuclei elong cell moving |
| 1 | 19 | 0 | 0 | 0 | -0.3730997 | 0 | |
| 1 | 20 | 0 | 0 | 0 | -9.2438375 | 0 | |
| 2 | 2 | 0 | 1 | 0 | 0.86547764 | 0 | |
| 2 | 3 | 1 | 1 | 1 | 0.17303847 | 0 | extend pseudopod ignore! |
| 2 | 4 | 0 | 1 | 0 | 0.49156052 | 0 | |
| 2 | 5 | 1 | 1 | 1 | 3.12728426 | 0 | Some bias up-right |
| 2 | 6 | 0 | 1 | 0 | 2.42080113 | 0 | |
| 2 | 7 | 0 | 1 | 0 | 1.23222885 | 0 | |
| 2 | 8 | 0 | 1 | 0 | 2.13907157 | 0 | |
| 2 | 9 | 0 | 1 | 0 | 2.32304259 | 0 | |
| 2 | 10 | 0 | 1 | 0 | 0.74768958 | 0 | |
| 2 | 11 | 0 | 0 | 0 | -2.019226 | 0 | |
| 2 | 12 | 0 | 0 | 0 | -1.7800501 | 0 | |
| 2 | 13 | 1 | 1 | 1 | -0.071932 | 0 | grow pseudopod up-left |
| 2 | 14 | 0 | 1 | 0 | -1.0690688 | 0 | |
| 2 | 15 | 0 | 1 | 0 | -3.2328266 | 0 | |
| 2 | 16 | 0 | 1 | 0 | -2.8734268 | 0 | |
| 2 | 17 | 1 | 1 | 1 | -0.5993773 | 0 | grow upper left corner |
| 2 | 18 | 1 | 1 | 1 | -0.3091252 | 0 | |
| 2 | 19 | 0 | 1 | 0 | -1.3325034 | 0 | |
| 2 | 20 | 0 | 1 | 0 | -1.7431717 | 0 | |
| 2 | 21 | 0 | 0 | 0 | -0.7711765 | 0 | |
| 2 | 22 | 0 | 1 | 0 | -0.1170125 | 0 | |
| 2 | 23 | 0 | 1 | 0 | 0.28539944 | 0 | |
| 2 | 24 | 1 | 1 | 1 | 0.98879567 | 0 | ignore, if none Zeroline over |
| 2 | 25 | 0 | 1 | 0 | -0.2899605 | 0 | |

170925 - TL - 13^{1,2}

170925 - TL - 3

| | | | | | | |
|---|----|---|---|---|------------|--------------------------|
| 2 | 26 | 0 | 1 | 0 | -1.9185896 | 0 |
| 2 | 27 | 0 | 0 | 0 | -0.9683975 | 0 |
| 2 | 28 | 1 | 1 | 1 | 1.25491593 | 0 |
| 2 | 29 | 0 | 1 | 0 | -0.012866 | 0 |
| 2 | 30 | 1 | 1 | 1 | -2.7319212 | 0 |
| 2 | 31 | 1 | 1 | 1 | -2.2639451 | 0 |
| 2 | 32 | 0 | 1 | 0 | -0.3219558 | 0 |
| 2 | 33 | 0 | 1 | 0 | 0.08238665 | 0 |
| 2 | 34 | 0 | 1 | 0 | -0.4716006 | 0 |
| 2 | 35 | 0 | 1 | 0 | 0.66147832 | 0 |
| 2 | 36 | 0 | 1 | 0 | 0.49089115 | 0 |
| 2 | 37 | 1 | 1 | 1 | -1.510175 | 0 |
| 2 | 38 | 1 | 1 | 1 | -1.2904291 | 0 Contract back down |
| 2 | 39 | 1 | 1 | 1 | -0.7007478 | 0 |
| 2 | 40 | 1 | 1 | 1 | -0.8383726 | 0 |
| 2 | 41 | 1 | 1 | 1 | -0.2669204 | 0 nucleus very round |
| 2 | 42 | 0 | 1 | 0 | 0.21871897 | 0 |
| 2 | 43 | 1 | 1 | 1 | 0.41907211 | 0 |
| 2 | 44 | 0 | 1 | 0 | 0.40278047 | 0 |
| 2 | 45 | 0 | 1 | 0 | 0.69169324 | 0 |
| 2 | 46 | 0 | 1 | 0 | 0.78898824 | 0 |
| 2 | 47 | 1 | 1 | 1 | -0.6048505 | 0 grow back up left |
| 2 | 48 | 1 | 1 | 1 | -1.3697187 | 0 |
| 2 | 49 | 1 | 1 | 1 | -1.1159311 | 0 |
| 2 | 50 | 1 | 1 | 1 | -0.509362 | 0 |
| 2 | 51 | 1 | 1 | 1 | 2.29682165 | 0 cell elongates |
| 2 | 52 | 0 | 1 | 0 | 3.33467855 | 0 |
| 2 | 53 | 0 | 1 | 0 | 0.71289528 | 0 |
| 2 | 54 | 1 | 1 | 1 | -0.8322882 | 0 |
| 2 | 55 | 1 | 0 | 0 | -0.9437334 | 0 |
| 2 | 56 | 0 | 1 | 0 | -0.5539361 | 0 |
| 2 | 57 | 0 | 1 | 0 | 1.16967128 | 0 |
| 2 | 58 | 0 | 1 | 0 | 3.93902353 | 0 |
| 2 | 59 | 0 | 1 | 0 | 4.68915223 | 0 |
| 2 | 60 | 0 | 1 | 0 | 4.20112555 | 0 |
| 2 | 61 | 1 | 1 | 1 | 2.22510875 | 0 changes shape |
| 2 | 62 | 1 | 1 | 1 | -2.2311197 | 0 |
| 2 | 63 | 1 | 1 | 1 | -2.474633 | 0 |
| 2 | 64 | 1 | 1 | 1 | 1.3904151 | 0 Starts to curve around |
| 2 | 65 | 1 | 1 | 1 | 1.50232692 | 0 |
| 2 | 66 | 1 | 1 | 1 | 0.62541015 | 0 |
| 2 | 67 | 1 | 1 | 1 | 0.28925148 | 0 |
| 2 | 68 | 1 | 1 | 1 | -0.1848759 | 0 |
| 2 | 69 | 1 | 1 | 1 | 3.6764347 | 0 |
| 2 | 70 | 1 | 1 | 1 | 6.29833628 | 0 |

| | | | | | | | |
|---|------------|---|---|---|------------|---|----------------------|
| 2 | <u>71</u> | 1 | 1 | 1 | 8.22984681 | 0 | v-shape |
| 2 | <u>72</u> | 1 | 1 | 1 | 31.5567249 | 1 | move down left |
| 2 | <u>73</u> | 1 | 1 | 1 | 29.6768505 | 1 | |
| 2 | <u>74</u> | 1 | 1 | 1 | 0.55609235 | 0 | move left |
| 2 | <u>75</u> | 1 | 1 | 1 | -7.9139315 | 0 | |
| 2 | <u>76</u> | 1 | 1 | 1 | -2.4994228 | 0 | |
| 2 | <u>77</u> | 1 | 1 | 1 | -5.2874506 | 0 | |
| 2 | <u>78</u> | 1 | 1 | 1 | -6.4267053 | 0 | |
| 2 | <u>79</u> | 1 | 1 | 1 | -1.127008 | 0 | |
| 2 | <u>80</u> | 1 | 1 | 1 | 2.93264418 | 0 | |
| 2 | <u>81</u> | 1 | 0 | 0 | 1.70253688 | 0 | |
| 2 | <u>82</u> | 1 | 1 | 1 | -1.4316534 | 0 | Changing Shape |
| 2 | <u>83</u> | 1 | 1 | 1 | -2.5270998 | 0 | |
| 2 | <u>84</u> | 1 | 1 | 1 | -1.3070506 | 0 | |
| 2 | <u>85</u> | 1 | 1 | 1 | -1.9493402 | 0 | |
| 2 | <u>86</u> | 1 | 1 | 1 | -3.9198084 | 0 | |
| 2 | <u>87</u> | 0 | 1 | 0 | -3.8350062 | 0 | |
| 2 | <u>88</u> | 1 | 1 | 1 | -3.1975239 | 0 | Stretching arms down |
| 2 | <u>89</u> | 1 | 1 | 1 | -3.6403218 | 0 | |
| 2 | <u>90</u> | 1 | 1 | 1 | -3.8891111 | 0 | |
| 2 | <u>91</u> | 1 | 1 | 1 | -3.7466913 | 0 | |
| 2 | <u>92</u> | 1 | 1 | 1 | -4.5816892 | 0 | |
| 2 | <u>93</u> | 1 | 0 | 0 | -4.7650627 | 0 | |
| 2 | <u>94</u> | 1 | 0 | 0 | -2.9057653 | 0 | |
| 2 | <u>95</u> | 1 | 1 | 1 | -0.8428627 | 0 | nucleus round |
| 2 | <u>96</u> | 1 | 1 | 1 | 1.78984024 | 0 | |
| 2 | <u>97</u> | 1 | 1 | 1 | 2.53073354 | 0 | |
| 2 | <u>98</u> | 1 | 1 | 1 | 0.86245651 | 0 | |
| 2 | <u>99</u> | 1 | 1 | 1 | -0.3135123 | 0 | |
| 2 | <u>100</u> | 1 | 1 | 1 | -0.62759 | 0 | |
| 2 | <u>101</u> | 1 | 1 | 1 | 0.59032698 | 0 | |
| 2 | <u>102</u> | 1 | 1 | 1 | 0.69557223 | 0 | |
| 2 | <u>103</u> | 0 | 0 | 0 | -1.1438095 | 0 | |
| 2 | <u>104</u> | 0 | 0 | 0 | -0.9011938 | 0 | |
| 2 | <u>105</u> | 0 | 1 | 0 | 1.39242041 | 0 | |
| 2 | <u>106</u> | 0 | 1 | 0 | 1.27844585 | 0 | |
| 2 | <u>107</u> | 1 | 1 | 1 | -0.2093244 | 0 | |
| 2 | <u>108</u> | 1 | 1 | 1 | 2.18834953 | 0 | |
| 2 | <u>109</u> | 1 | 1 | 1 | 6.65213743 | 0 | |
| 2 | <u>110</u> | 1 | 1 | 1 | 9.30426128 | 0 | |
| 2 | <u>111</u> | 1 | 1 | 1 | 8.59848897 | 0 | |
| 2 | <u>112</u> | 1 | 1 | 1 | 8.80754183 | 0 | |
| 2 | <u>113</u> | 1 | 1 | 1 | 10.7299458 | 0 | |
| 2 | <u>114</u> | 1 | 1 | 1 | 5.68762504 | 0 | |
| 2 | <u>115</u> | 1 | 1 | 1 | -4.3303049 | 0 | v-shape |

| | | | | | | |
|---|-----|---|---|---|------------|-----------------|
| 2 | 116 | 1 | 1 | 1 | -10.419341 | 0 |
| 2 | 117 | 1 | 1 | 1 | -7.3436573 | 0 |
| 2 | 118 | 1 | 1 | 1 | -0.7783249 | 0 |
| 2 | 119 | 0 | 1 | 0 | 1.34344247 | 0 |
| 2 | 120 | 1 | 1 | 1 | 0.85725267 | 0 move up left |
| 2 | 121 | 1 | 1 | 1 | -2.2479198 | 0 |
| 2 | 122 | 1 | 1 | 1 | -7.3171956 | 0 |
| 2 | 123 | 1 | 1 | 1 | -8.7160073 | 0 o-shape → |
| 2 | 124 | 1 | 1 | 1 | -3.6279217 | 0 |
| 2 | 125 | 0 | 1 | 0 | -0.1109815 | 0 |
| 2 | 126 | 1 | 1 | 1 | -0.6443003 | 0 |
| 2 | 127 | 0 | 1 | 0 | 0.04253239 | 0 |
| 2 | 128 | 0 | 1 | 0 | 2.09231892 | 0 |
| 2 | 129 | 0 | 1 | 0 | 1.76521501 | 0 |
| 2 | 130 | 0 | 1 | 0 | -0.7407162 | 0 |
| 2 | 131 | 1 | 1 | 1 | -5.5774024 | 0 straighten up |
| 2 | 132 | 1 | 1 | 1 | -11.953028 | 0 |
| 2 | 133 | 1 | 1 | 1 | -10.957053 | 0 |
| 2 | 134 | 1 | 1 | 1 | -4.7465972 | 0 |
| 2 | 135 | 1 | 1 | 1 | -2.0071964 | 0 |
| 2 | 136 | 1 | 1 | 1 | -0.3365034 | 0 |
| 2 | 137 | 1 | 1 | 1 | 0.48872362 | 0 |
| 2 | 138 | 0 | 1 | 0 | 0.77791408 | 0 |
| 2 | 139 | 1 | 1 | 1 | 3.07191438 | 0 |
| 2 | 140 | 1 | 1 | 1 | 13.428891 | 1 Y-shaped |
| 2 | 141 | 1 | 1 | 1 | 14.9632419 | 1 |
| 2 | 142 | 1 | 1 | 1 | 20.478786 | 1 |
| 2 | 143 | 1 | 1 | 1 | 23.2875725 | 1 charge right |
| 2 | 144 | 1 | 1 | 1 | 2.13026885 | 0 |
| 2 | 145 | 1 | 1 | 1 | -12.058865 | 0 |
| 2 | 146 | 1 | 1 | 1 | -11.879348 | 0 |
| 2 | 147 | 1 | 1 | 1 | -8.3356022 | 0 |
| 2 | 148 | 1 | 1 | 1 | -5.482387 | 0 |
| 2 | 149 | 1 | 1 | 1 | -4.2104676 | 0 |
| 2 | 150 | 1 | 1 | 1 | -2.6292146 | 0 |
| 3 | 2 | 1 | 0 | 0 | 3.87062728 | 0 |
| 3 | 3 | 1 | 0 | 0 | 7.78617 | 0 u-shape |
| 3 | 4 | 1 | 0 | 0 | -1.7360871 | 0 u-shape |
| 3 | 5 | 1 | 0 | 0 | -5.3122341 | 0 |
| 3 | 6 | 0 | 0 | 0 | 5.4496959 | 0 |
| 3 | 7 | 0 | 0 | 0 | 7.41783317 | 0 |
| 3 | 8 | 0 | 1 | 0 | -1.4246579 | 0 p 0 |
| 3 | 9 | 0 | 1 | 0 | -7.3477422 | 0 c 0 |
| 3 | 10 | 0 | 1 | 0 | -0.5224036 | 0 |
| 3 | 11 | 0 | 1 | 0 | 16.9846484 | 1 elong |

176929 - Timeline - 6A
174022 - 1A - 2B

| | | | | | | |
|---|----|---|---|---|------------|------------|
| 3 | 12 | 0 | 1 | 0 | 18.2567258 | 1 |
| 4 | 2 | 1 | 0 | 0 | 1.11606083 | 0 |
| 4 | 3 | 1 | 0 | 0 | 1.65721011 | 0 |
| 4 | 4 | 0 | 0 | 0 | -1.4513896 | 0 |
| 4 | 5 | 0 | 0 | 0 | -4.6454406 | 0 |
| 4 | 6 | 0 | 0 | 0 | -3.9885477 | 0 |
| 4 | 7 | 1 | 0 | 0 | -2.7922063 | 0 |
| 4 | 8 | 0 | 0 | 0 | -2.1308397 | 0 |
| 4 | 9 | 0 | 0 | 0 | -0.2223873 | 0 |
| 4 | 10 | 1 | 0 | 0 | 2.17527579 | 0 |
| 4 | 11 | 1 | 1 | 1 | 3.7547388 | 0 movement |
| 4 | 12 | 0 | 0 | 0 | 2.46723132 | 0 |
| 4 | 13 | 0 | 0 | 0 | -0.1945019 | 0 |
| 4 | 14 | 0 | 0 | 0 | -1.7525868 | 0 |
| 4 | 15 | 0 | 0 | 0 | -0.8924862 | 0 |
| 4 | 16 | 1 | 0 | 0 | 2.71425122 | 0 |
| 4 | 17 | 1 | 0 | 0 | 4.3445018 | 0 |
| 4 | 18 | 1 | 0 | 0 | 1.3802256 | 0 |
| 4 | 19 | 0 | 0 | 0 | -0.9383151 | 0 |
| 4 | 20 | 1 | 0 | 0 | -0.4203785 | 0 |
| 4 | 21 | 0 | 0 | 0 | -0.273012 | 0 |
| 4 | 22 | 0 | 0 | 0 | -0.3758465 | 0 |
| 4 | 23 | 0 | 0 | 0 | -0.398808 | 0 |
| 4 | 24 | 1 | 0 | 0 | 3.6129132 | 0 |
| 4 | 25 | 1 | 0 | 0 | 12.2138942 | 1 elong |
| 4 | 26 | 1 | 1 | 1 | 12.0709958 | 1 elong |
| 4 | 27 | 1 | 1 | 1 | 4.77602835 | 0 movement |
| 4 | 28 | 1 | 1 | 1 | 0.2443854 | 0 movement |
| 4 | 29 | 1 | 1 | 1 | -0.1066735 | 0 movement |
| 4 | 30 | 1 | 1 | 1 | 0.06163282 | 0 movement |
| 4 | 31 | 1 | 1 | 1 | -2.1629915 | 0 |
| 4 | 32 | 1 | 1 | 1 | -3.9700364 | 0 |
| 4 | 33 | 1 | 1 | 1 | 0.23513592 | 0 Y-shape |
| 4 | 34 | 0 | 1 | 0 | 7.83311425 | 0 Y-shape |
| 4 | 35 | 0 | 1 | 0 | 7.8868557 | 0 |
| 5 | 2 | 0 | 1 | 0 | -3.2580351 | 0 |
| 5 | 3 | 0 | 1 | 0 | -6.6886871 | 0 |
| 5 | 4 | 1 | 1 | 1 | 0.45471865 | 0 |
| 5 | 5 | 1 | 1 | 1 | 15.1780297 | 1 |
| 5 | 6 | 1 | 1 | 1 | 48.6253967 | 1 |
| 5 | 7 | 1 | 1 | 1 | 61.826582 | 1 |
| 5 | 8 | 1 | 1 | 1 | 30.9594696 | 1 |
| 5 | 9 | 1 | 1 | 1 | 8.91667562 | 0 |
| 5 | 10 | 1 | 1 | 1 | 1.95778145 | 0 |
| 5 | 11 | 1 | 1 | 1 | -1.7498256 | 0 |

| | | | | | | |
|---|----|---|---|---|------------|---|
| 5 | 12 | 0 | 1 | 0 | -3.1483169 | 0 |
| 5 | 13 | 0 | 0 | 0 | -2.2167363 | 0 |
| 5 | 14 | 0 | 1 | 0 | -3.5235624 | 0 |
| 5 | 15 | 0 | 1 | 0 | -6.5693616 | 0 |
| 5 | 16 | 0 | 0 | 0 | -6.2791774 | 0 |
| 5 | 17 | 0 | 1 | 0 | -1.2335507 | 0 |
| 5 | 18 | 0 | 1 | 0 | 2.90009508 | 0 |
| 5 | 19 | 0 | 1 | 0 | 3.08582911 | 0 |
| 5 | 20 | 0 | 1 | 0 | 2.10697274 | 0 |
| 5 | 21 | 0 | 0 | 0 | 0.31097628 | 0 |
| 5 | 22 | 0 | 0 | 0 | -1.1130394 | 0 |
| 5 | 23 | 0 | 1 | 0 | 0.04403848 | 0 |
| 5 | 24 | 0 | 1 | 0 | 1.38110245 | 0 |
| 5 | 25 | 1 | 1 | 1 | 3.09219874 | 0 |
| 5 | 26 | 1 | 0 | 0 | 6.32856485 | 0 |
| 5 | 27 | 1 | 1 | 1 | 6.41182015 | 0 |
| 5 | 28 | 1 | 0 | 0 | 2.9352382 | 0 |
| 5 | 29 | 1 | 0 | 0 | 1.50910324 | 0 |
| 5 | 30 | 1 | 1 | 1 | 2.73113771 | 0 |
| 5 | 31 | 1 | 1 | 1 | 3.48490458 | 0 |
| 5 | 32 | 1 | 1 | 1 | 5.17361345 | 0 |
| 5 | 33 | 1 | 1 | 1 | 7.15348764 | 0 |
| 5 | 34 | 1 | 1 | 1 | 6.77722298 | 0 |
| 5 | 35 | 1 | 1 | 1 | 2.83233569 | 0 |
| 5 | 36 | 1 | 1 | 1 | -2.3946312 | 0 |
| 5 | 37 | 0 | 1 | 0 | -3.5454933 | 0 |
| 5 | 38 | 0 | 1 | 0 | -2.4200056 | 0 |
| 5 | 39 | 0 | 1 | 0 | -2.7768861 | 0 |
| 5 | 40 | 0 | 1 | 0 | -2.383822 | 0 |
| 5 | 41 | 0 | 1 | 0 | -4.0469136 | 0 |
| 5 | 42 | 0 | 1 | 0 | -7.4366228 | 0 |
| 5 | 43 | 0 | 0 | 0 | -5.2482488 | 0 |
| 5 | 44 | 1 | 1 | 1 | -1.686381 | 0 |
| 5 | 45 | 1 | 0 | 0 | -1.8428195 | 0 |
| 5 | 46 | 0 | 0 | 0 | -2.0497318 | 0 |
| 5 | 47 | 0 | 0 | 0 | -1.2306546 | 0 |
| 5 | 48 | 0 | 0 | 0 | 1.86491753 | 0 |
| 5 | 49 | 0 | 1 | 0 | 4.23976334 | 0 |
| 5 | 50 | 0 | 1 | 0 | 2.80071307 | 0 |
| 5 | 51 | 0 | 1 | 0 | 0.67419383 | 0 |
| 5 | 52 | 0 | 1 | 0 | -1.3115384 | 0 |
| 5 | 53 | 0 | 1 | 0 | -3.0361518 | 0 |
| 5 | 54 | 0 | 0 | 0 | -3.3609214 | 0 |
| 5 | 55 | 0 | 1 | 0 | -4.3336249 | 0 |
| 5 | 56 | 1 | 1 | 1 | -5.3113994 | 0 |

| | | | | | | |
|---|----|---|---|---|------------|--------------------|
| 5 | 57 | 1 | 1 | 1 | -3.6361062 | 0 |
| 5 | 58 | 1 | 1 | 1 | -2.2187228 | 0 |
| 5 | 59 | 0 | 1 | 0 | -1.8207535 | 0 |
| 5 | 60 | 0 | 0 | 0 | 0.56336751 | 0 |
| 5 | 61 | 0 | 1 | 0 | 2.70062204 | 0 |
| 5 | 62 | 0 | 0 | 0 | 1.80275831 | 0 |
| 5 | 63 | 0 | 0 | 0 | -0.0346502 | 0 |
| 5 | 64 | 0 | 1 | 0 | -0.9683726 | 0 |
| 5 | 65 | 1 | 1 | 1 | -1.0829136 | 0 |
| 5 | 66 | 0 | 1 | 0 | -3.1226108 | 0 |
| 5 | 67 | 1 | 1 | 1 | -5.5045278 | 0 |
| 5 | 68 | 0 | 1 | 0 | -2.8164865 | 0 |
| 5 | 69 | 0 | 0 | 0 | 0.83262362 | 0 |
| 5 | 70 | 1 | 1 | 1 | 0.3369066 | 0 |
| 5 | 71 | 1 | 1 | 1 | -2.321825 | 0 |
| 5 | 72 | 1 | 1 | 1 | -3.4673871 | 0 |
| 6 | 2 | 0 | 0 | 0 | -12.993431 | 0 |
| 6 | 3 | 0 | 1 | 0 | -5.1049368 | 0 |
| 6 | 4 | 0 | 1 | 0 | 18.8208585 | 1 nuclei elong |
| 6 | 5 | 1 | 1 | 1 | 33.2189913 | 1 elong |
| 6 | 6 | 1 | 1 | 1 | 21.6746356 | 1 elong |
| 6 | 7 | 1 | 1 | 1 | -4.8832082 | 0 moving |
| 6 | 8 | 1 | 1 | 1 | -6.3456916 | 0 moving |
| 6 | 9 | 1 | 1 | 1 | 9.60128587 | 0 moving |
| 6 | 10 | 1 | 1 | 1 | 8.59038712 | 0 moving |
| 6 | 11 | 0 | 0 | 0 | -5.2931315 | 0 U-shape |
| 6 | 12 | 0 | 0 | 0 | -20.027061 | 0 U-shape |
| 6 | 13 | 0 | 1 | 0 | -13.86869 | 0 |
| 6 | 14 | 1 | 1 | 1 | 11.9055406 | 0 nuclei elong |
| 6 | 15 | 0 | 1 | 0 | 2.0242326 | 0 V-shape |
| 6 | 16 | 0 | 0 | 0 | -15.738688 | 0 |
| 6 | 17 | 0 | 0 | 0 | -15.47831 | 0 |
| 6 | 18 | 0 | 0 | 0 | -6.6572001 | 0 |
| 6 | 19 | 1 | 0 | 0 | 18.2164371 | 1 |
| 6 | 20 | 1 | 1 | 1 | 31.9037588 | 1 v-shape |
| 6 | 21 | 1 | 1 | 1 | 12.401977 | 1 nuclei elongated |
| 6 | 22 | 1 | 1 | 1 | -3.436258 | 0 moving |
| 6 | 23 | 1 | 1 | 1 | -11.10905 | 0 moving |
| 6 | 24 | 1 | 1 | 1 | -7.3262352 | 0 moving |
| 6 | 25 | 1 | 1 | 1 | 5.80978292 | 0 moving |
| 6 | 26 | 1 | 0 | 0 | 0.52256873 | 0 |
| 6 | 27 | 1 | 0 | 0 | -2.0563024 | 0 |
| 6 | 28 | 1 | 0 | 0 | 13.5194953 | 1 elong |
| 6 | 29 | 1 | 1 | 1 | 17.6029272 | 1 |
| 7 | 2 | 0 | 1 | 0 | -1.2777265 | 0 |

| | | | | | | |
|---|----|---|---|---|------------|------------|
| 7 | 3 | 0 | 1 | 0 | 1.59418687 | 0 |
| 7 | 4 | 0 | 1 | 0 | 0.24736014 | 0 |
| 7 | 5 | 0 | 1 | 0 | -6.7020968 | 0 |
| 7 | 6 | 0 | 1 | 0 | -9.2335158 | 0 |
| 7 | 7 | 0 | 1 | 0 | -3.9957472 | 0 |
| 7 | 8 | 0 | 1 | 0 | 1.3217268 | 0 |
| 7 | 9 | 0 | 1 | 0 | 0.45302003 | 0 |
| 7 | 10 | 1 | 1 | 1 | 5.12546288 | 0 u-shape |
| 7 | 11 | 1 | 0 | 0 | 8.3685999 | 0 u-shape |
| 7 | 12 | 1 | 1 | 1 | 1.7458781 | 0 u-shape |
| 7 | 13 | 1 | 1 | 1 | -1.3477566 | 0 movement |
| 7 | 14 | 1 | 1 | 1 | -4.4731392 | 0 movement |
| 7 | 15 | 0 | 1 | 0 | -9.9767367 | 0 |
| 7 | 16 | 0 | 0 | 0 | -12.837152 | 0 |
| 7 | 17 | 1 | 1 | 1 | -10.016916 | 0 |
| 7 | 18 | 1 | 0 | 0 | -6.0810227 | 0 |
| 7 | 19 | 1 | 0 | 0 | -4.5623303 | 0 |
| 7 | 20 | 1 | 0 | 0 | -0.159417 | 0 |
| 8 | 2 | 0 | 0 | 0 | 2.48131629 | 0 |
| 8 | 3 | 0 | 0 | 0 | 13.7319992 | 1 |
| 8 | 4 | 1 | 1 | 1 | 47.947285 | 1 |
| 8 | 5 | 1 | 1 | 1 | 35.1077356 | 1 |
| 8 | 6 | 1 | 1 | 1 | 2.86127742 | 0 |
| 8 | 7 | 1 | 1 | 1 | -3.0354152 | 0 |
| 8 | 8 | 1 | 1 | 1 | 1.74622711 | 0 |
| 8 | 9 | 1 | 1 | 1 | 0.51940512 | 0 |
| 8 | 10 | 1 | 1 | 1 | 6.02112701 | 0 |
| 8 | 11 | 1 | 1 | 1 | 8.94495902 | 0 |
| 8 | 12 | 1 | 1 | 1 | -2.1944066 | 0 |
| 8 | 13 | 0 | 0 | 0 | -11.665921 | 0 |
| 8 | 14 | 0 | 0 | 0 | -13.039159 | 0 |
| 8 | 15 | 0 | 0 | 0 | -10.543364 | 0 |
| 8 | 16 | 0 | 0 | 0 | -3.3467187 | 0 |
| 8 | 17 | 0 | 0 | 0 | 9.64858086 | 0 |
| 8 | 18 | 1 | 0 | 0 | 18.369332 | 1 |
| 8 | 19 | 1 | 0 | 0 | 11.5268597 | 0 |
| 8 | 20 | 1 | 0 | 0 | 4.78175601 | 0 |
| 8 | 21 | 1 | 0 | 0 | 5.43507054 | 0 |
| 8 | 22 | 1 | 1 | 1 | 2.85043396 | 0 |
| 8 | 23 | 1 | 0 | 0 | -2.5621926 | 0 |
| 8 | 24 | 1 | 0 | 0 | -0.833178 | 0 |
| 8 | 25 | 0 | 0 | 0 | 1.34022856 | 0 |
| 8 | 26 | 0 | 0 | 0 | -2.9720033 | 0 |
| 8 | 27 | 0 | 0 | 0 | -3.6813569 | 0 |
| 8 | 28 | 0 | 0 | 0 | 2.32698412 | 0 |

| | | | | | | |
|----|----|---|---|---|------------|---|
| 8 | 29 | 0 | 0 | 0 | 6.2504534 | 0 |
| 8 | 30 | 0 | 0 | 0 | 1.84056588 | 0 |
| 8 | 31 | 0 | 0 | 0 | -4.7677147 | 0 |
| 8 | 32 | 0 | 0 | 0 | -5.1543929 | 0 |
| 9 | 2 | 0 | 0 | 0 | -3.5324434 | 0 |
| 9 | 3 | 0 | 0 | 0 | -5.4223409 | 0 |
| 9 | 4 | 0 | 0 | 0 | -4.2250473 | 0 |
| 9 | 5 | 0 | 0 | 0 | -1.3161577 | 0 |
| 9 | 6 | 0 | 0 | 0 | 0.52923003 | 0 |
| 9 | 7 | 0 | 0 | 0 | 0.39788969 | 0 |
| 9 | 8 | 0 | 0 | 0 | -0.7476442 | 0 |
| 9 | 9 | 0 | 0 | 0 | -0.0770782 | 0 |
| 9 | 10 | 0 | 0 | 0 | 2.21409305 | 0 |
| 9 | 11 | 0 | 1 | 0 | 2.77863014 | 0 |
| 9 | 12 | 0 | 1 | 0 | 7.4865593 | 0 |
| 9 | 13 | 0 | 1 | 0 | 12.3879214 | 1 |
| 9 | 14 | 0 | 1 | 0 | 5.14269762 | 0 |
| 9 | 15 | 0 | 1 | 0 | -3.4911683 | 0 |
| 9 | 16 | 1 | 1 | 1 | -0.0902073 | 0 |
| 9 | 17 | 1 | 1 | 1 | 17.830871 | 1 |
| 9 | 18 | 1 | 1 | 1 | 20.1664152 | 1 |
| 9 | 19 | 1 | 1 | 1 | 5.62527986 | 0 |
| 9 | 20 | 1 | 1 | 1 | -1.8619581 | 0 |
| 9 | 21 | 1 | 1 | 1 | -3.8876634 | 0 |
| 10 | 2 | 1 | 1 | 1 | -2.134413 | 0 |
| 10 | 3 | 1 | 1 | 1 | -3.7884242 | 0 |
| 10 | 4 | 1 | 1 | 1 | -6.3320741 | 0 |
| 10 | 5 | 1 | 1 | 1 | 1.82132657 | 0 |
| 10 | 6 | 1 | 1 | 1 | 14.2778183 | 1 |
| 10 | 7 | 1 | 1 | 1 | 1.2716946 | 0 |
| 10 | 8 | 1 | 1 | 1 | -12.766939 | 0 |
| 10 | 9 | 1 | 1 | 1 | -6.4750909 | 0 |
| 10 | 10 | 1 | 1 | 1 | 1.5033674 | 0 |
| 10 | 11 | 1 | 1 | 1 | -6.0558734 | 0 |
| 10 | 12 | 1 | 1 | 1 | -10.603482 | 0 |
| 10 | 13 | 1 | 1 | 1 | -3.7806582 | 0 |
| 10 | 14 | 1 | 1 | 1 | -0.0729131 | 0 |
| 10 | 15 | 1 | 1 | 1 | 3.77878786 | 0 |
| 10 | 16 | 1 | 1 | 1 | 18.4227732 | 1 |
| 10 | 17 | 0 | 1 | 0 | 16.7336301 | 1 |
| 10 | 18 | 1 | 1 | 1 | 1.62244798 | 0 |
| 10 | 19 | 1 | 1 | 1 | -3.1701866 | 0 |
| 10 | 20 | 1 | 1 | 1 | 1.49927383 | 0 |
| 10 | 21 | 1 | 1 | 1 | -0.9054071 | 0 |
| 10 | 22 | 0 | 1 | 0 | -8.5218207 | 0 |

| | | | | | | |
|----|----|---|---|---|------------|---------------|
| 10 | 23 | 1 | 1 | 1 | -7.873969 | 0 |
| 10 | 24 | 1 | 1 | 1 | -3.8433039 | 0 |
| 10 | 25 | 1 | 1 | 1 | -5.2634618 | 0 |
| 10 | 26 | 1 | 1 | 1 | -3.3542517 | 0 |
| 10 | 27 | 1 | 1 | 1 | -3.6194183 | 0 |
| 10 | 28 | 1 | 1 | 1 | -2.3251527 | 0 |
| 10 | 29 | 1 | 1 | 1 | 14.9385274 | 1 |
| 10 | 30 | 1 | 1 | 1 | 17.4105684 | 1 |
| 10 | 31 | 1 | 1 | 1 | 1.54453632 | 0 |
| 10 | 32 | 1 | 1 | 1 | -8.071578 | 0 |
| 10 | 33 | 1 | 1 | 1 | -7.9042236 | 0 |
| 10 | 34 | 1 | 1 | 1 | 4.0738124 | 0 |
| 10 | 35 | 1 | 1 | 1 | 13.3270224 | 1 |
| 11 | 2 | 0 | 1 | 0 | 0.68203849 | 0 |
| 11 | 3 | 0 | 1 | 0 | 9.1552759 | 0 |
| 11 | 4 | 1 | 1 | 1 | 5.2093428 | 0 |
| 11 | 5 | 1 | 1 | 1 | -2.7548512 | 0 |
| 11 | 6 | 0 | 1 | 0 | 8.93363836 | 0 |
| 11 | 7 | 0 | 1 | 0 | 13.5830498 | 1 along |
| 11 | 8 | 0 | 1 | 0 | 1.19987755 | 0 |
| 11 | 9 | 0 | 1 | 0 | -3.8372974 | 0 |
| 11 | 10 | 0 | 1 | 0 | -4.5153453 | 0 |
| 11 | 11 | 0 | 1 | 0 | -10.618855 | 0 |
| 11 | 12 | 1 | 1 | 1 | 3.19346263 | 0 movement |
| 11 | 13 | 1 | 1 | 1 | 14.10284 | 1 Y-shape |
| 11 | 14 | 1 | 1 | 1 | -6.2217497 | 0 Y-shape |
| 11 | 15 | 1 | 1 | 1 | 4.64387581 | 0 |
| 11 | 16 | 1 | 1 | 1 | 32.3636217 | 1 close |
| 11 | 17 | 1 | 1 | 1 | 16.6207131 | 1 close |
| 11 | 18 | 1 | 1 | 1 | 0.09999833 | 0 |
| 11 | 19 | 1 | 1 | 1 | -2.7570486 | 0 |
| 11 | 20 | 0 | 1 | 0 | -6.7466023 | 0 |
| 11 | 21 | 0 | 1 | 0 | -11.450787 | 0 |
| 11 | 22 | 0 | 0 | 0 | -7.2951242 | 0 |
| 11 | 23 | 1 | 1 | 1 | -0.1133097 | 0 V-shape |
| 11 | 24 | 1 | 1 | 1 | 9.54624726 | 0 V-shape |
| 11 | 25 | 1 | 1 | 1 | 13.333856 | 1 V-shape |
| 11 | 26 | 1 | 1 | 1 | 2.76789808 | 0 close |
| 11 | 27 | 1 | 1 | 1 | 4.71099394 | 0 |
| 11 | 28 | 1 | 1 | 1 | 9.30995375 | 0 |
| 11 | 29 | 1 | 1 | 1 | -4.867094 | 0 |
| 11 | 30 | 0 | 1 | 0 | -12.250852 | 0 |
| 11 | 31 | 1 | 1 | 1 | -10.76872 | 0 Y-shape |
| 11 | 32 | 1 | 1 | 1 | 4.53333144 | 0 |
| 11 | 33 | 1 | 1 | 1 | 16.4380006 | 1 Y-shape/ele |

| | | | | | | | |
|----|----|---|---|---|------------|---|----------|
| 11 | 34 | 1 | 1 | 1 | -4.316442 | 0 | Y-shape |
| 11 | 35 | 1 | 1 | 1 | -15.335277 | 0 | — |
| 12 | 2 | 1 | 0 | 0 | 0.591471 | 0 | U-shape |
| 12 | 3 | 1 | 0 | 0 | -1.1114164 | 0 | U-shape |
| 12 | 4 | 1 | 0 | 0 | -2.6338361 | 0 | U-shape |
| 12 | 5 | 1 | 0 | 0 | -3.1788786 | 0 | U-shape |
| 12 | 6 | 0 | 0 | 0 | -4.2449823 | 0 | U-shape |
| 12 | 7 | 0 | 0 | 0 | -6.6628741 | 0 | U-shape |
| 12 | 8 | 1 | 0 | 0 | -0.0019274 | 0 | U-shape |
| 12 | 9 | 1 | 0 | 0 | 14.9342511 | 1 | → elong |
| 12 | 10 | 1 | 0 | 0 | 13.9203512 | 1 | elang |
| 12 | 11 | 1 | 0 | 0 | 4.58078338 | 0 | U-turn |
| 12 | 12 | 1 | 0 | 0 | -0.4835757 | 0 | U-shape |
| 12 | 13 | 1 | 1 | 1 | -5.472507 | 0 | movement |
| 12 | 14 | 1 | 1 | 1 | -13.641718 | 0 | Y-shape |
| 12 | 15 | 1 | 1 | 1 | -17.007778 | 0 | Y-shape |
| 12 | 16 | 1 | 0 | 0 | -7.9335872 | 0 | — |
| 12 | 17 | 0 | 0 | 0 | 2.70840907 | 0 | — |
| 12 | 18 | 1 | 0 | 0 | 9.47846415 | 0 | — |
| 12 | 19 | 1 | 1 | 1 | 10.9824069 | 0 | movement |
| 12 | 20 | 0 | 1 | 0 | -1.0287683 | 0 | — |
| 12 | 21 | 0 | 1 | 0 | -13.338913 | 0 | Y-shape |
| 12 | 22 | 1 | 1 | 1 | -8.9963806 | 0 | movement |
| 12 | 23 | 1 | 1 | 1 | 9.98580567 | 0 | movement |
| 12 | 24 | 0 | 1 | 0 | 9.35976837 | 0 | — |
| 12 | 25 | 0 | 1 | 0 | -0.0623742 | 0 | — |
| 12 | 26 | 0 | 1 | 0 | 1.21505786 | 0 | — |
| 12 | 27 | 0 | 1 | 0 | -0.7935728 | 0 | — |
| 12 | 28 | 0 | 1 | 0 | -7.238083 | 0 | — |
| 12 | 29 | 0 | 1 | 0 | -8.0517875 | 0 | — |
| 12 | 30 | 1 | 1 | 1 | -4.7201513 | 0 | — |
| 12 | 31 | 0 | 1 | 0 | -2.4895811 | 0 | — |
| 12 | 32 | 0 | 1 | 0 | -1.1162549 | 0 | Y-shape |
| 12 | 33 | 1 | 0 | 0 | -1.6119061 | 0 | Y-shape |
| 12 | 34 | 1 | 0 | 0 | -0.7551025 | 0 | U-shape |
| 12 | 35 | 1 | 0 | 0 | 4.40945469 | 0 | U-shape |
| 13 | 2 | 0 | 1 | 0 | -3.5122277 | 0 | — |
| 13 | 3 | 0 | 1 | 0 | -3.7017673 | 0 | — |
| 13 | 4 | 0 | 1 | 0 | -1.5413044 | 0 | — |
| 13 | 5 | 0 | 1 | 0 | -0.5463695 | 0 | — |
| 13 | 6 | 0 | 1 | 0 | 0.01922023 | 0 | — |
| 13 | 7 | 0 | 1 | 0 | -2.9931798 | 0 | — |
| 13 | 8 | 1 | 1 | 1 | -9.1730295 | 0 | — |
| 13 | 9 | 1 | 1 | 1 | -10.940774 | 0 | — |
| 13 | 10 | 0 | 0 | 0 | -6.4461629 | 0 | — |

| | | | | | | |
|----|----|---|---|---|------------|---|
| 13 | 11 | 0 | 1 | 0 | -3.1269855 | 0 |
| 13 | 12 | 0 | 1 | 0 | -2.7659697 | 0 |
| 13 | 13 | 0 | 0 | 0 | -2.817551 | 0 |
| 13 | 14 | 0 | 0 | 0 | -1.9013708 | 0 |
| 13 | 15 | 0 | 0 | 0 | -0.5341511 | 0 |
| 13 | 16 | 0 | 1 | 0 | 0.35676381 | 0 |
| 13 | 17 | 1 | 1 | 1 | 1.14299825 | 0 |
| 13 | 18 | 1 | 1 | 1 | 1.6060227 | 0 |
| 13 | 19 | 1 | 1 | 1 | 4.35422941 | 0 |
| 13 | 20 | 1 | 1 | 1 | 7.60064138 | 0 |
| 13 | 21 | 1 | 0 | 0 | 16.9240304 | 1 |
| 13 | 22 | 1 | 0 | 0 | 20.0619564 | 1 |
| 13 | 23 | 1 | 0 | 0 | 4.12564164 | 0 |
| 13 | 24 | 1 | 0 | 0 | -8.7836327 | 0 |
| 13 | 25 | 1 | 0 | 0 | -8.8012575 | 0 |
| 14 | 2 | 1 | 1 | 1 | -7.3721753 | 0 |
| 14 | 3 | 1 | 1 | 1 | -0.9146562 | 0 |
| 14 | 4 | 0 | 1 | 0 | 4.57557366 | 0 |
| 14 | 5 | 0 | 0 | 0 | -1.1190563 | 0 |
| 14 | 6 | 0 | 0 | 0 | -2.9945056 | 0 |
| 14 | 7 | 0 | 0 | 0 | -0.1575257 | 0 |
| 14 | 8 | 1 | 0 | 0 | 1.94048229 | 0 |
| 14 | 9 | 1 | 1 | 1 | 7.09956992 | 0 |
| 14 | 10 | 0 | 1 | 0 | 7.28721791 | 0 |
| 15 | 2 | 0 | 1 | 0 | 5.44079156 | 0 |
| 15 | 3 | 1 | 1 | 1 | -1.8548831 | 0 |
| 15 | 4 | 1 | 0 | 0 | -9.1979819 | 0 |
| 15 | 5 | 1 | 1 | 1 | 13.426183 | 1 |
| 15 | 6 | 1 | 1 | 1 | 28.099766 | 1 |
| 15 | 7 | 1 | 1 | 1 | 9.51326111 | 0 |
| 15 | 8 | 1 | 1 | 1 | -3.8014131 | 0 |
| 15 | 9 | 1 | 1 | 1 | -13.158528 | 0 |
| 15 | 10 | 0 | 1 | 0 | -17.356244 | 0 |
| 15 | 11 | 0 | 1 | 0 | -16.318161 | 0 |
| 15 | 12 | 0 | 1 | 0 | -16.92664 | 0 |
| 15 | 13 | 0 | 1 | 0 | -10.590602 | 0 |
| 15 | 14 | 0 | 0 | 0 | -1.5946573 | 0 |
| 15 | 15 | 0 | 0 | 0 | -0.267828 | 0 |
| 16 | 2 | 1 | 0 | 0 | 13.4676876 | 1 |
| 16 | 3 | 1 | 0 | 0 | 3.20501598 | 0 |
| 16 | 4 | 0 | 1 | 0 | -4.0836678 | 0 |
| 16 | 5 | 0 | 1 | 0 | -0.7940344 | 0 |
| 16 | 6 | 1 | 1 | 1 | 5.73309497 | 0 |
| 16 | 7 | 1 | 1 | 1 | 0.68059817 | 0 |
| 16 | 8 | 1 | 1 | 1 | -8.8024116 | 0 |

2020-12-28

2020-12-21

2020-12-14 - 1H

2020-12-15 - S

| | | | | | | |
|----|----|---|---|---|------------|---|
| 16 | 9 | 1 | 0 | 0 | 0.62072529 | 0 |
| 16 | 10 | 1 | 0 | 0 | 15.4879294 | 1 |
| 16 | 11 | 1 | 0 | 0 | 5.47974149 | 0 |
| 16 | 12 | 1 | 1 | 1 | 0.9527184 | 0 |
| 16 | 13 | 1 | 1 | 1 | 9.29375685 | 0 |
| 16 | 14 | 1 | 1 | 1 | 1.70243316 | 0 |
| 16 | 15 | 1 | 1 | 1 | -8.2051011 | 0 |
| 16 | 16 | 0 | 1 | 0 | -6.979988 | 0 |
| 16 | 17 | 0 | 1 | 0 | -4.4512744 | 0 |
| 16 | 18 | 0 | 1 | 0 | -4.961522 | 0 |
| 16 | 19 | 0 | 1 | 0 | -6.0407934 | 0 |
| 16 | 20 | 0 | 0 | 0 | -4.1568901 | 0 |
| 16 | 21 | 0 | 0 | 0 | -2.7096434 | 0 |
| 16 | 22 | 0 | 0 | 0 | -5.3611055 | 0 |
| 16 | 23 | 0 | 0 | 0 | -9.3732678 | 0 |
| 16 | 24 | 0 | 1 | 0 | -8.4129349 | 0 |
| 16 | 25 | 0 | 1 | 0 | 0.08581227 | 0 |
| 16 | 26 | 1 | 1 | 1 | 12.1870603 | 1 |
| 16 | 27 | 1 | 1 | 1 | 18.2823524 | 1 |
| 16 | 28 | 1 | 1 | 1 | 11.2171422 | 0 |
| 16 | 29 | 1 | 1 | 1 | 2.34368023 | 0 |
| 16 | 30 | 0 | 1 | 0 | -0.9044658 | 0 |
| 17 | 2 | 1 | 1 | 1 | -8.3212829 | 0 |
| 17 | 3 | 0 | 1 | 0 | -6.8428296 | 0 |
| 17 | 4 | 0 | 1 | 0 | -2.5264699 | 0 |
| 17 | 5 | 0 | 1 | 0 | -1.9035211 | 0 |
| 17 | 6 | 1 | 1 | 1 | 0.18723263 | 0 |
| 17 | 7 | 1 | 1 | 1 | 7.14822924 | 0 |
| 17 | 8 | 1 | 1 | 1 | 17.5288999 | 1 |
| 17 | 9 | 1 | 1 | 1 | 18.7723078 | 1 |
| 17 | 10 | 1 | 1 | 1 | 9.42707564 | 0 |
| 17 | 11 | 1 | 1 | 1 | 0.25878872 | 0 |
| 17 | 12 | 0 | 1 | 0 | -3.4311013 | 0 |
| 17 | 13 | 0 | 1 | 0 | -2.9699105 | 0 |
| 17 | 14 | 0 | 1 | 0 | -2.4384715 | 0 |
| 17 | 15 | 1 | 1 | 1 | -1.5715742 | 0 |
| 17 | 16 | 0 | 1 | 0 | -1.0027137 | 0 |
| 17 | 17 | 1 | 1 | 1 | -3.1554173 | 0 |
| 17 | 18 | 1 | 1 | 1 | -4.0242529 | 0 |
| 17 | 19 | 0 | 1 | 0 | -2.5633887 | 0 |
| 17 | 20 | 0 | 1 | 0 | -1.7152253 | 0 |
| 18 | 2 | 0 | 0 | 0 | -7.9611551 | 0 |
| 18 | 3 | 0 | 0 | 0 | -5.4730627 | 0 |
| 18 | 4 | 0 | 0 | 0 | 1.97675695 | 0 |
| 18 | 5 | 1 | 0 | 0 | 23.844549 | 1 |

186214-π - 6A

186205 - TL - 18

186205 - TL - 17

| | | | | | | |
|----|----|---|---|---|------------|---|
| 18 | 6 | 1 | 1 | 1 | 33.8664925 | 1 |
| 18 | 7 | 1 | 1 | 1 | 13.469265 | 1 |
| 18 | 8 | 1 | 1 | 1 | 1.29584304 | 0 |
| 18 | 9 | 1 | 1 | 1 | 1.3911959 | 0 |
| 18 | 10 | 1 | 1 | 1 | -2.3262773 | 0 |
| 18 | 11 | 1 | 1 | 1 | -4.6645303 | 0 |
| 18 | 12 | 1 | 1 | 1 | -2.0930151 | 0 |
| 18 | 13 | 0 | 1 | 0 | -4.3958015 | 0 |
| 18 | 14 | 0 | 0 | 0 | -8.5125585 | 0 |
| 18 | 15 | 0 | 0 | 0 | -8.7440064 | 0 |
| 18 | 16 | 1 | 0 | 0 | -9.3347109 | 0 |
| 18 | 17 | 1 | 1 | 1 | -10.978243 | 0 |
| 18 | 18 | 1 | 1 | 1 | -6.7076983 | 0 |
| 18 | 19 | 0 | 1 | 0 | -1.3765707 | 0 |
| 18 | 20 | 0 | 0 | 0 | -0.9324046 | 0 |
| 19 | 2 | 0 | 1 | 0 | 4.95688485 | 0 |
| 19 | 3 | 1 | 1 | 1 | 1.57556793 | 0 |
| 19 | 4 | 1 | 1 | 1 | 2.09750559 | 0 |
| 19 | 5 | 1 | 1 | 1 | 2.92090546 | 0 |
| 19 | 6 | 1 | 1 | 1 | -3.8765422 | 0 |
| 19 | 7 | 0 | 1 | 0 | -11.673126 | 0 |
| 19 | 8 | 0 | 0 | 0 | -13.82868 | 0 |
| 19 | 9 | 0 | 0 | 0 | -14.041958 | 0 |
| 19 | 10 | 0 | 1 | 0 | -3.5727037 | 0 |
| 19 | 11 | 0 | 1 | 0 | 24.1004947 | 1 |
| 19 | 12 | 1 | 1 | 1 | 26.8988134 | 1 |
| 19 | 13 | 1 | 1 | 1 | 8.0852577 | 0 |
| 19 | 14 | 1 | 0 | 0 | -6.1553481 | 0 |
| 19 | 15 | 1 | 1 | 1 | -5.3460124 | 0 |
| 19 | 16 | 0 | 1 | 0 | -4.3638592 | 0 |
| 19 | 17 | 0 | 1 | 0 | -11.565826 | 0 |
| 19 | 18 | 0 | 0 | 0 | -4.8233048 | 0 |
| 19 | 19 | 0 | 0 | 0 | 9.67957188 | 0 |
| 19 | 20 | 0 | 0 | 0 | 13.0027685 | 1 |
| 19 | 21 | 0 | 0 | 0 | 15.164025 | 1 |
| 19 | 22 | 1 | 1 | 1 | 15.5570482 | 1 |
| 19 | 23 | 1 | 1 | 1 | 13.9812345 | 1 |
| 19 | 24 | 1 | 0 | 0 | 14.9658554 | 1 |
| 19 | 25 | 1 | 0 | 0 | 10.2762773 | 0 |
| 20 | 2 | 0 | 1 | 0 | 20.6259614 | 1 |
| 20 | 3 | 0 | 1 | 0 | 10.9815922 | 0 |
| 20 | 4 | 0 | 1 | 0 | -4.2026235 | 0 |
| 20 | 5 | 0 | 1 | 0 | -4.173725 | 0 |
| 20 | 6 | 0 | 1 | 0 | 0.52752112 | 0 |
| 20 | 7 | 0 | 0 | 0 | 0.24322391 | 0 |

cell & nuclei
elongate

| | | | | | | |
|----|----|---|---|---|------------|---|
| 20 | 8 | 1 | 0 | 0 | -2.0033004 | 0 |
| 20 | 9 | 1 | 0 | 0 | -8.2500531 | 0 |
| 20 | 10 | 1 | 0 | 0 | -12.665054 | 0 |
| 20 | 11 | 1 | 1 | 1 | -8.9502899 | 0 |
| 20 | 12 | 1 | 1 | 1 | -3.4131851 | 0 |
| 20 | 13 | 1 | 1 | 1 | 0.9683787 | 0 |
| 21 | 2 | 0 | 1 | 0 | 0.11454133 | 0 |
| 21 | 3 | 0 | 1 | 0 | -5.838227 | 0 |
| 21 | 4 | 0 | 1 | 0 | -7.8944305 | 0 |
| 21 | 5 | 1 | 1 | 1 | -4.6046935 | 0 |
| 21 | 6 | 1 | 1 | 1 | -4.7721874 | 0 |
| 21 | 7 | 0 | 1 | 0 | -5.4581392 | 0 |
| 21 | 8 | 1 | 1 | 1 | 0.47949297 | 0 |
| 21 | 9 | 1 | 1 | 1 | 12.8939356 | 1 |
| 21 | 10 | 1 | 1 | 1 | 17.5138858 | 1 |
| 21 | 11 | 1 | 1 | 1 | 5.9857234 | 0 |
| 21 | 12 | 1 | 1 | 1 | -2.7103732 | 0 |
| 21 | 13 | 1 | 1 | 1 | 5.1003093 | 0 |
| 21 | 14 | 1 | 1 | 1 | 15.839271 | 1 |
| 21 | 15 | 1 | 1 | 1 | 4.19380983 | 0 |
| 21 | 16 | 1 | 1 | 1 | -12.127964 | 0 |
| 21 | 17 | 1 | 1 | 1 | -12.448533 | 0 |
| 21 | 18 | 0 | 1 | 0 | -6.0982434 | 0 |
| 21 | 19 | 0 | 1 | 0 | -4.877467 | 0 |
| 21 | 20 | 0 | 0 | 0 | -3.1966863 | 0 |
| 21 | 21 | 1 | 1 | 1 | -1.4704449 | 0 |
| 21 | 22 | 1 | 0 | 0 | -0.4032691 | 0 |
| 21 | 23 | 0 | 1 | 0 | -0.4012631 | 0 |
| 21 | 24 | 0 | 1 | 0 | -1.4132387 | 0 |
| 21 | 25 | 0 | 1 | 0 | -4.9226106 | 0 |
| 21 | 26 | 0 | 1 | 0 | -9.4929868 | 0 |
| 21 | 27 | 0 | 1 | 0 | -8.5554992 | 0 |
| 21 | 28 | 0 | 1 | 0 | -4.8658636 | 0 |
| 21 | 29 | 0 | 1 | 0 | -1.5095439 | 0 |
| 21 | 30 | 1 | 1 | 1 | 17.9895445 | 1 |
| 21 | 31 | 1 | 1 | 1 | 43.3140666 | 1 |
| 21 | 32 | 1 | 1 | 1 | 25.5230549 | 1 |
| 21 | 33 | 1 | 1 | 1 | -3.0186198 | 0 |
| 21 | 34 | 1 | 1 | 1 | -13.24476 | 0 |
| 21 | 35 | 1 | 1 | 1 | -10.141434 | 0 |
| 22 | 2 | 0 | 0 | 0 | -1.6699466 | 0 |
| 22 | 3 | 0 | 0 | 0 | 1.56270035 | 0 |
| 22 | 4 | 0 | 1 | 0 | 3.83692778 | 0 |
| 22 | 5 | 0 | 1 | 0 | 1.41594747 | 0 |
| 22 | 6 | 0 | 1 | 0 | -2.1655575 | 0 |

n shape

| | | | | | | |
|----|----|---|---|---|------------|---|
| 22 | 7 | 0 | 1 | 0 | -1.2274306 | 0 |
| 22 | 8 | 0 | 1 | 0 | 1.44945581 | 0 |
| 22 | 9 | 0 | 0 | 0 | 0.97692372 | 0 |
| 22 | 10 | 0 | 0 | 0 | 1.1919425 | 0 |
| 22 | 11 | 0 | 0 | 0 | 0.93943085 | 0 |
| 22 | 12 | 1 | 1 | 1 | -0.5259607 | 0 |
| 22 | 13 | 1 | 1 | 1 | 3.92794623 | 0 |
| 22 | 14 | 0 | 1 | 0 | 7.40204014 | 0 |
| 22 | 15 | 0 | 1 | 0 | 4.26421402 | 0 |
| 22 | 16 | 1 | 1 | 1 | 1.15797866 | 0 |
| 22 | 17 | 1 | 0 | 0 | -1.7387075 | 0 |
| 22 | 18 | 1 | 0 | 0 | 0.2863408 | 0 |
| 22 | 19 | 1 | 0 | 0 | 11.267437 | 0 |
| 22 | 20 | 1 | 0 | 0 | 23.2300958 | 1 |
| 22 | 21 | 1 | 0 | 0 | 22.6958944 | 1 |
| 22 | 22 | 1 | 0 | 0 | 11.0896342 | 0 |
| 22 | 23 | 1 | 0 | 0 | 1.88380951 | 0 |
| 23 | 2 | 0 | 0 | 0 | -0.7124409 | 0 |
| 23 | 3 | 0 | 1 | 0 | 0.1847943 | 0 |
| 23 | 4 | 0 | 1 | 0 | 0.43772574 | 0 |
| 23 | 5 | 0 | 0 | 0 | 1.71018201 | 0 |
| 23 | 6 | 0 | 1 | 0 | 2.98411302 | 0 |
| 23 | 7 | 0 | 0 | 0 | 3.06171117 | 0 |
| 23 | 8 | 0 | 0 | 0 | -0.121216 | 0 |
| 23 | 9 | 0 | 1 | 0 | -5.1494447 | 0 |
| 23 | 10 | 1 | 1 | 1 | -5.3540914 | 0 |
| 23 | 11 | 1 | 1 | 1 | -1.7306543 | 0 |
| 23 | 12 | 0 | 1 | 0 | 1.51035521 | 0 |
| 23 | 13 | 0 | 1 | 0 | 4.664071 | 0 |
| 23 | 14 | 0 | 0 | 0 | 5.2481823 | 0 |
| 23 | 15 | 0 | 0 | 0 | 1.2108942 | 0 |
| 23 | 16 | 0 | 0 | 0 | -1.2115665 | 0 |
| 23 | 17 | 0 | 1 | 0 | 3.43778383 | 0 |
| 23 | 18 | 0 | 1 | 0 | 6.90943985 | 0 |
| 23 | 19 | 0 | 1 | 0 | 2.87229414 | 0 |
| 23 | 20 | 1 | 1 | 1 | -3.257446 | 0 |
| 23 | 21 | 0 | 1 | 0 | -6.5632312 | 0 |
| 23 | 22 | 0 | 1 | 0 | -8.0786612 | 0 |
| 23 | 23 | 0 | 1 | 0 | -8.8718453 | 0 |
| 23 | 24 | 1 | 1 | 1 | -6.2957187 | 0 |
| 23 | 25 | 1 | 1 | 1 | -3.0887402 | 0 |
| 23 | 26 | 1 | 1 | 1 | -2.0887951 | 0 |
| 23 | 27 | 0 | 1 | 0 | -1.3545739 | 0 |
| 23 | 28 | 1 | 1 | 1 | 0.28206259 | 0 |
| 23 | 29 | 1 | 1 | 1 | 1.4920757 | 0 |

| | | | | | | |
|----|----|---|---|---|------------|---|
| 23 | 30 | 1 | 1 | 1 | 1.50208425 | 0 |
| 23 | 31 | 1 | 1 | 1 | 1.66219535 | 0 |
| 23 | 32 | 1 | 1 | 1 | 2.13570085 | 0 |
| 23 | 33 | 1 | 1 | 1 | 0.38965441 | 0 |
| 23 | 34 | 1 | 1 | 1 | -2.3554303 | 0 |
| 23 | 35 | 1 | 1 | 1 | -2.5511032 | 0 |
| 24 | 2 | 0 | 0 | 0 | 4.27313464 | 0 |
| 24 | 3 | 1 | 1 | 1 | 12.3952708 | 1 |
| 24 | 4 | 1 | 1 | 1 | 15.4559507 | 1 |
| 24 | 5 | 1 | 1 | 1 | 10.3175169 | 0 |
| 24 | 6 | 1 | 1 | 1 | 8.03492432 | 0 |
| 24 | 7 | 0 | 0 | 0 | 5.13707857 | 0 |
| 24 | 8 | 1 | 1 | 1 | -1.1503412 | 0 |
| 24 | 9 | 1 | 1 | 1 | -5.7619406 | 0 |
| 24 | 10 | 1 | 1 | 1 | -6.806712 | 0 |
| 24 | 11 | 1 | 1 | 1 | -5.87555 | 0 |
| 24 | 12 | 0 | 0 | 0 | -6.1200406 | 0 |
| 24 | 13 | 0 | 0 | 0 | -4.069973 | 0 |
| 24 | 14 | 0 | 0 | 0 | -0.3380035 | 0 |
| 24 | 15 | 0 | 0 | 0 | -0.0607827 | 0 |
| 24 | 16 | 0 | 0 | 0 | -1.5095538 | 0 |
| 24 | 17 | 1 | 1 | 1 | -0.9795178 | 0 |
| 24 | 18 | 0 | 1 | 0 | -0.1641492 | 0 |
| 24 | 19 | 0 | 0 | 0 | -2.7176629 | 0 |
| 24 | 20 | 0 | 0 | 0 | -3.7178507 | 0 |
| | | | | | 0.74261407 | 0 |

= elongation

= code marked elong
I = I believe elons

08/14/19

| caseNumber | Frame | PvX | PvY | Elongation % | PVX > | PVY > | Shape |
|------------------------|-------|-----|----------|--------------------|-------------|-------|--------------------|
| | | | | PROGRESSIVE CHANGE | PROGRESSIVE | FINAL | frame |
| 170925_TL_B | 1 | 2 | -1.0997 | -1.5062 | 31.3393 | 1 | 0 |
| Group 2 | 1 | 3 | -1.702 | -2.9462 | 14.2364 | 1 | 0 |
| | 1 | 4 | -2.2507 | -5.8438 | | 1 | 0 shrink |
| | 1 | 5 | -1.9473 | -7.8891 | | 1 | 1 adjustment |
| | 1 | 6 | -0.85532 | -7.6819 | | 0 | 1 elongation |
| | 1 | 7 | -0.55642 | -8.1839 | | 0 | 1 |
| | 1 | 8 | -1.1377 | -9.3929 | | 1 | 1 shrink |
| | 1 | 9 | -1.541 | -8.472 | | 1 | 1 shift left |
| | 1 | 10 | -1.6708 | -5.0728 | 18.6002 | 1 | 1 pseudopod |
| | 1 | 11* | -2.4068 | -2.5883 | 32.8630 | 1 | 0 |
| | 1 | 12 | -3.1926 | -3.9804 | | 1 | 0 |
| | 1 | 13 | -2.778 | -7.37 | | 1 | 1 shift straight |
| | 1 | 14 | -1.4719 | -9.3113 | | 1 | 1 |
| | 1 | 15 | -0.57592 | -9.497 | | 0 | 1 |
| | 1 | 16* | -0.26044 | -8.9468 | | 0 | 1 |
| | 1 | 17 | 0.9667 | -7.2895 | | 0 | 1 |
| | 1 | 18 | 1.8398 | -6.1405 | 15.4438 | 1 | 0 |
| | 1 | 19 | 0.76534 | -6.2664 | | 0 | 0 |
| | 1 | 20 | -0.10356 | -4.6291 | | 0 | 0 |
| Look into.... | 2 | 2 | -4.4056 | 1.7257 | | 1 | 0 |
| 170929_TL_S | 2 | 3 | -6.4219 | -0.56602 | | 1 | 0 |
| Group 2 | 2 | 4 | -7.636 | -2.8377 | | 1 | 0 U-Turn |
| X, Y plot shows change | 2 | 5 | -6.0474 | -2.6392 | | 1 | 0 shrink |
| A plot 3 does not | 2 | 6 | -2.2318 | -2.4965 | | 0 | 0 straightening |
| | 2 | 7 | -0.55386 | -3.5263 | | 0 | 0 |
| | 2 | 8 | -0.92535 | -4.695 | | 0 | 0 |
| See return | 2 | 9 | -0.7997 | -5.5738 | | 0 | 1 |
| | 2 | 10* | 0.36736 | -6.4953 | | 0 | 1 |
| | 2 | 11* | 1.1634 | -7.162 | 16.9846 | 0 | 1 straight |
| | 2 | 12 | 0.58338 | -5.457 | 18.2867 | 0 | 1 |
| + red | 3 | 2 | 1.4737 | 0.041155 | | 1 | 0 |
| 170929_TL_GA3 | 3 | 3 | 1.2149 | -0.092374 | | 1 | 0 circular |
| Group 2 | 3 | 4 | 0.2159 | 0.0082787 | | 0 | 0 nuclei |
| | 3 | 5 | -0.32356 | 0.17893 | | 0 | 0 |
| | 3 | 6 | -0.68058 | 0.25328 | | 0 | 0 |
| | 3 | 7 | -0.77924 | 0.29046 | | 1 | 0 |
| | 3 | 8 | -0.53913 | 0.16128 | | 0 | 0 |
| | 3 | 9 | 0.40727 | -0.15051 | | 0 | 0 |
| | 3 | 10 | 1.6469 | -0.58563 | | 1 | 0 |
| | 3 | 11 | 1.5178 | -0.70723 | | 1 | 1 cell extends out |
| | 3 | 12 | 0.66746 | -0.21273 | | 0 | 0 |
| | 3 | 13 | 0.058172 | 0.44955 | | 0 | 0 contracts back |
| | 3 | 14 | -0.47073 | 0.53112 | | 0 | 0 |
| | 3 | 15 | -0.40289 | 0.21684 | | 0 | 0 |
| | 3 | 16 | 0.78028 | -0.073162 | | 1 | 0 |

| | | | | | |
|---|-----|-----------|------------|---|---------------------|
| 4 | 29 | 1.8337 | 0.14221 | 1 | 0 |
| 4 | 30 | 1.83 | 0.34965 | 1 | move down time |
| 4 | 31* | 2.413 | 0.62792 | 1 | 1 |
| 4 | 32 | 3.4014 | 0.87946 | 1 | 1 |
| 4 | 33* | 3.7318 | 0.84086 | 1 | 1 |
| 4 | 34 | 2.928 | 0.73938 | 1 | 1 |
| 4 | 35 | 1.8812 | 0.75823 | 1 | 1 |
| 4 | 36* | 1.4668 | 0.8463 | 1 | Stop exten- size |
| 4 | 37 | 0.97586 | 0.46828 | 0 | 1 |
| 4 | 38 | -0.027677 | -0.31879 | 0 | 1 |
| 4 | 39 | -0.22076 | -0.57307 | 0 | 1 |
| 4 | 40 | 0.19378 | -0.37925 | 0 | 1 |
| 4 | 41 | -0.030414 | -0.37046 | 0 | 1 |
| 4 | 42 | -0.17455 | -0.38194 | 0 | 1 |
| 4 | 43 | 0.87839 | 0.091726 | 0 | 0 |
| 4 | 44 | 1.6536 | 0.39914 | 1 | 1 |
| 4 | 45 | 1.0309 | 0.20176 | 1 | 0 |
| 4 | 46 | 0.012188 | -0.044406 | 0 | 0 |
| 4 | 47 | -0.45395 | -0.18539 | 0 | 0 |
| 4 | 48 | -0.050339 | 0.071144 | 0 | 0 |
| 4 | 49 | 0.20394 | 0.34764 | 0 | 1 |
| 4 | 50 | -0.084182 | 0.45612 | 0 | 1 |
| 4 | 51 | -0.19419 | 0.79943 | 0 | 1 |
| 4 | 52 | 0.41244 | 0.95725 | 0 | 1 |
| 4 | 53* | 0.94275 | 0.36812 | 0 | 1 |
| 4 | 54 | 0.79493 | -0.059262 | 0 | 0 |
| 4 | 55 | 0.92235 | 0.33506 | 0 | 1 |
| 4 | 56 | 1.17 | 0.85988 | 1 | use seeded |
| 4 | 57 | 1.263 | 1.0739 | 1 | 1 |
| 4 | 58 | 1.0953 | 0.71627 | 1 | 1 |
| 4 | 59 | 0.543 | 0.31544 | 0 | 1 |
| 4 | 60 | -0.17765 | 0.063368 | 0 | 0 |
| 4 | 61 | -0.74722 | -0.32323 | 0 | 1 |
| 4 | 62 | -0.67791 | -0.14733 | 0 | 0 |
| 4 | 63 | 0.066829 | -0.0010474 | 0 | 0 |
| 4 | 64 | 0.98827 | -0.51827 | 0 | 1 |
| 4 | 65 | 1.0489 | -0.90475 | 1 | 1 change angle |
| 4 | 66 | 0.82082 | -0.91976 | 0 | 1 change angle |
| 4 | 67 | 1.107 | -0.62396 | 1 | 1 |
| 4 | 68 | 0.89222 | -0.33637 | 0 | 1 |
| 4 | 69 | 0.54737 | -0.14809 | 0 | 0 |
| 4 | 70 | 1.0428 | 0.27319 | 1 | 1 shape chart |
| 4 | 71 | 1.5735 | 0.62825 | 1 | 1 |
| 4 | 72 | 1.1908 | 0.50318 | 1 | 1 |
| 5 | 2 | -0.94287 | 0.94974 | 0 | 0 |
| 5 | 3 | 0.76662 | 3.2009 | 0 | 1 |

71002 - TL - 2C

| | | | | | | |
|---|-------|-----------|----------------|---------|---|--------------------|
| 7 | 3 - | 1.5061 | 0.65689 | 13.7320 | 0 | 0 |
| 7 | 4 - | 2.9445 | 5.157 | 47.9473 | 1 | 1 long extend down |
| 7 | 5 *- | 3.1862 | 8.6545 | 35.1077 | 1 | 1 |
| 7 | 6 | 3.0488 | 9.5024 | | 1 | 1 |
| 7 | 7 | 3.6834 | 9.9519 | | 1 | 1 |
| 7 | 8 | 4.1773 | 10.323 | | 1 | 1 |
| 7 | 9 | 4.0971 | 9.5932 | | 1 | 1 |
| 7 | 10 | 3.8632 | 8.6138 | | 1 | 1 |
| 7 | 11 * | 4.0993 | 8.82 | | 1 | 1 |
| 7 | 12 | 3.8813 | 7.5621 | | 1 | 1 |
| 7 | 13 | 1.6892 | 3.833 | | 0 | 0 |
| 7 | 14 | -0.5567 | 1.3133 | | 0 | 0 |
| 7 | 15 | -0.7882 | 0.97086 | | 0 | 0 net moving |
| 7 | 16 | 0.12166 | 1.4757 | | 0 | 0 |
| 7 | 17 | 1.1989 | 2.1825 | | 0 | 0 |
| 7 | 18 *- | 2.1601 | 2.6828 | 18.3493 | 1 | 0 |
| 7 | 19 | 3.4473 | 3.0798 | | 1 | 0 |
| 7 | 20 | 4.4372 | 3.4182 | | 1 | 0 |
| 7 | 21 | 4.7794 | 3.8678 | | 1 | 0 |
| 7 | 22 | 5.2036 | 4.3225 nucleus | | 1 | 1 move down |
| 7 | 23 | 4.6098 | 3.9815 | | 1 | 0 |
| 7 | 24 | 2.9058 | 2.6304 | | 1 | 0 |
| 7 | 25 | 1.2501 | 1.3684 | | 0 | 0 |
| 7 | 26 | -0.070919 | 1.0848 | | 0 | 0 |
| 7 | 27 | -0.72246 | 1.6477 | | 0 | 0 |
| 7 | 28 | -0.29894 | 2.8988 | | 0 | 0 |
| 7 | 29 * | 0.57824 | 3.8788 | | 0 | 0 |
| 7 | 30 | 0.72191 | 3.1908 | | 0 | 0 |
| 7 | 31 | 0.51376 | 1.8926 | | 0 | 0 |
| 7 | 32 | 0.44932 | 1.1313 | | 0 | 0 |

H002_TL - 6
Group 2

| | | | | | | |
|---|------|----------|----------|---------|---|-----------------------|
| 8 | 2 | 0.94076 | -0.88951 | | 0 | 0 |
| 8 | 3 | 0.67145 | -0.56971 | | 0 | 0 |
| 8 | 4 | 0.18725 | -0.34602 | | 0 | 0 |
| 8 | 5 | 0.089408 | -0.81454 | | 0 | 0 |
| 8 | 6 | 0.24419 | -0.96362 | | 0 | 0 |
| 8 | 7 | 0.34877 | -0.48039 | | 0 | 0 |
| 8 | 8 | 0.20526 | -0.25361 | | 0 | 0 |
| 8 | 9 | 0.026576 | -0.30855 | | 0 | 0 |
| 8 | 10 | -0.18497 | -1.2959 | | 0 | 0 |
| 8 | 11 | -0.53473 | -2.9873 | | 0 | 1 pseudopod extension |
| 8 | 12 * | -0.48854 | -3.1462 | | 0 | 1 |
| 8 | 13 - | -0.18183 | -2.684 | 12.8879 | 0 | 1 |
| 8 | 14 | -0.44702 | -2.8645 | | 0 | 1 |
| 8 | 15 | -1.1218 | -3.0754 | | 0 | 1 |
| 8 | 16 | -2.0719 | -3.4015 | | 1 | 1 curve left |
| 8 | 17 - | -3.7905 | -4.7905 | 17.8309 | 1 | 1 |

| | | | | | |
|----|-----|---------|----------|---------|--------------------------|
| 10 | 10 | 0.16909 | 1.551 | 0 | 1 |
| 10 | 11 | 0.42672 | 3.2069 | 0 | 1 |
| 10 | 12 | 3.1819 | 4.6 | 1 | 1 move right bottom left |
| 10 | 13* | -5.6453 | 4.9574 | 14.1028 | 1 |
| 10 | 14 | 6.3361 | 4.0789 | 1 | 1 Y-shape |
| 10 | 15 | 6.3689 | 3.3565 | 1 | 1 arm 2 |
| 10 | 16 | -6.9057 | 5.3486 | 32.3636 | 1 move bottom left right |
| 10 | 17* | -7.7415 | 8.4895 | 16.6207 | 1 |
| 10 | 18 | 5.9824 | 8.7698 | 1 | 1 |
| 10 | 19 | 3.1664 | 6.0001 | 1 | 1 |
| 10 | 20 | 1.5391 | 3.3339 | 0 | 1 |
| 10 | 21 | 0.01982 | 1.6807 | 0 | 1 |
| 10 | 22 | 1.6337 | 0.06592 | 0 | 0 |
| 10 | 23 | 5.2186 | -2.7625 | 1 | 1 top right |
| 10 | 24 | 5.1349 | -4.2596 | 1 | 1 u-shape |
| 10 | 25 | -2.9171 | -2.9812 | 13.3339 | 1 |
| 10 | 26 | 2.1044 | -2.8968 | 1 | 1 |
| 10 | 27* | 3.069 | -6.3298 | 1 | 1 |
| 10 | 28* | 3.9311 | -10.25 | 1 | 1 |
| 10 | 29 | 2.8788 | -10.028 | 1 | 1 |
| 10 | 30 | 0.90295 | -9.043 | 0 | 1 |
| 10 | 31 | -2.3965 | -9.5858 | 1 | 1 Y-shape |
| 10 | 32 | -5.8958 | -7.7343 | 1 | 1 Top left |
| 10 | 33* | -6.1432 | -4.7533 | 14.4386 | 1 |
| 10 | 34 | -4.4844 | -2.3558 | 1 | 1 |
| 10 | 35 | -2.6382 | -0.44546 | 1 | 1 |

| | | | | | |
|----|-----|----------|-----------|---------|-------------------|
| 11 | 2 | -1.5241 | -0.20275 | 1 | 0 |
| 11 | 3 | -1.9937 | -0.54783 | 1 | 0 |
| 11 | 4 | -2.2439 | -0.70351 | 1 | 0 cell Y-shape |
| 11 | 5 | -1.7733 | -0.030751 | 1 | 0 |
| 11 | 6 | -0.86889 | 0.89005 | 0 | 0 |
| 11 | 7 | -0.64938 | 1.5641 | 0 | 0 |
| 11 | 8 | -1.7624 | 1.7798 | 1 | 0 granules moves |
| 11 | 9 | -3.9936 | 0.83976 | 14.9343 | 0 left |
| 11 | 10 | -5.0572 | -0.30067 | 13.9204 | 0 bow turn |
| 11 | 11* | -4.5442 | -0.82186 | 1 | 0 |
| 11 | 12* | -4.9371 | -1.8941 | 1 | 0 |
| 11 | 13* | -6.0844 | -4.0298 | 1 | 1 top left |
| 11 | 14 | -5.5034 | -4.9802 | 1 | 1 |
| 11 | 15 | -3.1175 | -3.4366 | 1 | 1 |
| 11 | 16 | -1.0048 | -1.2945 | 1 | 0 pseudopod moves |
| 11 | 17 | 0.46933 | -0.22872 | 0 | 0 |
| 11 | 18 | 1.8083 | -1.1209 | 1 | 0 |
| 11 | 19* | 1.8928 | -3.3516 | 10.9824 | 1 tip right |
| 11 | 20 | 0.51651 | -5.0159 | 0 | 1 |
| 11 | 21 | -0.54267 | -5.2789 | 0 | 1 |

| | | | | | | | | |
|-------------|----|----|-----------|-----------|---------|---|-------|----------------|
| | 13 | 10 | 2.3678 | 3.7257 | 7.0996 | 0 | | 1 |
| 8020S | 14 | 2 | 6.2842 | 1.7782 | | 0 | S | 1 |
| 8020S-TL-14 | 14 | 3 | 8.9845 | 1.5072 | | 1 | SE | 1 |
| Group 1 | 14 | 4 | 9.405 | 0.5528 | | 1 | NE | 0 |
| | 14 | 5 | 9.2528 | 0.67607 | 13.4262 | 1 | SE E | 1 |
| | 14 | 6 | 11.505 | 0.83152 | 28.0998 | 1 | SE E | 1 |
| | 14 | 7 | 16.732 | -0.77454 | | 1 | NE | 1 |
| | 14 | 8 | 17.286 | -3.2372 | | 1 | NE | 1 |
| | 14 | 9 | 10.207 | -3.4916 | | 1 | NE | 1 |
| | 14 | 10 | 3.8778 | -1.9231 | | 0 | N | 1 |
| | 14 | 11 | 2.0992 | -1.281 | | 0 | N | 1 |
| | 14 | 12 | 2.293 | -1.5541 | | 0 | N | 1 |
| | 14 | 13 | 2.0089 | -1.4842 | | 0 | N | 1 |
| | 14 | 14 | 0.46146 | -0.60914 | | 0 | — | 0 |
| | 14 | 15 | -0.5076 | -0.011981 | | 0 | V1 | V2 0 |
| 8020S-TL-15 | 15 | 2 | 5.1399 | -0.80761 | 13.4477 | 1 | EAST | E 0 |
| Group 1 | 15 | 3 | 3.9963 | 0.48875 | | 1 | EAST | E 0 |
| 2 | 15 | 4 | 1.7853 | 4.1271 | | 0 | WORK | S 1 |
| | 15 | 5 | 2.6336 | 7.406 | | 0 | NORTH | S 1 |
| | 15 | 6 | 5.1045 | 8.0838 | | 1 | NE | SE 1 |
| | 15 | 7 | 5.9766 | 5.9563 | | 1 | NE | SE 1 |
| | 15 | 8 | 4.195 | 2.5426 | | 1 | NE | SE 1 |
| | 15 | 9 | 3.2897 | 0.67657 | | 1 | E | E 0 |
| | 15 | 10 | 4.039 | 0.35519 | 15.4879 | 1 | E | E 0 |
| | 15 | 11 | 5.1448 | -1.3261 | | 1 | E | E 0 |
| | 15 | 12 | 6.2147 | -4.1828 | | 1 | SE | NE 1 |
| | 15 | 13 | 6.4829 | -6.7239 | 9.2958 | 1 | SE | NE 1 |
| | 15 | 14 | 6.7255 | -8.836 | | 1 | SE | NE 1 |
| | 15 | 15 | 5.2544 | -8.8864 | | 1 | SE | NE 1 |
| | 15 | 16 | 1.6889 | -6.4255 | | 0 | S | N 1 |
| | 15 | 17 | 0.16584 | -4.0718 | | 0 | S | N 1 |
| | 15 | 18 | 0.37225 | -3.3706 | | 0 | S | N 1 |
| | 15 | 19 | -0.30101 | -2.7653 | | 0 | S | N 1 |
| | 15 | 20 | -1.4555 | -1.8449 | | 0 | — | — 0 |
| | 15 | 21 | -1.7728 | -1.4725 | | 0 | — | — 0 |
| | 15 | 22 | -1.3758 | -1.4647 | | 0 | — | — 0 |
| | 15 | 23 | -0.95129 | -1.716 | | 0 | — | — 0 |
| | 15 | 24 | -0.017783 | -2.1905 | | 0 | S | N 1 |
| | 15 | 25 | 1.5479 | -3.1255 | | 0 | S | N 1 |
| | 15 | 26 | 3.0956 | -4.8042 | 12.1871 | 1 | NESE | NC1 top right! |
| | 15 | 27 | 3.9109 | -6.2606 | 18.2824 | 1 | NESE | NC1 elongate |
| | 15 | 28 | 4.1937 | -6.5138 | | 1 | NESE | NC1 |
| | 15 | 29 | 4.0588 | -5.6454 | | 1 | NESE | NC1 shrink |
| | 15 | 30 | 2.6392 | -3.4148 | | 0 | S | NC1 |
| 8020S-TL-16 | 16 | 2 | -0.95169 | -3.4288 | | 1 | | 1 |
| Group 1 | 16 | 3 | -0.78899 | -2.129 | | 0 | | 1 |

*weird video

| | | | | | | |
|----|-----|--------|----------|---------|---|---|
| 18 | 12* | 7.4425 | 2.5599 | 26.8988 | 1 | 1 |
| 18 | 13* | 9.9497 | 2.1534 | | 1 | 1 |
| 18 | 14 | 11.264 | -0.85976 | | 1 | 0 |
| 18 | 15 | 9.5832 | -5.0086 | | 1 | 1 |
| 18 | 16 | 6.2749 | -4.8711 | | 0 | 1 |
| 18 | 17 | 3.5036 | -2.0246 | | 0 | 1 |
| 18 | 18 | 2.5106 | -0.94089 | | 0 | 0 |
| 18 | 19 | 2.5723 | -1.05 | | 0 | 0 |
| 18 | 20 | 3.6172 | -0.61726 | 13.0028 | 0 | 0 |
| 18 | 21 | 5.1983 | 0.54886 | 15.1640 | 0 | 0 |
| 18 | 22* | 7.1565 | 1.9361 | 14.5570 | 1 | 1 |
| 18 | 23* | 10.519 | 1.9779 | 13.9312 | 1 | 1 |
| 18 | 24* | 12.926 | 0.94452 | 14.9659 | 1 | 0 |
| 18 | 25 | 10.173 | 0.52608 | | 1 | 0 |

| | | | | | | |
|----|-----|----------|-----------|---------|----|----|
| 19 | 2 | -0.31644 | -1.3866 | | 1 | 1 |
| 19 | 3 | -1.126 | -2.4591 | | 1 | 1 |
| 19 | 4 | -1.2596 | -2.6005 | | 1 | 1 |
| 19 | 5 | -0.30798 | -2.575 | | 1 | 1 |
| 19 | 6 | 0.38921 | -2.6098 | | 1 | 1 |
| 19 | 7 | 1.472 | 1.313 | | 1 | 1 |
| 19 | 8 | 2.5227 | 6.2006 | | 1 | 1 |
| 19 | 9 | 1.8577 | 4.8114 | | 1 | 1 |
| 19 | 10 | 0.87581 | 0.62672 | | 1 | 1 |
| 19 | 11 | 0.4896 | -1.1489 | | 1 | 1 |
| 19 | 12 | -0.17144 | -1.2053 | | 1 | 1 |
| 19 | 13 | -1.2068 | -1.0785 | | 1 | 1 |
| 19 | 14 | -1.8428 | -0.3571 | | 1 | 0 |
| 19 | 15 | -1.661 | 0.90439 | | 1 | 1 |
| 19 | 16 | -1.3468 | 1.2157 | | 1 | 1 |
| 19 | 17 | -1.2177 | 0.58228 | | 1 | 1 |
| 19 | 18 | -1.4379 | -0.15121 | | 1 | 0 |
| 19 | 19 | -2.4883 | -0.63472 | | 1* | 1* |
| 19 | 20 | -2.503 | -0.59209 | | 1 | 1 |
| 19 | 21 | -0.51533 | -0.069763 | | 1 | 0 |
| 19 | 22 | 0.61115 | 0.28463 | | 1 | 0 |
| 19 | 23 | 0.30512 | 0.17782 | | 1 | 0 |
| 19 | 24 | 1.1094 | 1.0783 | | 1 | 1 |
| 19 | 25 | 3.5931 | 3.298 | | 1 | 1 |
| 19 | 26 | 5.4699 | 4.4286 | | 1 | 1 |
| 19 | 27 | 4.5893 | 3.3206 | | 1 | 1 |
| 19 | 28 | 2.6813 | 1.543 | | 1 | 1 |
| 19 | 29 | 2.4757 | 0.97231 | 12.8675 | 1 | 1 |
| 19 | 30 | 2.4533 | 1.0756 | 12.3413 | 1 | 1 |
| 19 | 31 | 1.8853 | 1.4337 | | 1 | 1 |
| 19 | 32 | 2.0876 | 3.4627 | 12.7483 | 1 | 1 |
| 19 | 33* | 1.7725 | 5.7284 | | 1 | 1 |

large arm
to bottom
right

Start lowered
down

move arm
towards
bottom
center

80214-TL-4
*
* lots of
pseudo pod
but not
CCW
* lots of
quad moving
but
CCW

WRONG

180215-TL-4

Missing 80214-TL-6A

180925-TL-3

| | | | | | | |
|----|-----------------|-----------|-----------|----------------------|---|----------------------------------|
| 20 | 6 | 1.4587 | -1.7158 | | 1 | 1 |
| 20 | 7 | 0.34819 | -2.7133 | | 0 | 1 |
| 20 | 8 | 2.4539 | -4.2857 | | 1 | 1 |
| 20 | 9 ⁺ | 4.8716 | -6.213 | 12.834 | 1 | 1 |
| 20 | 10 ⁺ | 6.5934 | -7.0177 | 13.513 9 | 1 | 1 |
| 20 | 11 | 7.4404 | -5.3251 | | 1 | 1 |
| 20 | 12 | 7.5096 | -3.1495 | | 1 | 1 |
| 20 | 13 | 7.9622 | -2.8789 | | 1 | 1 |
| 20 | 14 ⁺ | 8.0276 | -3.073 | 15.8393 moving right | 1 | 1 |
| 20 | 15 ⁺ | 6.8858 | -2.6894 | | 1 | 1 move back up |
| 20 | 16 | 4.8643 | -2.2661 | | 1 | 1 |
| 20 | 17 | 2.2665 | -1.0598 | | 1 | 1 |
| 20 | 18 | 0.08588 | 0.74905 | | 0 | 1 stop moving |
| 20 | 19 | -0.33857 | 0.99554 | | 0 | 1 |
| 20 | 20 | 0.1854 | -0.23198 | | 0 | 0 |
| 20 | 21 | 1.0676 | -0.93806 | | 1 | 1 Pseudopod extent |
| 20 | 22 | 1.2149 | -0.18009 | | 1 | 0 |
| 20 | 23 | -0.18733 | 0.75949 | | 0 | 1 |
| 20 | 24 | -0.4484 | 0.78881 | | 0 | 1 |
| 20 | 25 | 0.27917 | 1.4864 | | 0 | 1 |
| 20 | 26 | -0.27571 | 2.8924 | | 0 | 1 Cell arm extends straight down |
| 20 | 27 | -0.61405 | 2.8949 | | 0 | 1 |
| 20 | 28 | 0.14489 | 1.9875 | | 0 | 1 |
| 20 | 29 | -0.57587 | 2.9733 | | 0 | 1 |
| 20 | 30 ⁺ | -3.1239 | 5.622 | 17.9895 | 1 | 1 move bottom center |
| 20 | 31 ⁺ | -5.1217 | 7.8029 | 43.3141 | 1 | 1 |
| 20 | 32 ⁺ | -6.0623 | 9.9252 | 28.5231 | 1 | 1 |
| 20 | 33 | -6.2452 | 10.571 | | 1 | 1 |
| 20 | 34 | -5.8783 | 8.0726 | | 1 | 1 |
| 20 | 35 | -4.3484 | 4.3101 | | 1 | 1 |
| 21 | 2 | -0.040337 | 0.25567 | rounded nucleus | 0 | 0 Pseudopod retracting into cell |
| 21 | 3 | -0.15816 | -0.57521 | | 0 | 0 |
| 21 | 4 | -0.27247 | -1.4596 | | 0 | 1 |
| 21 | 5 | -0.58231 | -1.5073 | | 0 | 1 |
| 21 | 6 | -0.79237 | -1.2182 | | 0 | 1 |
| 21 | 7 | -0.81604 | -1.0252 | | 0 | 1 |
| 21 | 8 | -0.62936 | -0.78286 | | 0 | 1 |
| 21 | 9 | -0.37389 | -0.53676 | | 0 | 0 |
| 21 | 10 | -0.33041 | -0.42705 | | 0 | 0 |
| 21 | 11 | -0.59023 | -0.43441 | | 0 | 0 |
| 21 | 12 | -1.7569 | -0.84611 | | 1 | 1 move left with pseudopod |
| 21 | 13 | -2.3276 | -1.2962 | | 1 | 1 |
| 21 | 14 | -1.3719 | -1.3856 | | 0 | 1 |
| 21 | 15 | -0.97728 | -1.213 | | 0 | 1 |
| 21 | 16 | -1.5912 | -0.73837 | | 1 | 1 |
| 21 | 17 | -2.0711 | -0.085263 | | 1 | 0 |

| | | | | | | |
|----|----|---------|---------|----------------------|---|---|
| 23 | 8 | -3.8152 | 2.6521 | | 1 | 1 |
| 23 | 9 | -6.7427 | 3.9879 | | 1 | 1 |
| 23 | 10 | -6.1478 | 3.7062 | | 1 | 1 |
| 23 | 11 | -3.304 | 2.4186 | nucleus shrinkage | 1 | 1 |
| 23 | 12 | -2.074 | 1.9089 | | 0 | 0 |
| 23 | 13 | -1.5167 | 1.1023 | | 0 | 0 |
| 23 | 14 | -1.0672 | 0.07385 | | 0 | 0 |
| 23 | 15 | -1.4085 | 0.34703 | | 0 | 0 |
| 23 | 16 | -2.4346 | 1.5937 | | 0 | 0 |
| 23 | 17 | -2.8626 | 2.7313 | | 1 | 1 |
| 23 | 18 | -1.8614 | 2.8818 | | 0 | 1 |
| 23 | 19 | -1.2272 | 2.0876 | | 0 | 0 |
| 23 | 20 | -1.2296 | 1.1121 | | 0 | 0 |

Shift from
to

F Screenshots of metrics data table

| 1 | Group | Video_Case | 3 | 4 | 5 | N_Vel | C_Vel | 6 | N_numEndP | 7 | N_numEndP_Skel | 8 | N_numBranches_Skel | 9 | N_Major_Axis_um | 10 | C_Major_Axis_um | 11 | N_Min_Axis_um | C_Min_Axis_um | 12 |
|----|-------|------------|----|--------|--------|--------|--------|--------|-----------|---|----------------|---------|--------------------|---------|-----------------|---------|-----------------|---------|---------------|---------------|----|
| 1 | 1 | 1 | 2 | 0.0963 | 0.0086 | 3 | 0.1377 | 0.2078 | 3 | 5 | 3 | 29.1277 | 33.3189 | 8.1597 | 5.4891 | 29.8853 | 29.8853 | 11.4675 | 11.4675 | | |
| 2 | 1 | 1 | 1 | 3 | 0.0972 | 0.0740 | 4 | 0.0972 | 0.0740 | 2 | 3 | 1 | 22.8125 | 32.2115 | 6.0061 | 9.5450 | | | 10.8435 | | |
| 3 | 1 | 1 | 1 | 5 | 0.1795 | 0.2011 | 5 | 0.1795 | 0.2011 | 2 | 4 | 2 | 25.6677 | 32.4491 | 5.4160 | 8.6728 | | | | | |
| 4 | 1 | 1 | 1 | 6 | 0.1299 | 0.1723 | 3 | 0.1299 | 0.1723 | 5 | 3 | 3 | 18.8094 | 22.7236 | 6.5541 | 12.3439 | | | | | |
| 5 | 1 | 1 | 1 | 7 | 0.1313 | 0.0823 | 3 | 0.1313 | 0.0823 | 3 | 3 | 1 | 11.8855 | 22.7014 | 5.6963 | 13.4522 | | | | | |
| 6 | 1 | 1 | 1 | 8 | 0.1044 | 0.0350 | 3 | 0.1044 | 0.0350 | 3 | 3 | 1 | 10.3315 | 28.5569 | 6.0303 | 14.3539 | | | | | |
| 7 | 1 | 1 | 1 | 9 | 0.0499 | 0.0894 | 4 | 0.0499 | 0.0894 | 4 | 4 | 2 | 16.4494 | 21.4241 | 5.1813 | 11.4246 | | | | | |
| 8 | 1 | 1 | 10 | 0.0649 | 0.0978 | 2 | 0.0649 | 0.0978 | 4 | 4 | 2 | 15.5560 | 25.8726 | 5.5959 | 11.9412 | | | | | | |
| 9 | 1 | 1 | 11 | 0.0764 | 0.0233 | 4 | 0.0764 | 0.0233 | 3 | 3 | 1 | 14.4792 | 27.8149 | 5.6625 | 14.4481 | | | | | | |
| 10 | 1 | 1 | 12 | 0.0560 | 0.0080 | 3 | 0.0560 | 0.0080 | 3 | 3 | 1 | 13.8535 | 25.9409 | 5.5707 | 18.5582 | | | | | | |
| 11 | 1 | 1 | 13 | 0.0560 | 0.0158 | 3 | 0.0560 | 0.0158 | 3 | 3 | 1 | 13.7286 | 26.9715 | 5.4387 | 10.5957 | | | | | | |
| 12 | 1 | 1 | 14 | 0.0169 | 0.0037 | 3 | 0.0169 | 0.0037 | 3 | 3 | 1 | 14.6904 | 27.9600 | 5.4697 | 9.5061 | | | | | | |
| 13 | 1 | 1 | 15 | 0.0486 | 0.0863 | 3 | 0.0486 | 0.0863 | 4 | 4 | 2 | 20.9382 | 27.0141 | 6.4105 | 9.3607 | | | | | | |
| 14 | 1 | 1 | 16 | 0.0134 | 0.0358 | 3 | 0.0134 | 0.0358 | 6 | 6 | 4 | 19.4513 | 25.3278 | 6.8388 | 10.0390 | | | | | | |
| 15 | 1 | 1 | 17 | 0.0456 | 0.0082 | 4 | 0.0456 | 0.0082 | 5 | 5 | 3 | 17.0335 | 22.5363 | 6.5913 | 15.1755 | | | | | | |
| 16 | 1 | 1 | 18 | 0.0255 | 0.0523 | 3 | 0.0255 | 0.0523 | 4 | 4 | 2 | 13.0498 | 20.9067 | 5.5479 | 18.2331 | | | | | | |
| 17 | 1 | 1 | 19 | 0.1071 | 0.0444 | 3 | 0.1071 | 0.0444 | 4 | 4 | 2 | 9.9592 | 23.9238 | 6.1891 | 11.9197 | | | | | | |
| 18 | 1 | 1 | 20 | 0.0848 | 0.0410 | 4 | 0.0848 | 0.0410 | 4 | 4 | 2 | 10.2178 | 26.3063 | 6.0962 | 10.8258 | | | | | | |
| 19 | 1 | 1 | 21 | 0.0845 | 0.0604 | 3 | 0.0845 | 0.0604 | 3 | 4 | 2 | 11.0665 | 24.2164 | 7.0888 | 10.4817 | | | | | | |
| 20 | 1 | 1 | 22 | 0.0888 | 0.0430 | 3 | 0.0888 | 0.0430 | 4 | 4 | 2 | 12.0295 | 19.5480 | 7.4152 | 11.2224 | | | | | | |
| 21 | 1 | 1 | 23 | 0.0803 | 0.0129 | 4 | 0.0803 | 0.0129 | 5 | 3 | 3 | 12.5966 | 22.3747 | 7.0733 | 11.6559 | | | | | | |
| 22 | 1 | 1 | 24 | 0.0472 | 0.0318 | 3 | 0.0472 | 0.0318 | 3 | 1 | 1 | 13.0968 | 22.5166 | 6.0967 | 12.3757 | | | | | | |
| 23 | 1 | 1 | 25 | 0.0289 | 0.0176 | 3 | 0.0289 | 0.0176 | 5 | 3 | 3 | 12.8074 | 22.6040 | 6.0014 | 14.4419 | | | | | | |
| 24 | 1 | | | | | | | | | | | | | | | | | | | | |

FIGURE F.1: Rows 1 through 24 and Columns 1 through 12 of the final data set of metrics generated about the cells from the videos.

| ¹⁸ C_Area_um2 | ¹⁹ N_Area_um2 | ²⁰ N_C_A_Ratio | ²¹ Centroid_X | ²² Centroid_Y | ²³ Pct_Change | ²⁴ Elongation | ²⁵ Px | ²⁶ Py | ²⁷ Px_Mean | ²⁸ Py_Mean | ²⁹ Direction | ³⁰ Change_Direction | ³¹ Shapes |
|-----------------------------|-----------------------------|------------------------------|-----------------------------|-----------------------------|-----------------------------|-----------------------------|---------------------|---------------------|--------------------------|--------------------------|----------------------------|-----------------------------------|-------------------------|
| 187.9979 | 69.9294 | 0.3720 | 142.1392 | 332.1237 | 15.3038 | 1 | -5.1573 | 1.7377 | 1 | 1 South West | 0 | | 3 |
| 200.0327 | 102.6603 | 0.5132 | 126.6153 | 331.0561 | 68.1258 | 1 | -7.7619 | -0.5338 | 1 | 1 North West | 1 | | 3 |
| 190.2772 | 86.3404 | 0.4538 | 116.2477 | 327.4288 | -21.6810 | 0 | -5.1838 | -1.8136 | 1 | 1 North West | 0 | | 3 |
| 176.4190 | 87.3433 | 0.4951 | 96.0729 | 329.5333 | 12.5161 | 1 | -10.0874 | 1.0522 | 1 | 1 South West | 1 | | 3 |
| 172.0427 | 73.9410 | 0.4298 | 81.8309 | 333.0768 | -26.7196 | 0 | -7.1210 | 1.7718 | 1 | 1 South West | 0 | | 3 |
| 198.0269 | 49.5979 | 0.2505 | 69.1487 | 340.7826 | -36.8110 | 0 | -6.3411 | 3.8554 | 1 | 1 South West | 0 | | 3 |
| 236.0458 | 45.2216 | 0.1916 | 58.0467 | 344.7659 | -13.0747 | 0 | -5.5510 | 1.9912 | 1 | 1 South West | 0 | | 3 |
| 178.9718 | 64.0032 | 0.3576 | 60.0693 | 339.5084 | 59.2167 | 1 | 1.0113 | -2.6288 | 1 | 1 North East | 1 | | 1 |
| 223.0993 | 62.6356 | 0.2808 | 55.0638 | 334.1557 | -5.4317 | 0 | -2.5028 | -2.6764 | 1 | 1 North West | 1 | | 3 |
| 253.0040 | 59.1710 | 0.2339 | 46.4923 | 335.1784 | -6.9221 | 0 | -4.2857 | 0.5113 | 1 | 1 South West | 1 | | 3 |
| 238.5075 | 55.8888 | 0.2343 | 40.1755 | 334.8815 | -4.3213 | 0 | -3.1584 | -0.1484 | 1 | 1 North West | 1 | | 2 |
| 198.8474 | 55.0682 | 0.2769 | 39.8093 | 341.2022 | -0.9013 | 0 | -0.1831 | 3.1604 | 1 | 1 South West | 1 | | 3 |
| 195.0182 | 59.9004 | 0.3072 | 38.6966 | 342.7555 | 7.0056 | 0 | -0.5563 | 0.7766 | 1 | 1 South West | 0 | | 1 |
| 169.9457 | 84.2435 | 0.4957 | 36.1486 | 347.6218 | 42.5303 | 1 | -1.2740 | 2.4331 | 1 | 1 South West | 0 | | 3 |
| 169.7634 | 81.5083 | 0.4801 | 34.7755 | 348.2562 | -7.1015 | 0 | -0.6865 | 0.3172 | 1 | 1 South West | 0 | | 2 |
| 217.1731 | 73.0292 | 0.3363 | 36.4265 | 353.1380 | -12.4301 | 0 | 0.8235 | 2.4414 | 1 | 1 South East | 1 | | 3 |
| 225.5241 | 55.2462 | 0.2462 | 38.7530 | 354.8323 | -23.3877 | 0 | 1.1632 | 0.8466 | 1 | 1 South East | 0 | | 3 |
| 208.8764 | 47.6833 | 0.2283 | 34.6320 | 343.4553 | -23.6829 | 0 | -2.0605 | -5.6885 | 1 | 1 North West | 1 | | 1 |
| 204.2266 | 48.2303 | 0.2362 | 44.1326 | 342.2018 | 2.5966 | 0 | 4.7503 | -0.6267 | 1 | 1 North East | 1 | | 2 |
| 180.8864 | 59.5357 | 0.3291 | 53.6391 | 341.3548 | 8.3060 | 0 | 4.7533 | -0.4235 | 1 | 1 North East | 0 | | 3 |
| 151.8024 | 65.0061 | 0.4282 | 63.4324 | 343.5267 | 8.7021 | 0 | 4.8967 | 1.0899 | 1 | 1 South East | 1 | | 2 |
| 178.5159 | 63.1826 | 0.3539 | 70.2983 | 349.4612 | 4.7137 | 0 | 3.4329 | 2.9672 | 1 | 1 South East | 0 | | 3 |
| 185.0804 | 58.8063 | 0.3177 | 75.3837 | 351.0862 | 3.9710 | 0 | 2.5427 | 0.8125 | 1 | 1 South East | 0 | | 1 |
| 178.2424 | 56.5270 | 0.3171 | 78.3944 | 352.3458 | -2.2096 | 0 | 1.5053 | 0.6298 | 1 | 1 South East | 0 | | 1 |

FIGURE F.2: Rows 1 through 24 and Columns 18 through 31 of the final data set of metrics generated about the cells from the videos.